UNIVERSITY OF CAPE COAST

QUANTUM DOT SOLAR CELLS

ABBIEZIEH JOHN YANKEY

2009

UNIVERSITY OF CAPE COAST

QUANTUM DOT SOLAR CELLS

BY

ABBIEZIEH JOHN YANKEY

THESIS SUBMITTED TO THE DEPARTMENT OF PHYSICS OF THE SCHOOL OF PHYSICAL SCIENCES, UNIVERSITY OF CAPE COAST IN PARTIAL FULFILMENT OF THE REQUIREMENTS FOR THE AWARD OF A MASTER OF PHILOSOPHY DEGREE IN PHYSICS

NOVEMBER 2009

DECLARATION

CANDIDATE'S DECLARATION

I hereby declare that this thesis is the result of my own original research and that no part of it has been presented for another degree in this university or elsewhere.

……. Date…….

Yankey Abbiezieh John

(Candidate)

SUPERVISORS' DECLARATION

We hereby declare that the preparation and presentation of the thesis were supervised in accordance with the guidelines on supervision of thesis laid down by the University of Cape Coast.

…… Date:……

Prof. S. Y. Mensah

(Principal Supervisor)

…… Date……

Dr. Alfred Owusu

(Co-supervisor)

ABSTRACT

In this thesis, hot carrier relaxation dynamics in semiconductor quantum dots and quantum well structures have been investigated as the basis for improving on the efficiency of conventional solar cells to values between 40% and 60% beyond the Shockley and Queisser detailed balance limit of 30% hitherto.

Two schemes have been employed to obtain the shift in efficiency: The first is multiple exciton generation which occurs in semiconductor quantum dots. The output current as a function of the photogenerated voltage and the material band gap, is computed from the difference between the photogenerated and the recombination currents. The output voltage is obtained from corrections made to the voltages used in the splitting of water by standard photochemical processes.

The second is the formation of minibands in semiconductor quantum well structures which serve as the intermediate band required in the material bandgap in intermediate-band solar cell concept. Here, the output current is calculated from the difference between the photon flux absorbed by the cell and that emitted as a result of radiative recombination, all multiplied by a factor of the electronic charge. The output voltage is computed from the difference between the chemical potentials of the conduction and valence bands.

ACKNOWLEDGEMENTS

It is impossible to do justice to all the great people from whom I received help and support in various ways throughout my studies in only a few lines. Nevertheless, I will try to make an attempt to express my gratitude.

First, my special thanks go to Professor S. Y. Mensah of The Physics Department, UCC, under whose supervision this research was carried out. His patience, guidance, useful advice, critical comments and the many discussions either scientific or casual contributed immesurably to the success of this work. Also to Dr Owusu of the Physics Department UCC for his constructive critique of this work and providing answers to seemingly insurmountable problems that were encountered. Thanks also to the general staff and workers of the Physics Department of UCC.

I am also indebted to others whose work served as references in this research and to my fellow M. Phil students, Mr. Samuel Manu, Emmanuel Amewude, Nana Ama and Mathew Amekpewu not only for scientific inputs but sharing great conversations.

Finally, I want to thank my family; my parents, Egya Bekunludwo Yankey and Omo Adwo Yankey who always supported me in undertaking a scientific carrier and teaching me so many valuable lessons about important things outside Physics.

Thanks.

DEDICATION

To my sister Mrs. Faustina Avih and her family, Mr. Gabriel Ampah Sam, Mr. Fredrick Sam and Mr. John Korsah. Also to the Yankey family at Tikobo No1.

TABLE OF CONTENTS

LIST OF TABLES

LIST OF FIGURES

LIST OF SYMBOLS

DNA	deoxy-rebonucleic acid
QD	quantum dot
QDS	quantum dot supracrystal
2DEG	two-dimensional electron gas
S-Q	Shockley and Quiesser
MEG	multiple exciton generation
IBSC	Inter-mediate band solar cell
VB	Valence band
CB	Conduction band
0-D	zero dimensional
1-D	one dimensional
2-D	two dimensional
3-D	three dimensional
MOSFET	Metal oxide semiconductor field effect transistor
MQW	multiple quantum well
SL	superlattice
MBE	molecular beam epithaxy
MOCVD	metallo-orgarnic chemical vapour deposition
TMG	Trimethylgallium
TMA	Trimethyl Aluminium
TMI	TrimethylIndium

TOPO	Trioctylphosphine oxide
TOP	Trioctylphosphine
SK	Stanski-Krastanov
SET	single electron transistor
MDD	maximum density-droplet
TEM	Transmission electron micrograph
HOMO	Highest occupied molecular orbital
LUMO	Least unoccupied molecular orbital
CI	constant interaction
DC	direct current
AM-G	global air mass
PV	photovoltaic
AR	anti reflection
HH	heavy hole
LH	light hole
QY(E)	Quantum yield
QDS	quantum dot supracrystal

UNIVERSITY OF CAPE COAST

QUANTUM DOT SOLAR CELLS

ABBIEZIEH JOHN YANKEY

2009

UNIVERSITY OF CAPE COAST

QUANTUM DOT SOLAR CELLS

BY

ABBIEZIEH JOHN YANKEY

THESIS SUBMITTED TO THE DEPARTMENT OF PHYSICS OF THE SCHOOL OF PHYSICAL SCIENCES, UNIVERSITY OF CAPE COAST IN PARTIAL FULFILMENT OF THE REQUIREMENTS FOR THE AWARD OF A MASTER OF PHILOSOPHY DEGREE IN PHYSICS

NOVEMBER 2009

DECLARATION

CANDIDATE'S DECLARATION

I hereby declare that this thesis is the result of my own original research and that no part of it has been presented for another degree in this university or elsewhere.

……. Date…….

Yankey Abbiezieh John

(Candidate)

SUPERVISORS' DECLARATION

We hereby declare that the preparation and presentation of the thesis were supervised in accordance with the guidelines on supervision of thesis laid down by the University of Cape Coast.

…… Date:……

Prof. S. Y. Mensah

(Principal Supervisor)

…… Date……

Dr. Alfred Owusu

(Co-supervisor)

ABSTRACT

In this thesis, hot carrier relaxation dynamics in semiconductor quantum dots and quantum well structures have been investigated as the basis for improving on the efficiency of conventional solar cells to values between 40% and 60% beyond the Shockley and Queisser detailed balance limit of 30% hitherto.

Two schemes have been employed to obtain the shift in efficiency: The first is multiple exciton generation which occurs in semiconductor quantum dots. The output current as a function of the photogenerated voltage and the material band gap, is computed from the difference between the photogenerated and the recombination currents. The output voltage is obtained from corrections made to the voltages used in the splitting of water by standard photochemical processes.

The second is the formation of minibands in semiconductor quantum well structures which serve as the intermediate band required in the material bandgap in intermediate-band solar cell concept. Here, the output current is calculated from the difference between the photon flux absorbed by the cell and that emitted as a result of radiative recombination, all multiplied by a factor of the electronic charge. The output voltage is computed from the difference between the chemical potentials of the conduction and valence bands.

ACKNOWLEDGEMENTS

It is impossible to do justice to all the great people from whom I received help and support in various ways throughout my studies in only a few lines. Nevertheless, I will try to make an attempt to express my gratitude.

First, my special thanks go to Professor S. Y. Mensah of The Physics Department, UCC, under whose supervision this research was carried out. His patience, guidance, useful advice, critical comments and the many discussions either scientific or casual contributed immesurably to the success of this work. Also to Dr Owusu of the Physics Department UCC for his constructive critique of this work and providing answers to seemingly insurmountable problems that were encountered. Thanks also to the general staff and workers of the Physics Department of UCC.

I am also indebted to others whose work served as references in this research and to my fellow M. Phil students, Mr. Samuel Manu, Emmanuel Amewude, Nana Ama and Mathew Amekpewu not only for scientific inputs but sharing great conversations.

Finally, I want to thank my family; my parents, Egya Bekunludwo Yankey and Omo Adwo Yankey who always supported me in undertaking a scientific carrier and teaching me so many valuable lessons about important things outside Physics.

Thanks.

DEDICATION

To my sister Mrs. Faustina Avih and her family, Mr. Gabriel Ampah Sam, Mr. Fredrick Sam and Mr. John Korsah. Also to the Yankey family at Tikobo No1.

TABLE OF CONTENTS

LIST OF TABLES

LIST OF FIGURES

LIST OF SYMBOLS

DNA	deoxy-rebonucleic acid
QD	quantum dot
QDS	quantum dot supracrystal
2DEG	two-dimensional electron gas
S-Q	Shockley and Quiesser
MEG	multiple exciton generation
IBSC	Inter-mediate band solar cell
VB	Valence band
CB	Conduction band
0-D	zero dimensional
1-D	one dimensional
2-D	two dimensional
3-D	three dimensional
MOSFET	Metal oxide semiconductor field effect transistor
MQW	multiple quantum well
SL	superlattice
MBE	molecular beam epithaxy
MOCVD	metallo-orgarnic chemical vapour deposition
TMG	Trimethylgallium
TMA	Trimethyl Aluminium
TMI	TrimethylIndium

TOPO	Trioctylphosphine oxide
TOP	Trioctylphosphine
SK	Stanski-Krastanov
SET	single electron transistor
MDD	maximum density-droplet
TEM	Transmission electron micrograph
HOMO	Highest occupied molecular orbital
LUMO	Least unoccupied molecular orbital
CI	constant interaction
DC	direct current
AM-G	global air mass
PV	photovoltaic
AR	anti reflection
HH	heavy hole
LH	light hole
QY(E)	Quantum yield
QDS	quantum dot supracrystal

CHAPTER ONE

INTRODUCTION

Quantum Dots

The word nanometer is derived from the Greek word 'nano', meaning dwarf or extremely small. A nanometer (nm) is one billionth of a meter ie 10^{-9}m. For comparison, a single human hair is about 80,000 nm wide, a red blood cell is approximately 7,000 nm wide and a water molecule is almost 0.3nm across and DNA molecule is about 2.5nm wide. The nanoscale describes materials of dimensions from 100nm down to the size of atoms approximately 0.2nm. There has been an interest in the nanoscale because at this scale, the properties of materials show significant differences from those at a larger scale.

A nanostructure is any particle whose dimensions fall within the length scale specified, examples are quantum dots, carbon nanotubes, quantum wires, nanopolymers etc. There are many reasons for developing nanostructures. These are their ability to enhance optical absorption and emission, the continuing miniaturization of digital circuitry and the study of few-body quantum phenomena and possible exploitation for quantum computation.

The great diversity of matter making up our physical universe is composed of atoms exhibiting different physical properties depending on the chemical bonds binding them together. If we could concoct our own materials out of artificial atoms (quantum dots) that we could control, it would enable us

to fabricate a wide variety of new materials and useful devices with desirable properties.

The discovery of quantum dots took place when experimentalists measured the conductance through very small semiconductor field effect transistors [1]. But in the past two decades, progress in semiconductor micro fabrication has made it possible to confine a small number of electrons which is often reduced in dimensionality in the so called nanostructures. This means that electrons are moving freely in one, two dimensions or completely confined in all three spatial dimensions (zero-dimensional).

A quantum dot is a semiconductor nanostructure in which the charge carriers (electrons and holes) are confined in all three dimensions (zero dimensional) within a region of nanometer size. The size of the region is of the order of the electron De-Broglie wavelength of the charge carriers and as a result lead to discrete or quantized energy levels. These structures display a delta function density of states similar to real or naturally occurring atoms [2]. Usually, they are fabricated by restricting the two dimensional electron gas (2DEG) in a semiconductor heterostructure such as MOSFETs (metal-oxide-semiconductor field-effect transistors) or modulation-doped GaAs-AlGaAs, laterally by tiny electrostatic gates or vertically by etching techniques.

One can control the material composition, the number of electrons [3], vary the particle size and hence manipulate the confinement (discrete energy spectrum) or the energy gaps, the density and interaction strength of the dots as well as their absorption and luminescence properties. These structures can also hold and release electrons under the proper bias circumstances and thus constitute a two- state device. Figure 1 illustrates samples of quantum dots.

Fig 1: Quantum dot samples: (a) cylindrical, (b) rectangular (c) triangular pillar [4].

There are quantum dots of different materials and sizes; for instance, single molecules trapped between electrodes, metallic or superconducting particles, self assembled quantum dots, semiconductor lateral or vertical dots between closely spaced electrodes. Quantum dots or semiconductor nanocrystals and bulk semiconductors are made of the same materials. However, they exhibit different properties due to their size differences; the diameter of a quantum dot or nanocrystal semiconductor ranges between 2nm and 10 nm (10 and 50 atoms) and therefore exhibit quantum behavior whereas bulk semiconductor is much bigger than 10 nm. The jargon that 'small is different' is evident in this case.

The small size of a nanomaterial or quantum dot leads to three effects; first as a particle decreases in size, a greater proportion of atoms or molecules are present on the surface compared to those inside and this produces a large surface area to volume ratio than the same mass of material produced in larger form. For example, a particle of size 30 nm has 5% of its atoms on its surface, at 10 nm, 20% of its atoms reside on its surface and at

3 nm, 50% of its atoms reside on its surface. Since intrinsic reactivity or growth and catalytic chemical reactions are surface phenomena, this means that a given mass of material in nanoparticulate form will be much more chemically reactive than the same mass of material made up of larger particles. Thus the reduction in size has the potential for speeding up chemical reactions, biochemical and pharmaceutical separations and thus improving efficiency of many processes. In some cases, materials that are inert in their larger form are reactive when produced in their nano-size form, silver for example becomes a bactericide on a nanoscale.

Secondly, exceptional mechanical strength is observed for example in materials such as crystalline solids. As the size of their structural components decreases, there is much greater interface area within the material. Most metals are made up of small crystalline grains, the boundaries between the grain slow down or arrest the propagation of defects when the material is stressed, thus giving it strength. If these grains can be made very small, or even nanoscale in size, the interface area within the material greatly increases, which enhances its strength. For example, nanocrystalline nickel is as strong as hardened steel.

Thirdly, on accounts of its small size, the electron de Broglie wavelength begins to 'feel the boundaries' of the dot. Equivalently, as all the three spatial dimensions of the nanocrystal approach the Bohr exciton radius (BER), quantum confinement effects are observed. This means that the electron angular momentum, the hole and electron energy levels become discrete or quantized, i.e. there exist a small but finite separation between the energy levels [5]. Under these conditions, the nanostructured semiconductor

material ceases to resemble the bulk matrial and it can be called a quantum dot. This has large repercussions on the electronic and optical (absorptive and emissive) behavior of the semiconductor material. For example a blue shift of the absorption spectrum with decreasing dot size and a tunable emission wavelength by adjusting the dot size are examples of the size-dependent optical properties [6,7]. Hence the typical size of a quantum dot which produces a large surface to volume ratio and quantum confinement effects give the dot unique mechanical, electronic and optical properties which are distinct from those observed in the corresponding bulk semiconductor.

A number of theoretical approaches have been developed to analyze these phenomena observed in experimental work. The physics of quantum dots also show many similarities and differences with the behaviour of naturally occurring quantum systems in atomic and nuclear physics. Analogous atomic properties include an electronic shell structure, photon antibunching, controlled emission of quantum light and Rabi oscillations.

In contrast, quantum dots differ from real atoms in several respects. In quantum dots, the electrons are usually confined to a much larger volume than the electrons in real atoms. Typically a quantum dot structure resembles a two-dimensional box with a side length of ~ 100nm whereas in solids, the spacing between the atoms is of the order of a few Angstrom's (~ 0.2- 0.3) nm.

The shape of the confining potential is different in both structures. In real atoms the strong coulomb attraction of the nucleus is centripetal and restricts the electron motion into a small volume in the proximity of the nucleus resulting in a very high density and also, the effect of the mutual

coulomb repulsion is very small against the attractive force from the nucleus. In quantum dots, the potential is not a central attractive, but resembles more of a harmonic trap defined by the external electrodes (lateral quantum dot) or by physical dimensions (vertical quantum dots). Hence, the density in quantum dots can be much lower.

In a naturally occurring atom, one has little control over the spectrum of energies for adding or removing electrons. Here, the electrons interact with the fixed potential of the nucleus and with each other, and these two interactions determine the spectrum. The spacing of the energy levels in naturally occurring atoms are fixed and hence the absorption and emission properties are characteristic of the particular atom. In a quantum dot, the spacing of the energy levels is size-dependent and so are the absorption and emission wavelengths i.e. one can change this spectrum completely by altering the dot size at will, smaller dots emit blue light while larger dots emit red light.

A single semiconductor quantum dot consists of the order of 10^3-10^6 atoms. Most of the electrons in the material are bound to atoms but some of the electrons in the material can be made to move freely in the quantum dot region. While electrons are on the average further apart from each other, the electron-electron interaction becomes more important in comparison to the confinement strength. As the size and shape of the confinement potential differs from that of real atoms, so also, the energy scales are modified in quantum dots. Even though electrons are free to move in quantum dots, the mass of electrons is different from a free electron mass due to the surrounding host semiconductor material.

Unlike real atoms, current and voltage leads can be attached to probe a quantum dot's electronic state. When the charging energy of a small quantum dot is larger than the thermal energy, electrons in the lead cannot transfer onto the dot (Coulomb blockade effect). The interplay between quantum confinement and charging effects manifests itself in a wide range of physical phenomena. The single electron charging effect is one of these and will be discussed in the next chapter.

By coupling several quantum dots together, artificial molecules can be created [8-11]. An important feature of these artificial molecules is that the couplings between different dots can be tuned by changing the gate voltage or the inter-dot distance. This tunability also results in various interesting phenomena ranging from the formation of chemical bonds between coupled dots to covalent bonds. If a quantum dot is considered as a building block, quantum dot arrays can be created. Electrons in quantum dot arrays can move around and interact with each other through the Coulomb interactions and many interesting effects manifest themselves in magnetic, transport and optical properties.

When quantum dots are arranged on a periodic lattice and coupled to each other coherently, a band structure is obtained. This type of dot lattice or artificial crystal was first proposed by Sakaki [12] and it is called quantum dot super lattice. It is analogous to quantum well superlattice in which sequences of semiconductor layers with different band gaps produce new materials and devices. The energy spectrum of the superlattice is determined by the artificial periodicity in the quantum (dots) rather than the properties of the individual semiconductor materials.

Solar cells, alternative to dwindling traditional world energy resources

Amidst concerns, that the world's fossil fuel reserves are finite and depleting [13], much attention has been focused on finding other sustainable energy alternatives. Among the possible energy sources competing to replace fossil fuels, direct conversion of sunlight to electrical energy using photovoltaic solar cells is one of the important alternatives and a challenge that mankind faces today. Photvoltaic (solar) cells convert solar energy to electrical energy and offer many advantages including being low in maintenance and relatively environmentally friendly and could have a large number of applications, particularly in the energy, communications, military and space industries.

Even though solar radiation is free, plentiful and a clean source of power and also the technology for its conversion into useful energy has been around for over five decades, while researchers agree that when measured on a per watt basis, the amount of solar power that reaches the earth surface in an hour is more than the world's population energy requirement for a year, the major draw back to the wide-spread use of conventional silicon photovoltaic solar cells to date has been its prohibitive cost and low efficiency device.

The maximum power conversion efficiency obtainable with conventional single junction solar cell is given by the Shockley and Queisser limit. Using detailed balance approach, and assuming that each photon above the cell's material bandgap produces just one electron-hole pair while all photons with energies below the bandgap are lost, one obtains a theoretical maximum energy conversion efficiency of 30% [14]. The efficiency of conventional solar cells is small because of their inability to absorb all of the

incident solar energy and secondly their inability to convert all of the photons energy that is absorbed to free electrons and holes necessary to generate photocurrents and photovoltages in the material component.

This efficiency value is unsatisfactorily low. It would be incorrect if one considers the Shockley and Queisser limit as the ultimate limit achievable with photovoltaic cells since the actual limit could be much higher if transmission and thermalisation losses could be sufficiently reduced. Consider the sun as a blck body emitting at a temperature of 5760K and a solar cell (another black body) at 300K , the Carnot thermodynamic efficiency is 95%. Calculations of radiative losses from the solar cell by Lansberg et al [15] give an efficiency of 93.3%.

Taking into account entropy generation during energy conversion, one obtains a black body limit of about 86%. The large difference between the Shockley-Queisser and the thermodynamic limits is due to a mismatch between single materials which are characterized by only two energy levels with bandgaps in the range ; (1.0 eV - 1.7 eV) and the solar spectrum which contains photons with a wide range of energies in the interval (0.5 eV - 3.5 eV). From the foregoing, devices that rely on a single transition between energy levels are intrinsically not suitable for the broad solar spectrum.

Undoubtedly, large area and durable solar cells with cheap starting materials, inexpensive manufacturing techniques, and a reasonable level of efficiency are required to satisfy our growing energy demands. Unfortunately, contemporary photovoltaic solar cells fail on all counts. Notwithstanding, there is a potentially huge market for solar cells utilization if their cost were to approach or decrease past the cost of combusting fossil fuels especially for;

1. Areas where the cost of connecting to the power grid is prohibitive such as in developing nations that do not have a well developed electrical distribution network.
2. Military planners who are concerned at soldier's reliance on batteries to power the increasing amount of portable electronic equipments they carry into battle.
3. Areas connected to the grid yet located in geographical locations with favourable conditions of insolation (sun exposure). In these areas, demand will arise from individuals concerned when using clean energy sources to supplement their energy supply.

Several roots have been proposed to overcome this intrinsic property of semiconductor solar cells and thereby increase their power output. All these methods or concepts concentrate on a much better use of the solar spectrum [16].These methods can be achieved either through slight modification of the solar spectrum or the material of the semiconductor or by exploiting the excess bandgap energy of the photogenerated electrons through the application of nano-size materials (Quantum dots and quantum dot supracystals) which show unique and important strong quantization effect. The latter constituting the concept of 3rd generation solar cells.

In this thesis, we review the unique characteristics of quantum dots and the theoretical basis of using quantum dots to optimize the performance of conventional solar cells through multiple exciton generation (MEG) and intermediate band solar cell (IBSC) concepts. These schemes produce efficiency limits between 40% and 60% which constitute an improvement over the Shockley and Quiesser limit.

Thesis outlook

The organization of this thesis is as follows. Chapter One highlights some of the outstanding properties of quantum dots in comparison with naturally occurring atoms and their possible potential applications especially in solar cell technology. A brief commentary on conventional solar cells, the need to improve on their efficiency and their possible potential applications are also given.

Chapter Two discusses the synthesis methods and characterization of both 2-dimensional electron gas (2DEG) and quantum dots. It gives detailed experiments that describe the electronic structure of the dots including theoretical overview and the classification of quantum dot in artificial periodic table. The optical propertiesof quantum dots, in particular the absorption and emission spectroscopy and quantum efficiency are discussed extensively.

Chapter Three discusses briefly, conventional solar cells and the modification of their efficiency by incorporating quantum dots in them. This is based on a process referred to as impact-ionization or multiple exciton generation (MEG) which occurs in quantum dots on interaction with solar radiation. Intermediate band solar cell (IBSC) concepts are also discussed. Finally, conclusions and recommendations are given in Chapter Four.

CHAPTER TWO

SEMICONDUCTOR HETEROSTRUCTURE AND CHARACTERISATION OF QUANTUM DOT

Theoretical description of Semiconductor heterostructure

In solids, atoms are bonded closely together and their formerly discrete energy levels split into sub-levels or form degenerate levels. Due to the interactions of an enormous amount of atoms, the sublevels are closely spaced in such a way that quasi continuous bands of possible energies are formed. Quantum mechanical considerations show that the energy spectrum of a bulk semiconductor consists of energy bands separated by gaps. The lower energy band is called the valence band (VB) while the upper energy band is called the conduction band (CB).

In the ground state of an undoped perfect semi-conductor at 0K, an overwhelming majority of electrons occupy the valence band, filling it almost completely whereas an extremely small percentage of electrons occupy the conduction band. The electrons in a bulk semiconductor material have a range of energies. One electron with energy different from a second electron is described as being in a different energy level, and it is established that only two electrons can fit in any given state. It is also established that some energy levels are simply off- limits to electrons and this region of forbidden electron energies is called the bandgap. It is a fixed parameter for each semiconductor based on the material of the semiconductor.

Bulk semiconductor and semiconductor compounds are typically made from compounds containing an element from the periodic table that are in

groups II and VI, III and V or IV and VI. Through doping of the semiconductor, delocalized electrons may also be introduced into the CB and holes in the VB using impurity atoms that have more (donors) or fewer (acceptors) electrons in their external orbital than the atoms of the lattice. Here no excitation is involved and the semiconductor remains in the ground state. Electrons and holes or quasi-particles that carry electric charge are responsible for all observed phenomena that occur in semiconductors.

Band-structure engineering has made it possible to construct semiconductor heterostructures or artificial crystals [17] which is composed of different layers of semiconductors with the thickness of the layers along the growth axis being carefully controlled with atomic precision. Thus, making it possible, to create new materials and devices with pre-defined properties. In bulk metals and semiconductors, electrons (or holes) are generally free to move in all spatial directions. If this freedom is frozen or restricted in certain directions, the dimensionality of the system becomes reduced.

The reduced dimensionality actually increases the energy of charge carriers (electrons and holes) and has implications for the density of states of the system as a whole. For example in a 2-dimensional (2-D) system, the electrons can only move in one plane and may not travel perpendicular to this plane. An example of a naturally occurring material showing a quasi 2-dimensional behaviour is graphite where the resistance measured along the sheet is much lower than between sheets. Polymer sheets, electrons on the surface of liquid helium, semiconductor systems such as metal oxide semiconductor field effect transistors (MOSFET's), heterojunctions and quantum wells are other examples.

One dimensional systems where motion of charge carriers is permitted only along a line also occur naturally, as for example transport along a polymer chain. They may also be fabricated using semiconductors through advanced lithographic techniques where they are known as quantum wires.

Finally, all possibility of movement may be removed to form a zero-dimensional system. The fabricated ones are quantum dots, the natural versions being atoms. Electrons and holes confined by potential barriers to small regions of space where the dimensions of the confinement are less than the de-Broglie wavelength of these charge carriers produce pronounced quantization effects as already mentioned. The three quantization configurations are shown in figure 2. For typical semiconductors (group IV, III-V, II-VI elements), the length scale below which strong quantization

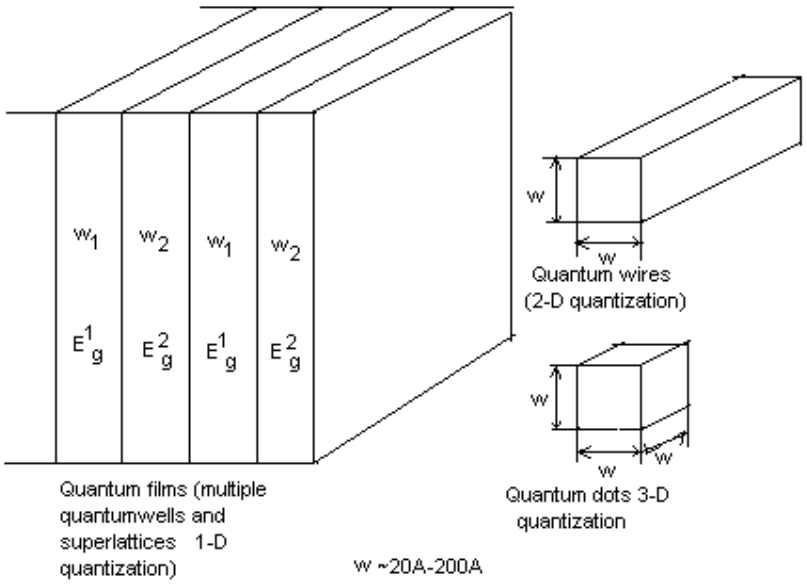

Fig 2: Three quantization configurations of quantum well structures [18].

effects begin to occur ranges from about 5nm to 25nm [19].

A single quantum well is formed from one semiconductor sandwiched between two layers of semiconductors having a larger bandgap. The centre layer with the smaller bandgap semiconductor forms the quantum well while the two layers sandwiching the center layer creates the potential barriers [20] as shown in figure 3.

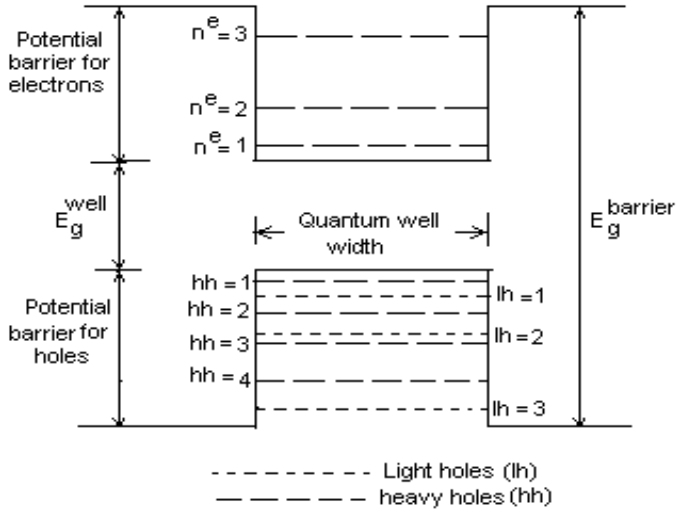

Fig 3: One-dimensionally confined quantum well [20].

Two potential wells are actually formed in the quantum well structure; one well is for conduction band electrons, the other for valence band holes. The well depth for electrons is the difference between the conduction band edges of the well and barrier semiconductor, while the well depth for holes is the corresponding valence band offset.

Multiple quantum well (MQW) structures consist of a series of quantum wells (i.e. a series of alternating layers of wells and barriers). If the barrier thickness between adjacent wells is sufficient to prevent significant electronic coupling between wells, then each well is electronically isolated.

This type of structure is referred to as multiple quantum well (MQW). On the other hand if the barrier thickness is sufficiently thin to allow electronic coupling between wells i.e. there is significant overlap of electronic wave functions between wells, then the electronic charge distribution becomes delocalized along the direction normal to the well layers. This coupling leads to broadening of the quantized states of the wells. The new broadened and delocalized quantized states are called minibands. If there is strong coupling between the wells, we obtain a superlattice (SL). The critical barrier thickness

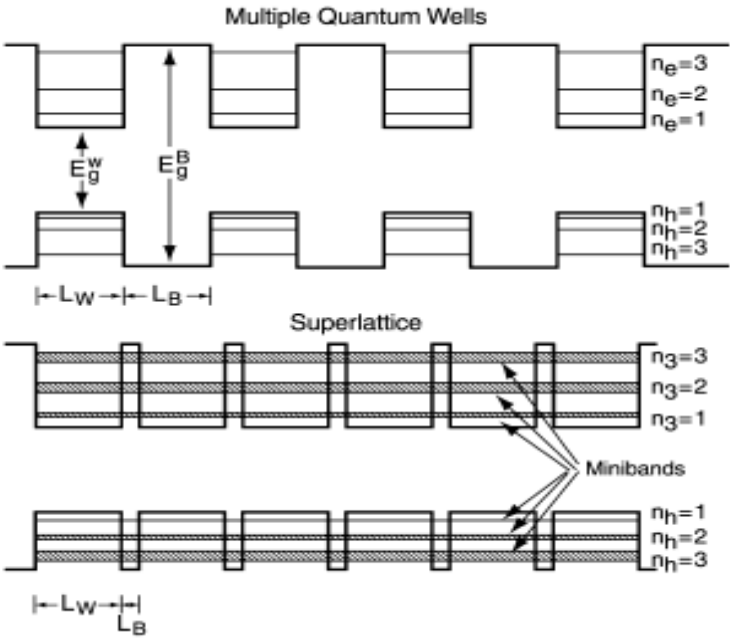

Fig 4: Energy levels of (a) multiple quantum well structures (barrier.4nm) and (b) superlattices (barrier <4nm) [19].

at which minibands formation begin to occur is about $40\,\mathring{A}$ [21-25]. The electronic coupling increases rapidly with decreasing barrier thickness, and miniband formation is very strong below $20\,\mathring{A}$ as shown in figure 4.

Superlattice structures yield efficient transport normal to the layers because the charge carriers can move through the minibands, the narrower the barriers, the wider the minibands and the higher the carrier mobility. Charge transport in multiple quantum wells with thick barriers requires thermionic emission of carriers over the barriers. However, if an electric field is applied, there would be field-assisted tunneling through the barriers [26].

Synthesis of Quantum well structures (2DEG)

Quantum wells are produced through epitaxial growth of crystalline films via either

1. molecular beam epitaxy (MBE) or
2. metallo-organic chemical vapour deposition [27-30].

Both techniques are capable of creating epitaxial layers of sufficient quality to produce quantization effects. These qualities include uniform thickness and interfacial abruptness (both within a few atomic layers), perfect crystallization and compositional uniformity.

Molecular Beam Epitaxy (MBE)

In the MBE technique, an ultra vacuum chamber is fitted with a number of evaporation (effusion) cells, each controlled by a separate shutter, which supply fluxes of molecular beams of the desired atomic species, illustrated in figure 5. The beam can be turned on and off within 0.1s. Growth rates are typically 5Å/s. An ion beam sputtering gun is used first to ion-etch the surfaces to remove impurities and imperfections. The substrates are maintained at ~500 – 700 ^{o}C during growth. Spectroscopic capabilities such as

mass spectrometry, auger spectrometry and reflection high-energy electron diffraction are included in the chamber to control the process and provide data on film quality.

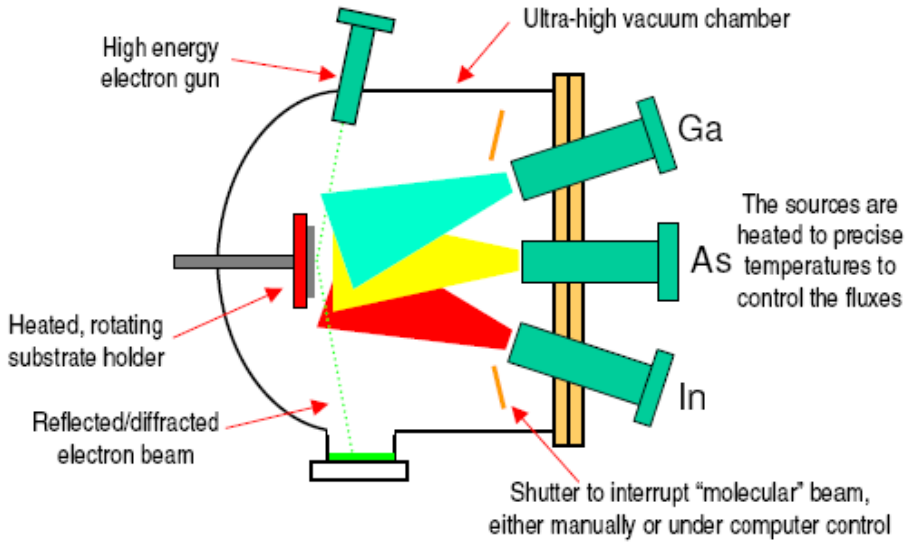

Fig 5: Schematic diagram of MBE apparatus [31]

Elemental species that can be produced by MBE include Ga, Al, In, Sb, Sn, Be, Ge, Se, Te, Cd, Hg, Zn, Mn, Pb and Si. The quantum well materials mostly produced by MBE are III-V semiconductors, binary and ternary compounds such as GaAs/$Al_XGa_{1-X}As$, GaSb/$Al_XGa_{1-X}Sb$, InAs/GaSb, $Ga_XIn_{1-X}As$/$AlIn_{1-x}As$, GaAs/$Ga_XIn_{1-X}P_2$ and InP/$Ga_XIn_{1-x}As$. In each case the well material is the first and the barrier material is the second compound. II-VI semiconductor materials such as CdTe/HgTe and ZnSe/$Zn_{1-X}Mn_XS$ have also been made.

Metallo-organic chemical vapour deposition (MOCVD)

This technique is used purely for preparing III-V semiconductor quantum wells. In this process, the group III metals are introduced into a reaction chamber in a form of metallo-organic vapours that react at high temperatures with gaseous precursors of the non-metalloid group V component of the desired semiconductor compound to form a crystalline, epitaxial film on a heated substrate. Ga, Al and In are commonly introduced as trimethyle gallium (TMG), trimethyl Aluminium (TMA) and trimethyl indium (TMI). As and P are usually introduced as arsine and phosphine, although less toxic compounds such as tertiary butyl arsine and tertiary butyl phosphine are also used.

The organometallic compounds are kept in liquid form at a sufficiently low but constant temperature and are swept into the reaction chamber at controlled composition by spraying hydrogen gas at a controlled flow rate through the liquid metallo-organics. Gaseous arsine or phosphine is fed directly into the system from gas cylinders through flow and pressure controllers. Ultra-pure hydrogen is used as the carrier gas for all reactant flows. The single crystal substrate is placed on a graphite block that is heated by resistance heaters to 650-750^{o}C. Growth rates are typically 5-10 Å/s. The reaction chamber is operated at either atmospheric or reduced pressure (50-100 torr). The low pressure system can yield very sharp interfaces between the semiconductor heterojunctions and very uniform epilayers, as shown in figure 6 where GaAs wells are 52 $\overset{o}{A}$ thick and the $Al_{0.32}Ga_{0.68}As$ barriers are 17 $\overset{o}{A}$ thick.

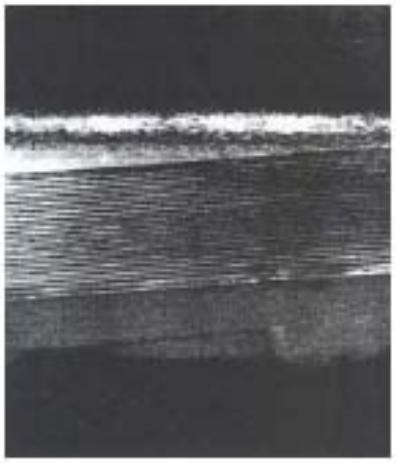

Fig 6: TEM of GaAs/$Al_{0.32}Ga_{0.68}As$ superlattice structure [32].

Carrier distribution in quantum well structures

Consider a low-dimensional system formed by a heterostructure consisting of a sandwich of different semiconductor materials such as GaAs/AlGaAs wafers where layers of gallium arsenide and aluminum gallium arsenide are stacked together in a specific way as shown in figure 7. GaAs is a III-V compound semiconductor material composed of the element gallium (Ga) from column III and the element arsenic (As) from column V of the periodic table of elements. AlGaAs is obtained when a fraction of the Ga ions in GaAs is substituted by aluminum (Al) ions, also from column III of the periodic table of elements. In this way, the band gap of GaAs $\Delta E_g \sim 1.42eV$ is increased. The resultant heterostructure is $Al_xGa_{1-x}As$. Usually an Al fraction of x = 0.3 is substituted resulting in a band gap of 1.79eV and when the two materials are put together, a band gap mismatch of $\Delta E_c \approx 0.37eV$ is formed at the interface of the two materials in figure 7. In this way a modulated band gap material or a superlattice is formed.

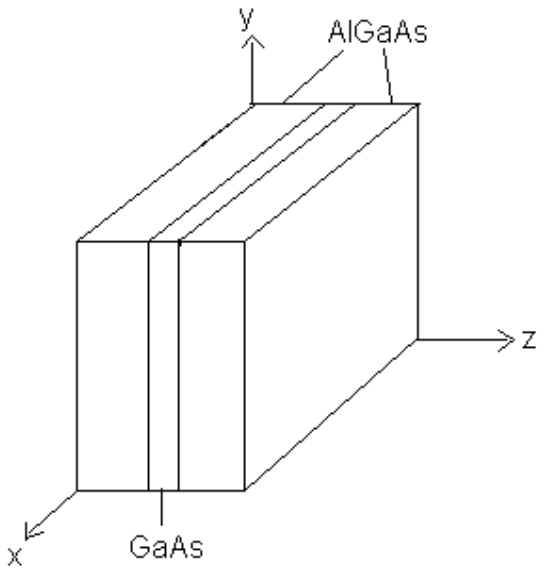

Fig 7: GaAs layer sandwiched between AlGaAs layers to form a heterostructure.

Subsequently, when silicon dopants are implanted in the AlGaAs regions (typically $1\times10^{18}cm^{-3}$ dopant in 65nm AlGaAs), they donate free electrons which fall into the GaAs because their energy is lower in the later material. The resulting positive charge on the Si atoms creates a potential that hold the electrons at the GaAs/AlGaAs interface in a quantum well. The electrons in this well are strongly confined in the growth direction, forming discrete states but are only allowed to move in the plane of the interface, where they form a two-dimensional electron gas (2DEG)

Modulation-doped Heterostructure

In an idealized system we are interested in free carriers, i.e. electrons in the CB and holes in the VB must propagate in delocalized states over the crystal [33]. The obvious way to introduce the carriers is by doping the regions where

the carriers are needed. However charged donors or acceptors are left behind when electrons or holes are released and these scatter the carriers by coulomb interaction-ionized impurity scattering. This obstructs the propagation of the carriers within the structure, blurs energy levels and disrupts the coherence of the electron and hole wave functions needed to observe the quantum effects.

The solution to this problem is modulation doping whereby the doping is grown in one region but carriers subsequently migrate to another as shown in fig ure 8 for the heterojuntion between negatively doped AlGaAs and undoped GaAs. The electrons in the conduction band travel around and some cross into the GaAs, lowering their energy as shown in figure 8a.

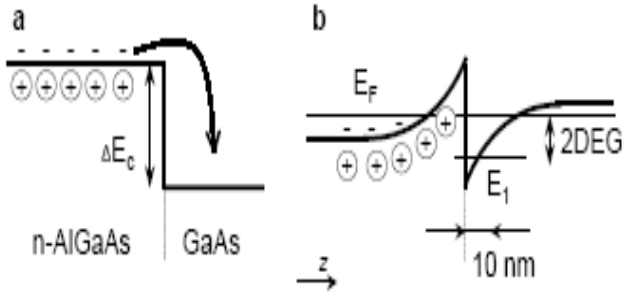

Fig 8: Conduction band around a heterojunction between negatively doped AlGaAs and undoped GaAs [33].

This motion separates the negatively charged electrons from their positively charged donors setting up an electrostatic potential that tends to drive the electrons into the n-AlGaAs. As a result, the edge of the conduction band has a slope as shown in fig 8b. Since the electrons cannot climb the barrier ΔEc, they become trapped at the heterointerface in the potential well. A detailed analysis shows that the potential well is roughly triangular [10] and spreads

over 10 nm along the growth direction at typical energy of the electrons E_1 in GaAs. The energy levels for motion along the z axis are quantized similar to those in square well.

Mostly electrons occupy the lowest quantized states along the z while remaining free in the other two dimensions x and y. This constitutes a two dimensional electron gas (2-DEG) which forms the basis for many electronic devices. Thus modulation doping achieves two benefits, firstly it has separated electrons from their donors to reduce scattering by ionized impurities and secondly, confined electrons to two dimensions.

Basic Properties of 2DEG

In this section, the basic quantum mechanical properties of two dimensional electron gas (2DEG) are examined. This includes the wave function, the energy dispersion, the density of states and the motion of the electrons in perpendicular magnetic field.

The wave function and energy dispersion of a 2DEG

In order to understand and predict the physical properties of heterostructure as described earlier, we need to address the two fundamental questions [34]. What is the ground state of given system? and how does the system behave under an external influence? Answering these questions remain one of the most challenging problems in modern physics mainly due to the many- body nature of nanostructures composed of many atoms or electrons.

Let us first consider electrons in the narrow gap semiconductor layer as shown in figure 7. If this layer is thin enough, the motion of carriers in the

direction perpendicular to the heterointerfaces is quantized, meaning that this motion involves discrete (quantum) energy levels. Let the z- axis be directed perpendicular to the plane of the 2DEG. In the direction parallel to the heterointerfaces, the electronic motion is not restricted. Hence, the wave function for a 2DEG can be presented as

$$\Psi(\vec{r},z) = \chi(z)\psi(\vec{r}) = \chi(z)\exp(ik_x x + ik_y y) \tag{1}$$

The term $\exp(ik_x x + ik_y y)$ in the wave function describes the electronic motion in directions x and y in the plane of the 2DEG similar to that of free electrons. This is understandable since electrons move freely in these directions while **r** is the position vector in the plane of the 2DEG. In the rest of the analysis, it will be assumed that all the distances are much larger than interatomic distances and that the electronic mass is the effective mass. A good approximation for the confining potential is a triangular one. Thus

$$\mathrm{U(z)} = \begin{cases} \infty & at \quad z < 0 \\ Fz & at \quad z > 0 \end{cases} \tag{2}$$

Then one can write the Schrödinger's equation for the wave function χ (z) as

$$\frac{\partial^2 \chi}{\partial z^2} + \frac{2m}{\hbar^2}(\mathrm{E - Fz})\chi = 0 \tag{3}$$

Instead of z, we introduce a dimensionless variable

$$\varsigma = \left(\mathrm{z} - \frac{\mathrm{E}}{\mathrm{F}}\right)\left(\frac{2m\mathrm{F}}{\hbar^2}\right)^{\frac{1}{3}} \tag{4}$$

The quantity

$$\ell_{\mathrm{F}} = \left(\frac{2m\mathrm{F}}{\hbar^2}\right)^{-\frac{1}{3}} \tag{5}$$

plays the role of characteristic localization length in the y direction. Equation (3) can be written in the form

$$\chi'' - \varsigma\chi = 0 \tag{6}$$

Which is solved with boundary conditions of finiteness at infinity and z = 0. At z = 0, the solution of equation (6) takes the form

$$\chi(\varsigma) = AAi(\varsigma) \tag{7}$$

Where Ai(ς) is the Airy function defined as

$$Ai(\varsigma) = \frac{1}{\sqrt{\pi}}\int_0^\infty \cos\left(\frac{\mu^3}{3} + \mu\varsigma\right)\mathrm{d}\mu \tag{8}$$

For large positive ς it decays exponentially,

$$Ai(\varsigma) \approx \frac{1}{2\varsigma^{1/4}} e^{-(2/3)\varsigma^{3/2}} \tag{9}$$

While for large negative ς, it is oscillatory,

$$Ai(\varsigma) \approx \frac{1}{|\varsigma|^{1/4}}\sin\left(\frac{2}{3}|\varsigma|^{3/2} + \frac{\pi}{4}\right) \tag{10}$$

The energy spectrum E_n, is defined by the roots ς_n of the equation

$$Ai(\varsigma) = 0, \rightarrow E_n = E_o\varsigma_n \tag{11}$$

Here

$$E_o = \left(\frac{\hbar^2 \mathrm{F}^2}{2m}\right)^{1/3} \tag{12}$$

The normalization constants A_n are defined as

$$A_n^{-1} = \int_0^\infty \mathrm{dz}\,|\,\chi_n(\mathrm{z})\,|^2 \tag{13}$$

The normalized electron densities $\gamma_n = A_n|\,\chi_n(\mathrm{z})\,|^2$ are shown in figure 9.

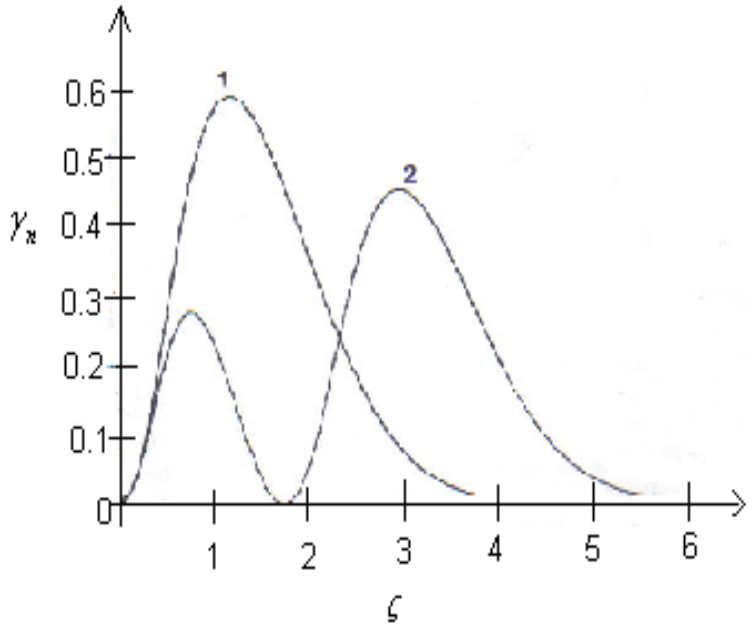

Fig 9: Normalized electron densities $\gamma_n = A_n \left| \chi_n(z/\ell_F) \right|^2$ for the first (1) and second (2) subbands in a triangular potential well.

Each level creates a sub-band for the in-plane motion, the energy being

$$E_{n,k} = E_n + E(k) = E_n + \frac{\hbar^2 k^2}{2m}, \tag{14}$$

Here n is the quantum number labelling the levels. Each quantum level, E_n corresponds to an energy subband. The effective mass m, being considerably smaller than the mass of the free electron. The dependence of the electron energy on the wave vector for a two-dimensional electron gas is given by

$$E - E_n = \frac{\hbar^2 (k_x^2 + k_y^2)}{2m} \tag{15}$$

For the quantization to be important, the difference between the levels should be much larger than the thermal energy, that is, $E_o >> k_B T$ where k_B is the Boltzmann constant and T is the temperature in kelvins.

Density of states

As in any physical system, electrons and holes try to occupy low energy positions in conduction and valence bands. Quantum mechanical considerations show that only certain amounts of carriers are allowed for any given energy.The quantity that speciifies how closely packed the energy levels are in some physical system is called the density of states (DOS). It is defined as the available number of states N per unit energy interval per unit volume of the material,

$$g(E) = \frac{2}{V} \cdot \frac{dN}{dE} \tag{16}$$

The factor 2, takes into accounts the fact that two electrons of opposite spins occupy each state. The Density of states shows profound changes with the dimensionality of quantization. For an ideal bulk semiconductors with simple parabolic bands, the DOS has a square-root dependence on the electron energy [35].

$$g^{3-D}(E) = \frac{1}{2\pi^2}\left(\frac{2m}{\hbar^2}\right)^{3/2} E^{1/2} \tag{17}$$

The super script 3-D, emphasizes the fact that in bulk material, the carriers move freely in all directions of space. While the DOS in 3-D case grows with the square root of the energy, it shows different behaviour for structures with reduced dimensionality.

The density of states for each subband in a 2DEG can be found using an approach similar to that used for a 3-D density of states, that is, by counting the number of states with wave vectors k between k and k + dk. The corresponding area in k-space is equal to 2πkdk. The density of allowed states

is equal to the number of allowed values of k in this area in k-space times two. The density of allowed points in k-space for the unit size sample is $1/(2\pi)^2$. Hence, the total number of states with values of k between k and k + dk is

$$dN = \frac{2 \times 2\pi k\, dk}{(2\pi)^2} \tag{18}$$

From equation (15)

$$k = \frac{\sqrt{2m(E - E_n)}}{\hbar} \tag{19}$$

where E_n is the bottom of the n^{th} subband and

$$k\, dk = m\, dE / \hbar^2 \tag{20}$$

we obtain

$$dN = \frac{4\pi \left[2m(E - E_n)\hbar^2\right]^{\frac{1}{2}} 2m\, dE / \hbar^2}{2\left[2m(E - E_n)\hbar^2\right]^{\frac{1}{2}} (2\pi)^2} = g(E)dE \tag{21}$$

where the density of states, g(E), for one subband is given by

$$g(E)^{2-D} = \frac{m}{\pi \hbar^2} \tag{22}$$

In the absence of a magnetic field, the DOS in a 2DEG is a constant, dependent only on fundamental constants and the effective mass of the confined electrons.The states of the first (bottom) subband overlap with the states of the second (from the bottom) subband for energies larger than the second energy level, and so on. As a consequence, the overall density of states has a staircase shape as shown in figure 10. It may be desribed by the equation $g(E)^{2-D} = \frac{m}{\pi \hbar^2} \sum_i H(E - E_i)$, where $H(E - E_i)$ is the Heaviside function. It takes the value of zero when E is less than E_i and 1, when E is equal or

graeter than E_i . E_i is the i-th energy level witin the well. With an increase in the well thickness, the steps in figure 10 gradually decrease and merge into an

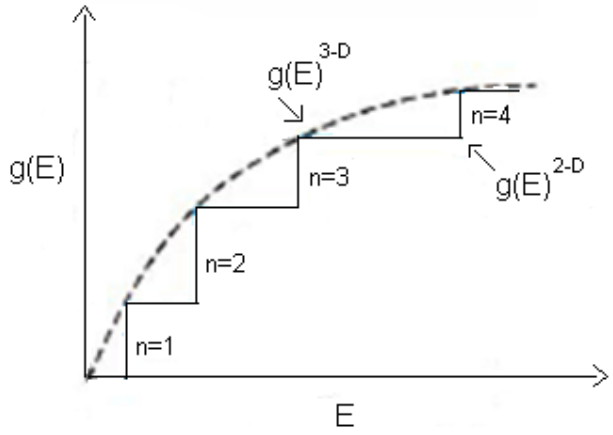

Fig 10: Density of states for a quasi 2-D system (step-like line) and of bulk semiconductor material (broken line) [19]

envelope parabolic function, which is equal to the three-dimensional density of states function multiplied by the well thickness. Once we find the densities of states, we can calculate the electron concentration in the conduction band and various optical properties such as the rate of absorption or emission. However, energy states in the valence band may play an equally important role.

Motion in a perpendicular magnetic field

There has been much interest in the effects of a perpendicularly applied magnetic field on a 2DEG. The reasons being that because of the confinement there is no dispersion in the direction of the magnetic field so that a magnetic field applied perpendicularly to the plane of a 2DEG creates highly

degenerate electron energy levels. In a single particle picture and with no disorder in the 2-D electron system, the magnetic field essentially places electrons in an identical harmonic oscillator potential well of number equal to the number of magnetic flux quanta passing through the 2-D system. The quantum energy levels, equally spaced in energy in the harmonic oscillator potential wells are known as Landau levels. Depending on the magnetic field strength, these levels can have enormous degeneracy.

According to classical theory, the Hamiltonian function of a charged particle in an external magnetic field is

$$\hat{H} = \frac{1}{2m}\left(\mathbf{p} - \frac{e}{c}\mathbf{A}\right)^2 + e\phi \ , \tag{23}$$

where ϕ is scalar and A is the vector potential of the magnetic field i.e. $\mathbf{B} = \nabla \times \mathbf{A}$, $\mathbf{p}$ is the generalized momentum of the particle and c is the velocity of light in vacuum. According to quantum mechanical rules, the canonical momentum $\mathbf{p}$, has to be replaced by the corresponding operator,

$$\mathbf{p} \rightarrow \hat{\mathbf{p}} = -i\hbar\nabla \tag{24}$$

and adding an extra spin term $-\boldsymbol{\mu}\mathbf{H}$ where $\boldsymbol{\mu} = \mu_B \hat{\mathbf{s}}/s$ is the magnetic moment. Here $\mu_B = e/2mc$ is the Bohr magneton while $\hat{\mathbf{s}}$ is the spin operator and $\mathbf{H}$ is the magnetic field intensity. Generally, interaction with the periodic potential of the crystalline lattice leads to renormalization of the spin splitting, $\mu_B \rightarrow \mu^{=} g_f \mu_B$ where g_f is called the spectroscopic spin splitting factor. Finally we obtain,

$$\hat{H} = \frac{1}{2m}\left(\hat{\mathbf{p}} - \frac{e}{c}\mathbf{A}\right)^2 - \boldsymbol{\mu}\mathbf{H} + e\phi =$$

$$\frac{\mathbf{p}^2}{2\mathrm{m}} - \frac{e}{2\mathrm{m}c}\left(\mathbf{A}\cdot\mathbf{p} + \mathbf{A}\cdot\mathbf{p}\right) + \frac{e^2\mathbf{A}^2}{\mathrm{m}c^2} - \frac{\mu}{s}\hat{\mathbf{s}}.\mathbf{H} + e\phi \qquad (25)$$

Since $\hat{\mathbf{p}}\cdot\mathbf{A} - \mathbf{A}\cdot\hat{\mathbf{p}} = -i\hbar\,\mathrm{div}\,\mathbf{A}$, those operators commute if $\mathrm{div}\,\mathbf{A} = 0$. It holds in a uniform magnetic field with $\mathbf{A} = \frac{1}{2}\mathbf{H}\times\mathbf{r}$. Thus $\mathbf{A}\cdot\hat{\mathbf{p}} = \hat{\mathbf{p}}\cdot\mathbf{A}$ and hence $\mathbf{A}\cdot\hat{\mathbf{p}} + \hat{\mathbf{p}}\cdot\mathbf{A} = 2\mathbf{A}\cdot\hat{\mathbf{p}} = 2\,\hat{\mathbf{p}}\cdot\mathbf{A}$.

The wave function in a magnetic field is not uniquely defined: it is defined only within the gauge transform $\mathbf{A}\to\mathbf{A}+\nabla f$, $\phi\to\phi-\frac{1}{c}\frac{\partial f}{\partial t}$, where f, is an arbitrary function of coordinates and time f(r,t). Under such a transformation only the phase of the wave function is changed by the quantity $e\,f/\hbar\,c$ that does not affect the observable quantities. In classical mechanics, the generalized momentum of the particles is related to its velocity by the Hamiltonian equation,

$$m\,\mathbf{v} = \mathbf{p} - e\mathbf{A}/c$$

(26)

In quantum mechanics, we arrive at a similar expression. However, different components of the velocity do not commute, the commutation rules being

$$\left\{\hat{v}_x, \hat{v}_y\right\} = i\left(e\hbar/m^2c\right)\mathrm{H}_z,$$

$$\left\{\hat{v}_y, \hat{v}_z\right\} = i\left(e\hbar/m^2c\right)\mathrm{H}_x,$$

$$\left\{\hat{v}_z, \hat{v}_x\right\} = i\left(e\hbar/m^2c\right)\mathrm{H}_y, \qquad (27)$$

This means that the particles cannot simultaneously have definite velocities in all three directions. The Cartesian components of the vector potential

A = (-yH, 0, 0) generate a uniform magnetic field which points in the y direction.i.e. H = (0, 0, H_z). Substituting this value of A into the Hamiltonian above gives the time-independent Schrödinger equation

$$\hat{H} = \frac{1}{2m}\left(\hat{p}_x + \frac{eHy}{c} \right)^2 + \frac{\hat{p}_y}{2m} + \frac{\hat{p}_z}{2m} - \frac{\mu}{s}\hat{\mathbf{s}}_z H_z \tag{28}$$

As the coordinates x and z are missing from the Hamiltonian,

$\frac{\partial \hat{H}}{\partial x} = -\hat{p}_x = 0, \Rightarrow \hat{p}_x = \text{constant}$ and $\frac{\partial \hat{H}}{\partial z} = -\hat{p}_z = 0 \Rightarrow \hat{p}_z = \text{constant}$, it follows that they commute with the Hamiltonian, i.e.

$$\left[\hat{p}_x, \hat{H} \right] = \left[\hat{p}_z, \hat{H} \right] = 0 \tag{29}$$

Following from the commutation relations, we may conclude that $\hat{p}_x, \hat{p}_z$ and $\hat{H}$ have simultaneous eigenstates. The eigenstates of $\hat{p}_x$ and $\hat{p}_z$ appear as

$$\beta_{k_x k_z} = e^{i(k_x x + k_z z)} \tag{30}$$

So that we may write the common eigenstates of $\hat{p}_x, \hat{p}_z$ and $\hat{H}$ in the form

$$\varphi = e^{i(p_x x + p_z z)/\hbar} \phi(y). \tag{31}$$

also the operator $\hat{s}_z$ commutes with the Hamiltonian. Thus the z - component of the spin is conserved and can be replaced by its eigenvalue σ. Hence, the Schrödinger's equation for the ordinary coordinate function, may be written as

$$\frac{1}{2m}\left[\left(\hat{p}_x + \frac{eH}{c} y \right)^2 + \hat{p}_y^2 + \hat{p}_z^2 \right] \varphi - \frac{\mu}{s}\sigma H \varphi = E\varphi \tag{32}$$

From $mv_z = \hat{p}_z - \frac{e\mathrm{A}_z}{c}$ with $\mathrm{A}_z = 0 \Rightarrow \hat{p}_z = mv_z$ and a similar equation for $\mathrm{A}_y = 0$ giving $\hat{p}_y = mv_y$ thus the eigenevalues $\hat{p_x}$ and $\hat{p_z}$ takes all values from - ∞ to ∞.

Following from this, the motion along magnetic field in a 3-D system is not quantized. Equation (32) reduces to

$$\left[\hat{p}_y{}^2 + \frac{e^2\mathrm{H}^2}{2mc^2}\left(\frac{c\hbar k_x}{e\mathrm{H}} + y\right)^2\right]\phi(y) = \left(E - \hat{p}_z{}^2 + \frac{\mu\sigma}{s}\mathrm{H}\right)\phi(y) \qquad \text{or}$$

$$\left[\frac{\hat{p}_y{}^2}{2m} + \frac{\mathrm{K}}{2}(y - y_o)^2\right]\phi(y) = \left(E - \frac{\hbar^2 k_z{}^2}{2m} + \frac{\mu\sigma}{s}\mathrm{H}\right)\phi(y) \qquad (33)$$

where $y_o \equiv -\frac{c\,\hat{p}_x}{e\mathrm{H}} = -a_H^2 k_x$, $a_H = (c\hbar/eH)^{1/2}$ -

, $\frac{\mathrm{K}}{m} \equiv \left(\frac{e\mathrm{H}}{mc}\right)^2 \equiv \Omega^2$, $\omega_c = |e|H/mc$, $\hat{p}_x = \hbar k_x$ and $\hat{p}_z = \hbar k_z$.

The frequency Ω is called the cyclotron frequency. This is the frequency of rotation corresponding to the classical motion of a charged particle in a uniform magnetic field. The Schrödinger equation (33) is the same as that for a simple harmonic oscillator constrained to move along the y-axis about the point y_o with natural frequency Ω. From the analysis of the harmonic oscillator, the eigen energies of this equation are

$$E_n = \hbar\Omega\left(n + \frac{1}{2}\right) + \frac{\hbar^2 k_z{}^2}{2m} - \frac{\mu\sigma}{s}\mathrm{H}, \ \mathrm{n} = 0, 1, 2\ldots \qquad (34)$$

But for an electron, $\mu/s = -|e|\hbar/mc$ and so the energy spectrum becomes

$$E_n = \hbar\Omega\left(n + \frac{1}{2} + \sigma\right) + \frac{\hbar^2 k_z{}^2}{2m} \qquad (35)$$

The first term in equation (35) gives discrete levels which correspond to the finite motion in the xy-plane, called the Landau levels. It corresponds to rotational motion normal to the direction of the magnetic field in this instance directed along the positive z-axis. The separation between the allowed values being equal to $\hbar\Omega$. The kinetic energy term $\frac{\hbar^2 k_z^2}{2m}$ corresponds to free, linear motion parallel to the z-axis. In the corresponding motion, the electron trajectories will be a set of circles around the lines of field. The electrons perform these orbits at the cyclotron frequency $\Omega = eH/m$ and a constant z velocity. Classically, such motion is unaffected by a magnetic field in the z direction. The projection of the motion onto the xy-plane is shown in figure 11.

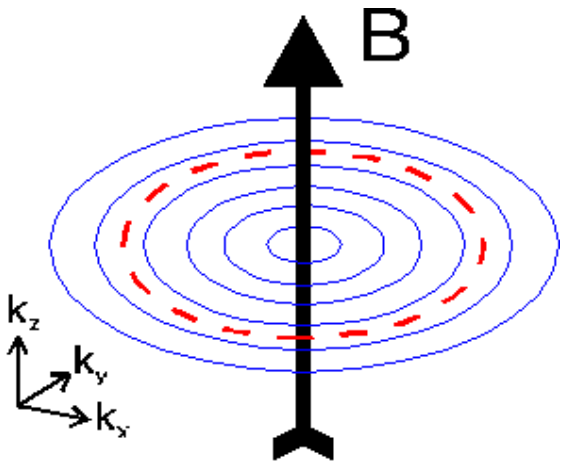

Fig 11: Magnetic quantization and Landau levels in a 2DEG

The eigenfuntion corresponding to the eigenenergy of equation (35) is

$$\phi_n(y) = \aleph_n H_n\left[\sqrt{\frac{m\Omega}{\hbar}}(y - y_o)\right] \exp\left[-\frac{1}{2}\sqrt{\frac{m\Omega}{\hbar}}(y - y_o)\right] \qquad (36)$$

where H_n is the nth-order Hermite polynomial and $\aleph_n$ is a normalization constant. Together with equation (25), this form for ϕ_n gives the wave function as

$$\varphi_n = \aleph_n H_n\left[\sqrt{\frac{m\Omega}{\hbar}}(y-y_o)\right]\exp\left[-\frac{1}{2}\sqrt{\frac{m\Omega}{\hbar}}(y-y_o)^2 + i(k_x x + k_z z)\right] \quad (37)$$

For a particle moving in a uniform magnetic field which is pointed in the z- direction. The other conserved quantity,

$$x_o = \frac{cp_y}{cH} + x \quad (38)$$

is the classical x coordinates of the center of the circle. It commutes with the Hamiltonian. However the operators $\hat{x}_o$ *and* $\hat{y}_o$ do not commute. This implies that the coordinates $\hat{x}_o$ *and* $\hat{y}_o$ cannot take definite values simultaneously. The coordinates *x* and *y* are not equivalent because the wave functions in equation (36) correspond to the energy independent of k_y. As a result, any function of the form $\sum_{k_x} C(k_x)\varphi_{N,k_x,k_z}$ corresponds to the same energy since one can chose convenient linear combinations to get a correct asymptotic behaviour.

Density of state in a magnetic field

In order to calculate the density of state in a magnetic field, we must first count the number of the values of k_y corresponding to the energy ε_α often called the degeneracy factor. As usual we apply cyclic boundary

conditions along y and z axis and obtain $k_y = \frac{2\pi}{L_y} n_{y,} \quad k_z = \frac{2\pi}{L_z} n_z$ at the same time, we assume that the solution exists only in the region $0 < y_o < L_y$.

So the degeneracy factor is

$$\frac{L_x}{2\pi}\left|k_x\right|^{\max} = \frac{L_x}{2\pi a_H{}^2} y_o^{\max} = \frac{L_y L_x}{2\pi a_H^2}$$

(39)

This is a very important relation which shows that one can imagine the Landau states as cells with area a_H^2. We may now calculate the number of states in a 2-D system treating the k_z as for the usual 1-D motion

$$\frac{2\left|k_z\right| L_z}{2\pi} = \frac{2\sqrt{2mL_x}}{2\pi\hbar}\sqrt{E - \hbar\omega_c\left(N + 1/2\right)} \tag{40}$$

for each state with a given N. Finally, the total number of states per unit volume for a given spin is

$$Z_s(E) = \sum_N Z_s N(E) = \frac{2\sqrt{2m}}{(2\pi)^2 \hbar a_H^2} \sum_N \sqrt{E - \hbar\omega_c\left(N + 1/2\right)} \tag{41}$$

where the sum is taken over all the values of N with non negative $E - \hbar\omega_c\left(N + 1/2\right)$. The total number of states is $Z(E) = 2Z\ (E)$.

To obtain DOS, we differentiate equation (41) with respect to E. The result is

$$g_s(E) = \frac{dZ(E)}{dE} = \frac{\sqrt{2m}}{(2\pi)^2 \hbar a_H^2} \sum_N \frac{\Theta\left[E - \hbar\omega_c\left(N + 1/2\right)\right]}{\sqrt{E - \hbar\omega_c\left(N + 1/2\right)}}. \tag{42}$$

where

$$\Theta(x) = \begin{Bmatrix} 1 & for & x > 0 \\ 1/2 & for & x = 0 \\ 0 & for & x < 0 \end{Bmatrix} \tag{43}$$

is the Heaviside step function. To take the spin into account, we add the spin splitting $\pm \mu_B g_f H$ to the energy levels. If we ignore the spin splitting, we can assume spin degeneracy and multiply all the formulas by the factor 2. Thus $g(E) = 2g(E)$.

The behaviour of the density of states could be interpreted qualitatively as follows. The landau levels as functions of magnetic field for a given value of p_z are shown in figure 12.

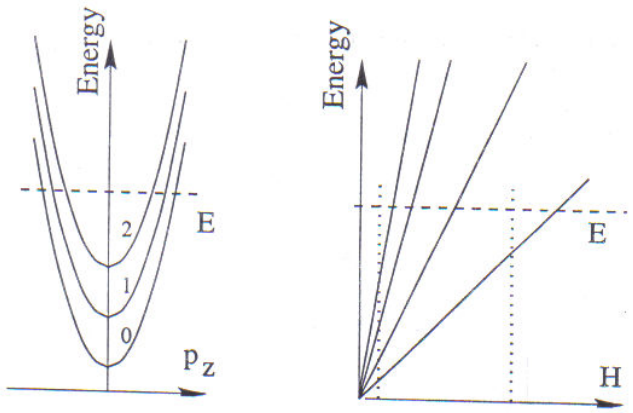

Fig 12: Landau levels as functions of p_z (left panel) and of H (right panel).

As a function of magnetic field they form the so called landau fan. The Fermi level is also shown. At low magnetic fields, its dependence on magnetic field is very weak. It is seen that if the magnetic field is small, many levels are filled. Suppose we start with some value of magnetic field and follow the upper filled level N, as the field increases. The slopes of the fan also increases and at a given threshold value H_N, for which

$$E_N(H_N) = \epsilon_F \tag{44}$$

, the electrons are transferred from the N-th Landau level to the other ones. Then for the field H_{N-1} which is determined from the equation $E_{N-1}(H_{N-1}) = \epsilon_F$, the (N-1)th level becomes empty. We obtain

$$H_N \approx \frac{m_c c}{e\hbar}\epsilon_F \frac{1}{N} \quad \text{so } \Delta\left(\frac{1}{H}\right) \approx \frac{e\hbar}{m_c c E_F} \tag{45}$$

Here m_c is the cyclotron effective mass which in the case of isotropic spectrum is the same as the density of states effective mass. We observe that DOS in a magnetic field oscillates with increasing energy just similar to the case of a quasi 1-D system. Here, the Landau subbands play the same role as the modes of transverse quantization for quantum channels. For a 2DEG, the motion along the z-direction is quantized, and instead of $e^{ip_z z/\hbar}$, we have $\chi_s(z)$. This means that for each subbands of spatial quantization, we have a sharp Landau level, the density of states (per unit area) being

$$g(E) = \frac{v_v eH}{4\pi^2\hbar^2 c}\sum_{n,s,\sigma}\delta\left(E - E_{n,s,\sigma}\right). \tag{46}$$

Thus the density of states has sharp maxima at the energy level that is a feature of zero-dimensional systems as shown in figure 13. In real samples, the peaks are smeared by disorder. In the presence of the magnetic field, the available states clump into Landau levels separated by the cyclotron energy with regions of energy between landau levels where there are no allowed states. As the magnetic field increases, the Landau levels move relative to the Fermi energy. When the Fermi energy lies in a gap between Landau levels, electrons cannot move to new states.

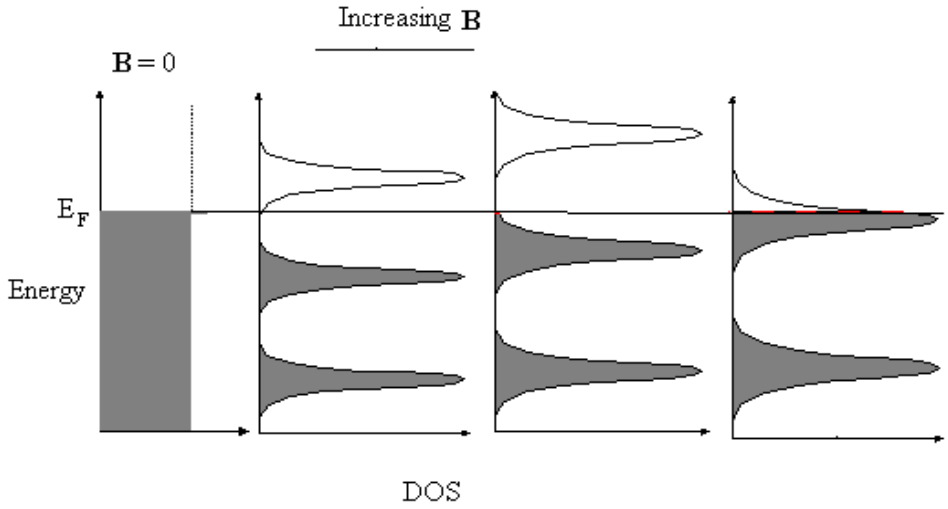

Figure 13: Energy versus DOS for a 2DEG in a magnetic field

Realization of a quantum dot from a 2DEG

In this section, we focus on two quantum dots (QD) structures that are commonly used in the study of single electron phenomena. One is the lateral quantum dot shown in figure 14a. Metal electrodes are patterned on the top and bottom surfaces of a two-dimensional electron gas (2DEG) heterostructure of GaAs\AlGaAs. These electrodes form a capacitor with the 2DEG in between them in order to control its density. If a positive or negative bias voltage is applied to the gate, the heterointerface region underneath it will be populated or depleted in the 2DEG respectively. A negative voltage applied to the gates raises the electrostatic potential and depletes the underlying 2DEG in the vicinity of the gates. In this way, electrons are confined to movement in only one direction forming a one-dimensional system or a quantum wire.

By restricting motion in the remaining direction with an additional gate electrode, a small region of 2DEG remains at the center of the structure,

separated from the rest of the 2DEG by two narrow constrictions. As the dimensions of the structure approach the electron de-Broglie wavelength, the resultant island of trapped electrons form a quasi-zero dimensional structure called a quantum dot [36-38]. When the electrostatic potential of the constriction is higher than the Fermi energy of the 2DEG, there arises an energy barrier under which electrons can tunnel.

The other structure is obtained in the vertical quantum dot illustrated in figure 14b. A narrow pillar is fabricated in a heterostructure where a disk of

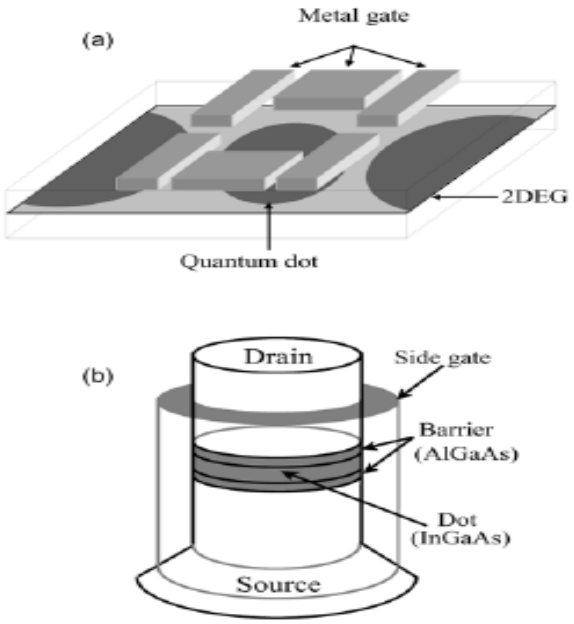

Fig 14: Schematic diagram of (a) a lateral and (b) a vertical quantum dots [36]

GaAs is sandwiched between two thin AlGaAs barriers. A negatively biased gate electrode surrounding the pillar depletes electrons in the outer region of the pillar and shrinks the quantum disk. Consequently, the electrons are confined at a very narrow region in the center of the pillar. Current flowing through the pillar is measured between the source and drain electrodes on the

top and bottom of the pillar. The lateral confining potential has a circular symmetry approximated by a two-dimensional parabolic potential. This allows us to observe a shell structure having highly degenerate levels.

Another type of vertical dot structure has been proposed by Ashoori et al [39,40]. In this case, the dot is located in the GaAs quantum well between AlGaAs barriers and its size is controlled by the top gate voltage as in the lateral quantum dot. Electrons tunnel vertically to the bottom electrode. The addition spectra are measured in a unique capacitance measurement by varying the gate voltage. Singlet-triplet transitions and Landau transitions have been observed in these kinds of structures [40].

Synthesis of quantum dots

The general technique for producing nanostructures (quantum dots) fall under two major categories;

Firstly, Top- down manufacturing where the approach involves starting with a large piece of material and etching, milling or machining a nanostructure from it by removing material from it as in fabrication of electronic chips. Another approach is to break up solids into nanoparticles using grinding or ballmilling.

Secondly, there is bottom-up manufacturing which involves the building of a structure, atom-by-atom or molecule-by-molecule through chemical synthesis, self or positional assembly.

There are three methods of synthesizing quantum dots; these are Lithography, colloidal chemistry and epitaxy.

Lithography is the process of producing patterns on semiconductor crystals [36]. This process is slow and has high instances of contamination and deformation. Epitaxy involves the growth of quantum dots on patterned substrates [41]. A disadvantage of this method is that the amount of producible quantum dot is limited by masked patterns. Quantum dots fabricated using colloidal chemistry methods [42] are typically composed of elements in the II and VI group of the periodic table (i.e. cadmium sulfide CdS, and cadmium selenide CdSe).

Colloidal quantum dots

The common approach to the synthesis of colloidal quantum dots is the controlled nucleation and growth of particles in a solution of chemical precursors containing the metal and the anion sources (controlled arrested precipitation) [43-45]. The technique of forming mono dispersed is very old and can be traced back to the synthesis of gold colloids by Michael Faraday in 1857 [43, 44]. A common method for II-VI colloids quantum dot formation is to rapidly inject a solution of chemical reagents containing the group II and group VI into hot and vigorously stirred solvent containing molecules that can coordinate with the surface of the precipitated quantum particles [44-46]. A large number of nucleation centers are initially formed and the coordinating ligands in the hot solvent prevent or limit particle growth via the normal process of Oswald ripening (i.e. the growth of smaller particles at the expense of larger particles).

Further improvement of the size distribution of the quantum dots particles can be achieved through size-selective precipitation whereby slow

addition of non-solvent to the colloidal solution of particles causes precipitation of large particles (the solubility of molecules with the same type of chemical structure decreases with increasing size). This process can be repeated several times to narrow the size distribution of II-VI colloidal quantum dots to a few percent of the mean diameter.

The synthesis of III-V colloidal quantum dot is more difficult than II-VI. This is because the synthesis must be conducted in a rigorously air-free and water-free atmosphere. It also requires higher reaction temperatures and much longer reaction times and it involves more complicated organo-metallic chemistry.

For example in the synthesis of InP quantum dots [47-51], an Indium salt, [$In(C_2O_4)_3$, InF_3 or $InCl_3$] is reacted with trimethylsilylphosphine [$P(Si(CH_3)_3)_3$] in a solution of trioctylphosphine Oxide (TOPO) and Trioctylphosphine (TOP) to form a soluble InP organometallic precursor species that contains In and P in a 1:1 ratio. The InP precursor species in the TOPO/TOP solution is then heated for several days at a temperature ranging from 270 to 290^{o}C depending on the desired properties. One difference between the synthesis of II-VI material and III-VI material is that more than one day of heating at the reaction temperature is required to form crystalline III-V quantum dots whereas II-VI quantum dots form immediately on injection of the reactants into the hot TOPO -TOP solution.

The resulting InP quantum dot contains a capping layer of TOPO, which can be readily exchanged for several other capping agents, such as thiols, ptridines, amines and polymers. The size distribution of the InP quantum dots can be further narrowed down to less than 10% through

selective precipitation techniques. Finally they can be synthesized in the form of colloidal solutions, powders or dispersed in transparent polymers or organic glasses (for low temperature studies). Capped InP quantum dots recovered as powders can also be redissolved to form transparent colloidal solutions.

In addition to InP quantum dots, similar methods have been used to produce III-VI quantum dots of GaP [47, 52], $GaInP_2$ [53] and InAs [54]; higher temperatures (400^oC) are required for GaP and $GaInP_2$ quantum dots. Spherical and cubical PbSe quantum dots obtained through colloidal synthesis are shown in figure 15.

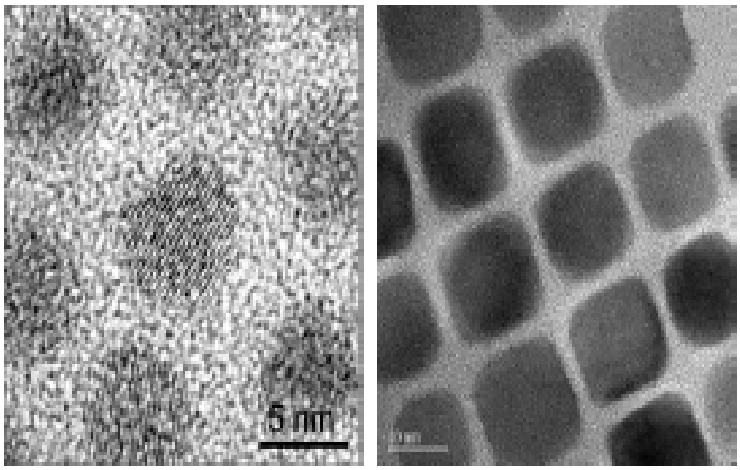

Fig 15: TEM of PbSe quantum dot spheres (5nm diameter) and Cube (10nm) [55].

Stranski-Krastanov epitaxial growth

Quantum dots can also be produced by epitaxial growth from the vapour phase on appropriate substrates; the growth can be effected using either MBE or MOCVD. In the Stanski-Krastanov (SK) mode of quantum dot formation, a thin semiconductor film is deposited by MBE or MOCVD onto

another semiconductor substrate material that has a mismatch in lattice constant with the material being deposited. If the lattice mismatch is sufficiently high, and the film has a higher surface energy than the substrate, after the initial growth of a few monolayers (called the wetting layer), subsequent deposition form small islands which are in the quantum dots regime. The size, shape, perfection and density of these SK quantum dots can be controlled by controlling the conditions in the MBE or MOCVD reaction. The bulk of work on these SK quantum dots has been on $InGa_XAs_{1-X}$ quantum dots grown on GsAs substrates [56]. InP quantum dots grown on GaAs as $Al_XGa_{1-X}As$ substrates has also been reported by Hanna et al, [57].

The SK quantum dots are generally larger than the colloidal quantum dots. They typically have a lateral dimension of 1000-2000Å and a height of 100-500Å. For III-V semiconductors, these sizes produce quantization effects because their Bohr radius is large but their degree of quantization is not as strong as that in colloidal quantum dots where the sizes ranges from 15Å to 100Å. The shape of the InAs/GaAs SK quantum dots has been reported to be a square based pyramid [58]. However, other results suggest a parallelogram base and C_{2V} symmetry [59, 60]. Another configuration of SK type quantum dots is possible. In this case a quantum well which has a thin outer barrier (about 100Å) is first formed. SK islands of another semiconductor material having a lattice mismatch with the barrier are then deposited on top of the barrier into the quantum well.

In the case of InP, SK islands (called stressor islands) formed on an AlGaAs/GaAs/AiGaAs quantum well, the strain field expands the GaAs and reduces the GaAs quantum well beneath the InP islands [61]. Thus the GaAs

quantum well beneath the InP stressor island is converted into a quantum dot since the one-dimensional confinement of carriers is transformed into 3-dimensional confinement. An important feature of this type of quantum dot is that both the well and barrier region of the quantum dot are made of the same material. This eliminates interface defects and interface states that complicates the relaxation behaviour of the photogenerated carriers.

Basic properties of quantum dots

In this section, the theoretical background of the basic properties of quantum dots which includes quantization of energy levels and density of states are discussed.

Quantization of energy in quantum dots

As stated previously the confinement of electrons in all three spatial directions in 2DEG produces a quantum dot. According to de Broglie, a particle can also be treated as a wave with a wavelength inversely proportional to the absolute value of the particle's linear momentum,

$$\lambda = \frac{h}{p} \tag{47}$$

The absolute value of the momentum is given by the product of the particle's mass and its velocity. Using the definition of the mean thermal velocity of free carriers, one arrive at the following equation;

$$p = m \cdot \langle v \rangle = m \cdot \sqrt{\frac{3kT}{m}} = \sqrt{3kTm} \tag{48}$$

In a semiconductor crystal, the mass of the free carriers needs to be replaced by the effective mass m of the carrier in the material. The de Broglie wavelength is thus

$$\lambda = \frac{h}{\sqrt{3kTm}} \tag{49}$$

For electrons in InAs, the effective mass is $m = 0.026m_o$ [60], where m_o is the free electron mass. The de Broglie wavelength of electrons in InAs at room temperature is therefore $\lambda =$ 39nm. It can therefore be expected that quantization effects become apparent for structures of a few tens of nanometers. The carrier wave functions (as solutions to the Schrödinger equation in the periodic potential lattice) are therefore localized in space and the corresponding energy eigenvalues are no longer quasi continuous but discrete.

Density of states in quantum dots

In quantum dots, the values of k are quantized in all directions. All the available states exist only at discrete energies and can be desribed by a delta function. This is illustrated in Fig.16 together with the DOS for bulk semiconductor for comparison. Quantum dots are therefore referred to as artificial atoms since the atomic levels are also discrete.

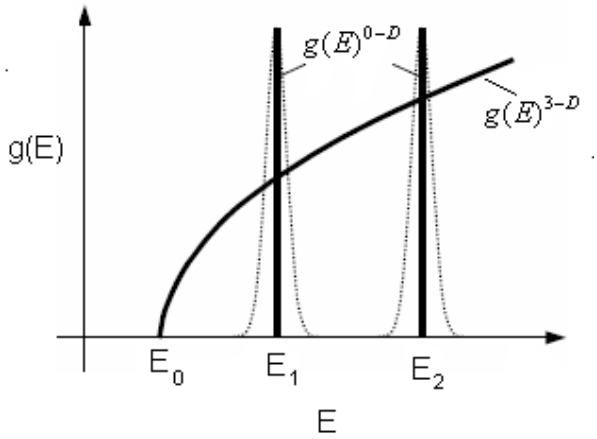

Fig 16: DOS versus energy for a 3-D and 0-D structure (QD) [62].

In real structures, homogenous and inhomogeneous broadening results in a narrow distribution of energy at each level. The homogenous level broadening is a result of the finite carrier lifetime, carrier-phonon [62] and carrier-carrier interaction [63]. Inhomogeneous broadening , shown as dashed lines on the other hand, arises from the superposition of many transitions in a quantum dot ensemble. Differences in environment (strain), size and composition, lead to slightly different energy levels for the individual quantum dots [64, 65].

Electronic structure of quantum dots

Atoms are studied by adding, removing or exciting electrons with light and quantum mechanical considerations show that the confinement of electrons in an atom coupled with the three-dimensional (3-D) spherically symmetric potential around them yields discrete quantized energy levels with degeneracies known as shells, 1s, 2s, 3s, 3p,. Each shell can hold a specific number of electrons. The electronic configuration is particularly stable when

these shells are completely filled with electrons, occurring at 'magic' atomic numbers 2, 8, 18, 32.

However, the energy levels of the confined electrons in quantum dot can be measured by several ways including the spectroscopy of single-electron tunneling which exploits the sequential tunneling of electrons via the localized quantum dot states. In this process the electrons tunnel one-by-one from one lead attached to the quantum dot and the next depending on the voltage drop in the dot and the presence of either the blocking or tunnel barrier and can either jump back to the same lead or tunnel further to the other lead.

The results show that the confinement of electrons and the symmetry of a two-dimensional disk-shaped quantum dot lead to discrete energy levels with a shell structure having magic numbers 2, 6, 12, 20.... Thus, the lower degree of symmetry in 2-D results in a different sequence of magic numbers from the case of the 3-D. By measuring electron transport through quantum dots, a periodic table of artificial 2-D elements has been obtained.

Theory and measurement techniques with the SET

Figure 17a shows a schematic diagram of a single electron transistor (SET) based on GaAs (semiconducting) and AlGaAs (insulating) and figure 17b, an electronmicrograph of the top surface of the SET used in the experiments of Goldhaber-Gordon et al [66,67]. The active region of the transistor is a 2DEG at the interface of GaAs/AlGaAs which is connected through two strong tunnel barriers due to the constriction in the top gate, to the source and drain. One can tune the density of the 2DEG. The set-up makes it possible to measure the conductance or the current flow through the dot. When

a positive voltage is applied to the bottom gate, more and more electrons accumulate in the dot. By application of a negative voltage to the top gate, electrons are repelled from under the lithographically patterned top metal electrodes, thus tuning the height of the barrier.

The small lake of electrons in the middle form the quantum dot, their confinement in the plane can be approximated as parabolic. Excitations in this plane have energies about a few meV, hence the experiment require very low temperatures. The Fermi level of the lake can be tuned by the bottom gate voltage. When the voltage on this gate is increased, the potential minimum in which the electrons are trapped become deeper. This causes the number of

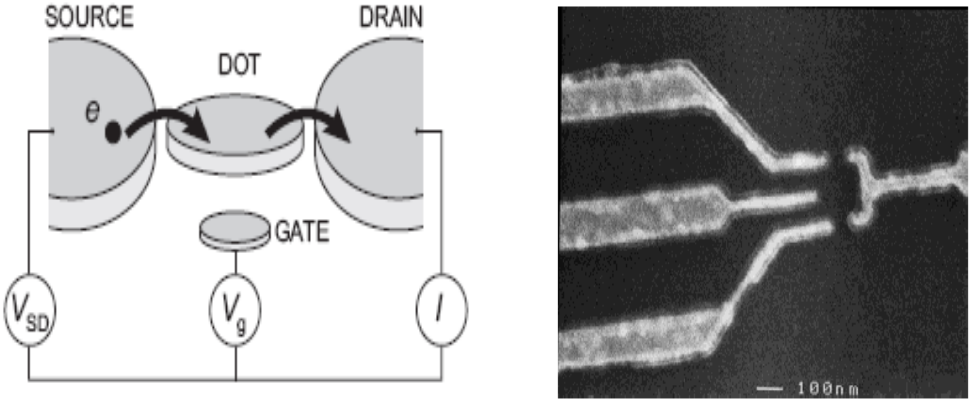

(a) (b)

Fig 17: (a) Schematic diagram of a Single-electron transistor (vertical quantum dot) and (b) electronmicrograph of the top surface of the SET [67].

trapped electrons to increase. However, unlike a conventional transistor in which the charge increase continuously, the charge in the trap increases in discrete steps and this is reflected in the conductance between the source and

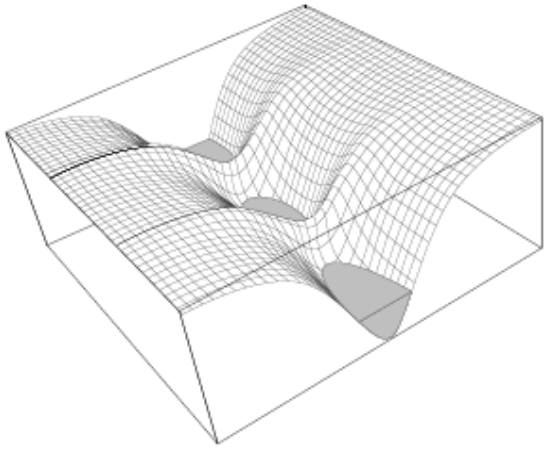

Fig 18: Potential landscape of the 2-D electrons in the SET [68].

Experimental results of Single-electron tunneling in vertical quantum Dots

The results obtained by the single-electron transistor for the three terminal quantum dot are presented in figures 19, 20, 21 and 22.

In figure 17a, a small biased voltage V_{sd} is applied between the source and drain and the current is measured as a function of the gate voltage V_g which is tuned in step, the results illustrated in figure 19. It shows the source-drain current as a function of the gate voltage for a quantum dot of diameter 0.5μm measured at a very small bias voltage $V_{sd} = 150\,\mu V$ and at a very low temperature ($T = 50mK$). A conventional transistor turns on only ones, when the gate voltage is raised. Here, nearly periodic peaks in the current are observed when the bottom gate voltage is increased. Also the current peaks are observed to occur at specific gate voltages. The name 'single-electron transistor' is due to the fact that the transistor turns on and off again every time a single electron is added to it.

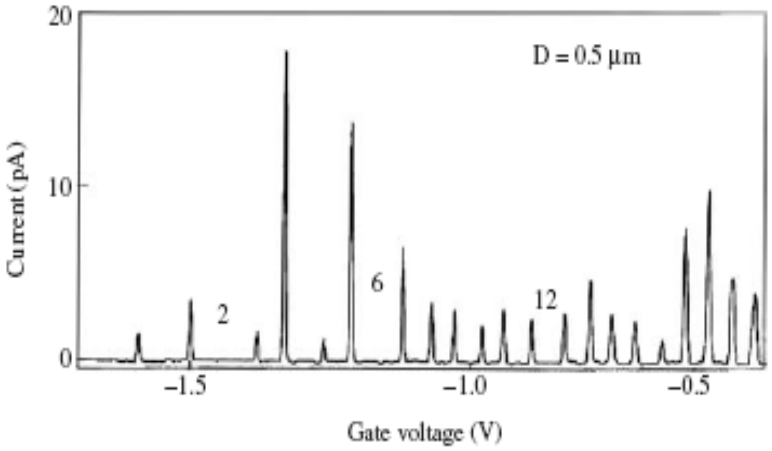

Fig 19: Source-drain current versus gate voltage at $V_{sd} = 150\mu V$ [69].

Each current peak results from many sequential single-electron tunneling processes. The time interval between the tunneling events was estimated to vary from 1ns to 100ns. For $V_g < -1.6V$, the quantum dot is empty. The first peak at $V_g \approx -1.6V$, corresponds to the tunneling of the first electron via the quantum dot. The relative distances between the peaks correspond to the filling of the subsequent shells of the artificial atom. The positions of the peaks are explained as follows: the large separations between the 2^{nd} and 3^{rd} peaks, the 6^{th} and 7^{th} peaks, the 12^{th} and 13^{th} peaks correspond to the complete filling of the first, second and third shells respectively. The slightly larger separation between the 4^{th} and 5^{th}, the 9^{th} and 10^{th} peaks results from the filling of the subsequent subshells according to Hund's rule.

The intervals of the gate voltage correspond to zero source-drain current, due to Coulomb blockade [69]. Then the electrons confined in the quantum dot prevent the flow of subsequent electrons.

If the source-drain voltage (V_{sd}) is tuned or increased, transport is also allowed in the excited states of the quantum dot. A plot of the conductance or differential current $\partial I/\partial V_{sd}$ on the gate voltage- source drain voltage (V_g-V_{sd}) plane is shown in figure 20 called the stability diagram [70]. In the white diamond shaped regions, $\partial I/\partial V_{sd}$ = 0 due to the coulomb blockade.

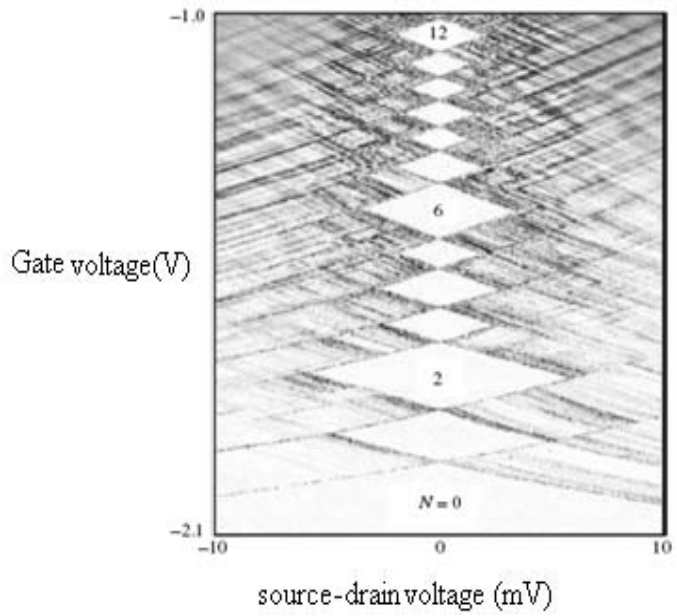

Fig 20: Differential conductance $\partial I/\partial V_{sd}$ plotted on the $V_g - V_{sd}$ plane at B = 0 [69, 70].

The number (N) of the quantum dot's confined electrons is fixed in each of the diamonds.

The application of an external magnetic field essentially modifies the electronic states in the quantum dot [40, 70, 71] and the accompanying evolution of the single-electron tunneling peaks was observed by Kouwenhoven et al [70]. A plot of the current peaks as a function of the gate

voltage and magnetic field plane at biased source and drain voltage V_{sd} = 0.1mV is shown in figure 21. The measurement show that, the ground state energy of the quantum dot-confined electron system undergoes symmetry transformation and the usual current (coulomb) oscillations broaden into current stripes.

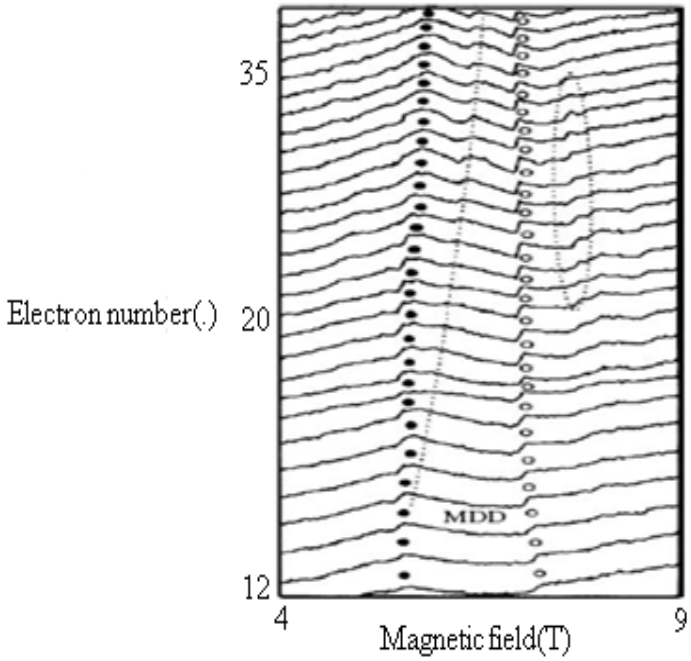

Fig 21: Source-drain current peaks as a function of gate voltage and magnetic field at V_{sd} = 0.1mV [69].

Then the N-electron ground state and the excited state electrochemical potentials within an energy window e V_{sd}, appear as kinks or peaks shown in figure 21.

The single-electron tunneling peaks at high magnetic field were measured by Oosterkamp et al [71]. If the magnetic-field is sufficiently strong, the N electron system becomes fully spin polarized and the electrons occupy the orbitals with the subsequent angular momenta. This state is called

maximum-density-droplet (MDD) [72]. If the magnetic field increases further, the MDD decays and a Wiegner molecule is formed [73] in which the electrons are localized at different spatial sites with an island-like electron density distribution. The formation and decay of the MDD are shown in figure 21 as abrupt steps marked by full and open circles.

The corresponding spin configurations shown by the arrows in the squares represent electrons arranged in the symmetric and anti symmetric set of the Fock-Darwin orbitals are shown in figure 22.

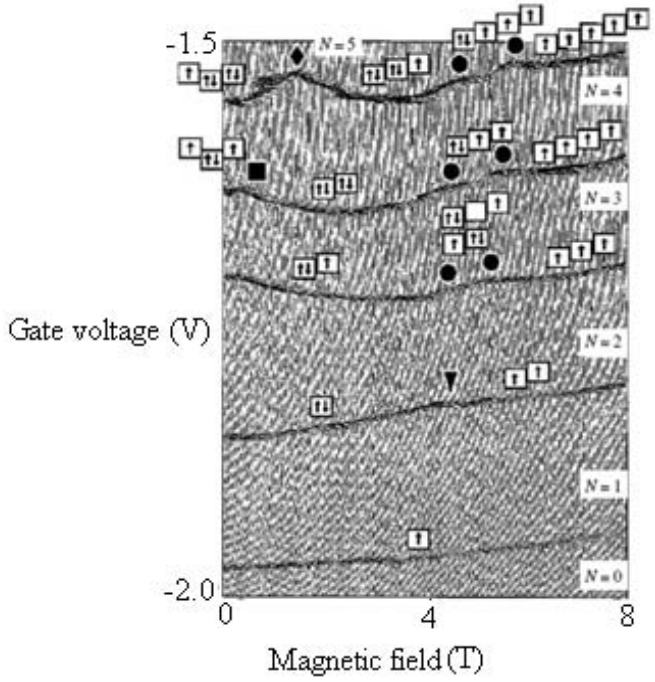

Fig 22: Gate voltage corresponding to the current peaks at V_{sd} = 100μV versus magnetic field for different numbers of electrons [71].

In the Weigner molecule regime, the additional steps were observed (dotted ovals in figure 22). The authors [71] argue that at all these steps, the electron charge distribution changes abruptly. The different symbols indicate the ground state transitions.

Theory of the single-electron tunneling

The phenomenon of the periodic conductance peaks observed in the experimental results may be explained by several models notably; the Coulomb blockade model and the constant interaction model.

The Coulomb Blockade model

The classical model of the Coulomb blockade is based on charge quantization. According to this model [4], a charging energy is required to add an extra electron to the dot. The gate voltage tunes the energy levels of the dot and as this energy reaches the Coulomb charging energy, an electron can enter the dot. When an energy level in the dot becomes aligned within the transport window eV_{sd}, which is determined by the electrochemical potentials of the source and drain, a current can pass through the dot. As the gate voltage is increased, the level moves out of the transport window as shown in figure 23 and no electron can tunnel inside or outside the dot resulting in no current (Coulomb blockade region). The current is zero until another electron is drawn into the dot.

This model leads to equally spaced tunneling current peaks which are observed in large quantum dots, called Coulomb oscillations. In the nanoscale regime, quantum effects appear, that is the energy levels of the electrons confined in the quantum dot are discrete but are not equally spaced. Therefore, the charging energies are different for different numbers of electrons and the single-electron peaks exhibit unequal spacing [74] as illustrated in figure 19. This is the manifestation of the quantum nature of the Coulomb blockade [75].

If one considers a quantum dot as a classical conductor having capacitance C, which depends on the dot's dimensions and the geometry with respect to the leads, the charging energy needed to add one electron to it is expressed as $U = e^2/2C$. At low temperatures, the charging energy can be

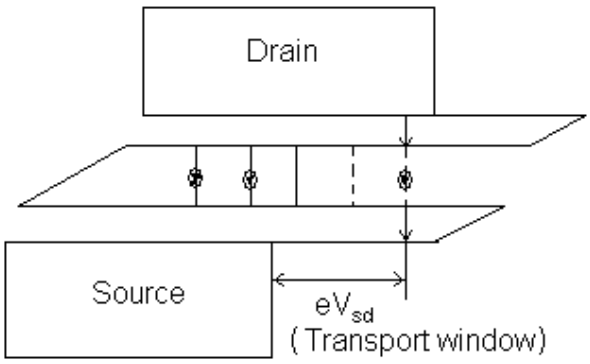

Fig 23: A schematic diagram of the transport window through the dot.

larger than the thermal energy $k_B T$ of the dot i.e. ($k_B T \leq \frac{e^2}{2C}$) and if the dot is very well isolated by the tunnel barriers, then the number of electrons N on it does not fluctuate and is a very well defined integer. This number changes when electrons tunnel to and from the dot. However, due to Coulomb repulsion between electrons, the energy of a dot containing N+1 electron is larger than when it contains N electrons. Extra energy is therefore needed to add an electron to the dot. Consequently, no current can flow, a phenomenon known as Coulomb blockade.

In order to transfer a charge Q from the source to the dot, the energy of the dot when it contains N and N+1 electron must be degenerate. Under biased conditions, the total energy E, of the dot can be written semi classically as

$$E = U + \Delta E \qquad (50)$$

where ΔE is particle in-a-box level spacing or the quantum mechanical energy levels of the dot. But for the lateral quantum dot in figure 17a, the level spectrum can be shifted by the bottom gate V_g. Hence , the energy E of the dot becomes

$$E = \frac{Q^2}{2C} + QV_g . \tag{51}$$

The first term in equation (51) is the charging energy due to the repulsion of the electrons on the dot. The second term is the electrostatic interaction between the dot and the positive underlying gate voltage which tunes the energy levels [66]. The graph of this function (a plot of E against Q) is a parabola with a minimum ($\frac{dE}{dQ} = 0$) at $Q = Q_m = - CV_g$. Hence, the charge transferred can be tuned by the gate voltage V_g. By varying V_g, any value of Q_m, the charge that minimizes the energy, can be chosen arbitrally, were not the charge quantized. However, because real charge is quantized, i.e. $Q_m = -Ne$, the dot's energy as a function of the number of electrons E(N), and the positive gate voltage V_g can only assume discrete or specific values.

Since the charges are transferred by the electrons with a charge - e, then the energy as a function of the number N of electrons on the dot is

$$E(N) = -N eV_g + \frac{N^2 e^2}{2C} \tag{52}$$

Now the energy difference when the dot contains N and N+1 electrons is given by

$$E(N+1) - E(N) = -eV_g + N\frac{e^2}{C} . \tag{53}$$

Since charge is transferred only when $E(N+1)$ and $E(N)$ are degenerate, the difference in energy must be zero which corresponds to certain values of V_g, such that

$$V_{g_N} = N\frac{e}{C}\ , \tag{54}$$

This can also be visualized in figure 24 where if the gate voltage V_g is adjusted such that when Q_m = - Ne, for which an integral number (N) of electrons minimizes the energy, the coulomb interaction results in the same energy difference U = $e^2/2C$ for increasing or decreasing (N) by one.

Thus there is an energy gap that suppresses charge fluctuation. Also, for all values Q_m , there is a small but non-zero energy gap for adding or subtracting an electron from the dot thus leading to no current. Only when the

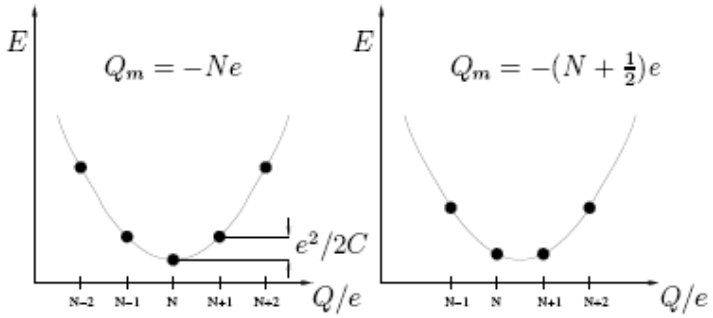

Fig 24: Energy versus charge on a semi classical dot. Left; $Q_m = -Ne$ and Right: $Q_m = -(N+\frac{1}{2})e$ [68].

gate voltage is adjusted such that $Q_m = -(N+\frac{1}{2})e$, the state with N and N+ 1 electrons are degenerate and the energy gap disappears. Under this condition, an electron then tunnels from the source to the dot increasing the number of electrons on it to N+1 and then subsequently tunnels out to the drain, reducing

the electron number to N again and the charge fluctuation results in the nearly periodic equidistant conductance peaks even at zero temperature only when the average charge on the artificial atom is $Q_m = -(N + \frac{1}{2})e$.

Thus the approximately equally spaced peaks in the conductance of the SET is due to charge quantization. This assertion seems to contradict the age long charge quantization concept since the discovery of the electron. However, since the wave function of electrons in conductors is extended over macroscopic distances, the charge in any small volume is not quantized. It is the localization of electrons to a small region of space that quantizes the charge. In this case, the degree of localization depends on the transmission of the tunnel barriers whose resistance R must be such that the RC time constant for an electron to tunnel off the dot into the leads be great enough that energy uncertainty is less than the charging energy.

This is achieved by RC > h/U or approximately, R > h/e^2 which is the fundamental unit of resistance that enters for instance in the quantum hall effect. Thus while the calculation of the charging energy is completely classical, Planck's constant determines whether the charge energy is present or not. This condition is valid at T = 0K, independent of C and therefore of the size of the dot. Notably, thermal charge fluctuation can overcome this localization, so charge fluctuation is observed only at kT < U, implying that this effect is observed in smaller quantum dots which have larger U.

Apart from the charge quantization, energy quantization is important when electrons are confined to small volumes. However, the criterion for charge and energy quantization are the same at T = 0K. Whereas U is the charging energy, there is a typical energy spacing ΔE necessary to excite the

artificial atom with fixed number of electrons. Also the levels of the dot are not perfectly sharp but rather have typical width caused by the life-time broadening because an electron in a level can tunnel into the leads. Alternatively, one can say that the eigen states of the system are mixtures of localized states on the dot and extended states in the leads. But energy quantization means that $\Delta E > \Gamma$, where Γ is the band width.

According to Thoules [76], the current through the SET for a single quantum level is the charge of the electron divided by the time t for an electron in a single state to traverse the dot while in that level. If dN/dE is the density of states in the dot, then $(dN/dE)eV_{sd}$ is the number of current-carrying channels between the Fermi energy in the source and that in the drain. Thus the current is $I = \frac{e}{t}(dN/dE)eV_{sd}$. The width gives the traversal time $t = h/\Gamma$ and $(dN/dE) = 1/\Delta E$, so that the condition for energy quantization is $R = V_{sd}/I > h/e^2$, the same as charge quantization. But while the condition for charge and energy quantization at T = 0K are the same, charge quantization often survives to higher temperatures and can be observed when $kT < U$, but energy quantization requires $kT < \Delta E$. Since $U > \Delta E$ for most SET's, made to date, energy quantization is more difficult to observe than charge quantization.

Energy quantization can be observed by measuring the variations between the peak positions from figure 19 while the energy level spectrum can be measured directly by observing the tunneling current at fixed V_g as a function of V_{sd}. The resonant transfer occurs only at specific gate voltages. Between the peaks, the current is zero and N remains constant. The distance

between consecutive peaks is proportional to the so-called addition energy, which is the difference in energy between dots with N+1 and N electrons. As a result of the Coulomb blockade [77- 80] electrons tunnel one-by-one and the conductance vs. gate dependence is a set of sharp peaks.

The constant interaction model (CI)

The constant interaction model [79,81] makes two important assumptions. First, the coulomb interactions among electrons in the dot, and between electrons in the dot and those in its environment, are parameterized by a single capacitance C. This capacitance can be thought of as the sum of the capacitances between the dot and the source C_S , the drain C_D and the gate C_g . Therefore $C = C_S + C_D + C_g$

Second, the discrete energy spectrum can be described independently of the number of electrons on the dot. Under these assumptions, the total energy of an N-electron dot in the ground state with the source and drain voltage $V_{sd,}$ applied to the source (with the drain grounded), is given by

$$E(N) = \left[\frac{-|e|(N - N_o) + C_S V_{sd} + C_g V_g}{\sqrt{2C}} \right]^2 + \sum_{n=1}^{N} E_n(B) \qquad (55)$$

where $-|e|$ is the electron charge, and N_o is the number of electrons on the dot at zero gate voltage, which compensates the positive background charge originating from the donors in the heterostructure. The terms $C_S V_{sd}$ and $C_g V_g$ can change continuously and represent the charge on the dot induced by the bias voltage (through the capacitance C_S) and by the gate voltage V_g (through the capacitance C_g) respectively. The last term in equation (55) is a sum over the occupied single-particle energy levels $E_n(B)$ which are

separated by energy $\Delta E_n = E_n - E_{n-1}$. These energy levels depend on the characteristics of the confinement potential. Notably, within the constant interaction model, only the single-particle states depend on magnetic field *B*.

To describe these transport experiments, it is often more convenient to use the electrochemical potential. The electrochemical potential of the electrons in the dot is defined as the energy required to add the nth electron to the dot

$$\mu(N) = E_N - E_{N-1} = (N - N_o - \tfrac{1}{2})U - \frac{U}{|e|}(C_S V_{sd} + C_g V_g) + E_n \qquad (56)$$

where $U = e^2/2C$ is the charging energy and E_n is the ground-state energies of the N-electron system confined in the dot. The expression denotes the transition between the N- electron ground state and N-1 ground-state. The electrochemical potential for the transitions between ground-states with a different number is shown in figure 25. The discrete levels are spaced by the so called addition energy.

$$E_{add}(N) = \mu(N+1) - \mu(N) = U + \Delta E = \alpha\left[V_g(N+1) - V_g(N)\right] \qquad (57)$$

Again, the addition energy consists of purely electrostatic part i.e. the charging energy U, plus the energy spacing between two discrete quantum levels, ΔE.

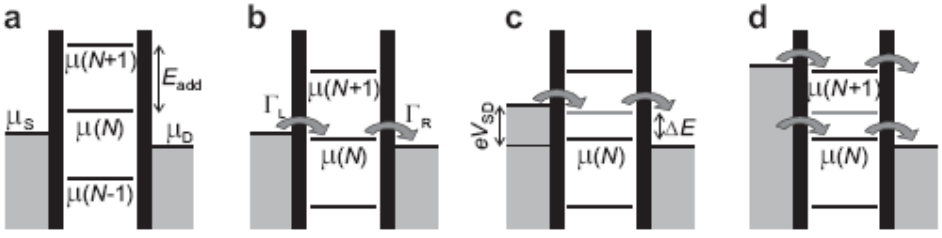

Fig 25: Schematic diagrams of the electrochemical potential of the quantum dot for different electron numbers [79].

The level spacing ΔE can be zero when two consecutive electrons are added to the same spin-degenerate level. The addition energy is related to the gate voltage simply by a dimensionless factor α which depends on the geometry of the dot. Equation (57) is the link between the gate voltages measured in the experiment and the ground-state energy.

For the metal electrodes at zero temperature and zero voltage, the chemical potential is identified with the Fermi energy as

$$\mu_\alpha = F_\alpha = \mu_\alpha^o - eV_\alpha \tag{58}$$

where μ_α^o is the chemical potential of the electrons in electrode α and V_α is the voltage applied to electrode α. For transport to occur, energy conservation needs to be satisfied. This is the case when an electrochemical level of the dot falls within the bias window between the electrochemical potential (Fermi energy), of the source (μ_S) and the drain (μ_D) i.e.

$$\mu_D \le \mu \le \mu_S \tag{59}$$

with the bias window

$$-|e|V_{sd} = \mu_D - \mu_S . \tag{60}$$

It is only when the condition in equation (59) is met, that an electron tunnels from the source onto the dot and then tunnels off to the drain without loosing energy. By reversing the bias voltage, the inequality sign in the condition in equation (59) is reversed and the electron tunnels from the drain to the source. Hence, the notion of source and drain is a matter of convention. The important point to realize is that since the dot is small, it has a very small capacitance and therefore a large charging energy. For a typical

dot, $U = e^2/2C \approx$ a few meV. If the electrochemical potential levels are as shown in figure 25a, this energy is not available at low temperatures and small bias voltage. So the number of electrons on the dot remains fixed and no current can flow through the dot. This is the phenomenon resembling coulomb blockade.

The coulomb blockade can be lifted by changing the voltage applied to the gate electrode. This changes the electrostatic potential of the dot with respect to the reservoirs, shifting the whole ladder of electrochemical potential levels up or down. When a level falls within the bias window, the current through the dot is switched on. In figure 25(b), $\mu(N)$ is aligned, so the electron number alternates between N-1 and N. This means that the nth electron can tunnel onto the dot from the source, but only after it tunnels off to the drain can another electron come onto the dot again from the source. This cycle is known as single electron tunneling.

At the positions of the peaks, an electrochemical potential level is aligned with the source and drain and a single-electron tunneling current flows. In the valleys between the peaks, the number of electrons on the dot is fixed due to Coulomb blockade. By tuning the gate voltage from one value to the next one, the number of electrons on the dot can be precisely controlled. The distance between the peaks corresponds to $U + \Delta E$ and can therefore give information about the energy spectrum of the dot.

A second way to lift the Coulomb blockade is by changing the source – drain voltage V_{sd}, as in figure 25(c). In general, we change the electrochemical potential of only one of the reservoirs, keeping the other one fixed. This increases the bias window and also drags the electrochemical potential level of

the dot along due to the capacitative coupling to the source. Suppose V_g is adjusted so that Q_m = - Ne and V_{sd} is increased. Current can flow only when an electrochemical potential of the dot falls within the bias window.

When V_{sd} is increased so much that both the ground state as well as an excited transition state fall within the bias window, there would be two channels available for electron tunneling through the dot and the current increases. For larger V_{sd}'s than the level spacing (ΔE), the current increases each time a new quantum state comes in the bias window set by the V_{sd}. But for small V_{sd}'s, the current always flow through one state. Measurements with different source-drain voltages V_{sd} as a function of the gate voltage, is displayed in figure 20

In general, the alignment of nth the ground state and an excited transition state in the transport window lead to a change in the current enabling us to perform energy spectroscopy of the excited states. The exact changes in the current depend on the tunneling rates of the two paths [82]. Usually, we measure the current or differential conductance (the derivative of the current with respect to the source-drain bias) while keeping the bias voltage, for series of different values of the gate voltage. Such measurements are plotted on a graph as shown in figure 20. Inside the diamond shaped region, the number of electrons is fixed due to Coulomb blockade, and no current flows. Outside the diamonds, Coulomb blockade is lifted and single-electron tunneling can take place (or for large bias voltages, even double electron-tunneling is possible) as shown in figure 25(d). Excited states are revealed as changes in the current i.e. as peaks or dips in the differential

conductance. For such Coulomb diamonds, the excited states as well as the charging energy can be read off directly as displayed in figure 20.

The simple model described above, explains successfully how quantization of charge and energy leads to effects like coulomb blockade and Coulomb oscillations. Nevertheless, it is too simplified in many respects. For instance the model considers only first-order tunneling processes in which an electron tunnels first from one reservoir onto the dot and then from the dot to the other reservoir. But when the tunnel rate between the dot and the leads, Γ is increased, higher- order tunneling via virtual intermediate states become important. Such processes are known as cotunneling. Furthermore, the simple model does not take into account the spin of the electrons, thereby excluding, for instance, exchange effects. Thus one can overcome the charging energy by changing either the source-drain voltage or the gate voltage. The magic numbers can be identified because significantly higher gate voltages are needed to add the 2nd, 6th and 12th electron. Quantum dots are therefore 2-D analogies for real atoms and are therefore referred to as 'Artificial atoms' [83].

So far, three different energy scales have been identified with the study of the SETs i.e. U, ΔE and Γ which are respectively the energy needed to add an electron to the dot, the energy to excite the dot with a fixed number of electrons and the broadening of the dot's energy levels by quantum mechanical tunneling to the leads. A last energy scale other than the three mentioned previously is the Kondo 'bond'. The tunneling results in a kind of chemical bond between the dot and the leads when the dot has a spin which is the origin of Kondo effect. This Kondo bond is very weak and could not be

observed for nearly a decade after its prediction by theorists but it is now a subject of intense research [66, 67, 84-86]

Electrostatic energy of a single quantum dot

The charge conservation requires that

$$-ne = Q_e + Q_c + Q_g$$

$$= C_e(V_e - U) + C_c(V_c - U) + C_g(V_g - U) \tag{61}$$

where U is the potential of the dot. The effective charge of the dot is

$$Q = CU = ne + \sum_{i=e,c,g} C_i V_i, \qquad C \equiv \sum_i C_i \tag{62}$$

This charge consists of four contributions, the charge of excess electrons and the charges induced by the electrodes. Thus, the electrostatic energy of the dot is

$$E = \frac{Q^2}{2C} = \frac{(ne)^2}{2C} + \frac{ne}{C}\sum_i C_i V_i + \frac{1}{2C}\left(\sum_i C_i V_i\right)^2 \tag{63}$$

The last term is unimportant because it is independent of n. In the stationary case, the current through both junctions is the same while in the non stationary situation, an electric charge can accumulate on the dot and the currents are different.

The tunneling current

For the artificial atom, the absorption and emission of electrons define the tunneling current. Suppose the gate voltage V_g is set at a conductance peak and an electron is tunneling back and forth between the atom and the leads. Since the electron spends a finite time τ on the dot, the uncertainty principle

tells us that the energy level of the electron has a width $\Gamma \approx h/\tau$. Further, since the probability of finding an electron on the atom decays as $e^{-t/\tau}$, the level will therefore have a Lorentzian shape. This line shape can be measured from the transition probability spectrum T(E) of the electron with energy E incident on the atom from the source. The spectrum is given by

$$T(E) = \frac{\Gamma^2}{\Gamma^2 + (E - E_N)^2} \tag{64}$$

where E_N is the energy of the Nth level. The probability that electrons are transmitted from the source to the drain is approximately proportional to the conductance, $G \approx (e^2/h)T(E)$ where e^2/h is the quantum conductance. Obviously, $G < e^2/h$ in each of the barriers separately, in order to observe conductance resonance.

This condition is equivalent to requiring that the separation of the levels is greater than the width Γ. But the electron spectroscopy has a finite width determined by the energy spread of the electrons in the source which are trying to enter the artificial atom. These electrons are distributed according to the Fermi Dirac distribution function

$$f(E) = \frac{1}{\exp\left(\frac{E - E_F}{k_B T}\right) + 1} \tag{65}$$

where E_F is the Fermi energy. The tunneling current is given by

$$I = \int \frac{e}{h} T(E)\left[f(E) - f(E - V_{sd})\right] dE \tag{66}$$

Equation (66) shows that the net current is proportional to the probability f(E)T(E) that there is an electron in the source with energy E and that the electron can tunnel between the source and drain minus the equivalent

probability for electrons going from the drain to the source. The best resolution is by making $V_{sd} \leq k_B T$. Then $\left[f(E) - f(E - V_{sd})\right] \approx eV_{sd}(df/dE)$ and I is then proportional to V_{sd}, so that the conductance

$$G = I/V_{sd} \ . \tag{67}$$

The model Hamiltonian

In quantum mechanics, particles are described with wave functions Ψ which are solutions of the non-relativistic Schrödinger equation

$$\hat{H}\Psi = i\hbar \frac{\partial \Psi}{\partial t} \tag{68}$$

where $\hat{H}$ is the Hamiltonian operator. In time independent systems, as considered in this thesis, the Schrödinger's equation reduces to the energy eigen value problem

$$\hat{H}\Psi = E\Psi \tag{69}$$

All other physical properties can be calculated from Ψ. For many-body quantum systems as in quantum dot, solving Ψ becomes exponentially difficult when the number of electrons increases. With the aid of modern computing power, accurate solutions of Ψ are achievable but for larger systems, some approximation schemes of solving equation (69) are necessary.

In the first place we assume that the heterostructure is an idealized defect-free semiconductor crystal where ions are arranged in a regular periodic array. Secondly, any crystal is composed of two groups of electrons, valence electrons which contribute to the chemical bonding and core electrons which are tightly bound in the core shell ions. In semiconductors, valence electrons fill in the valence band and core electrons scarcely influence the properties of

the crystal and for that reason is usually not considered. An important role is played by the adiabatic approximation. It is based on the fact that ions are much heavier than electrons.

Therefore, the ions move so slowly on the scale of velocities of electrons, that at any moment, the electrons will be in their ground state for that particular instantaneous ionic arrangement. In other words, the ions can respond only slowly to a change in the electron configuration, while the electrons respond adiabatically to a change in the positions of the ions. Thus the motion of the ions can be effectively decoupled from the motion of the electrons.

A key assumption is the one-particle approximation whereby the many-particle problem is reduced to the motion of an electron in the potential created both by the periodic ion lattice and all electrons in the system including itself. It enormously simplifies the problem of many interacting electrons by effectively removing pair potentials and thus allowing us to describe it with a single particle Schrödinger equation. However, this one particle point of view does not completely neglect electron-electron interactions but rather summarizes their effect by an average global contribution to the potential. In this way the single particle Schrödinger equation does not treat an electron independently of all the others, since the wave functions of other electrons are present through the form of that average contribution.

As explained earlier, only a couple of electrons at a time can be made to move in a quantum dot region. The only constriction in the two-dimensional semiconductor interface is created by the external electrodes which define the

shape and size of the quantum dot. Although an electron is effectively free to move, its motion is affected by the surrounding ion lattice in the semiconductor material. One can rather accurately describe electron motion in a quantum dot by substituting the mass of a free electron with the effective mass tensor $m^*_{\alpha\beta}(r)$ of the electron of the host semiconductor material in the Hamiltonian. This is called the effective mass approximation [87] and it has shown to be fairly accurate for GaAs conduction band electrons in quantum dots. The problem of an electron moving under the simultaneous influence of external forces and the lattice potential can then be simplified to an equivalent problem where quasi electrons, distinguishable from free electrons only by their different masses, move only under the influence of the external forces.

The approximation is valid in the same conditions where the concentration of electrons is mostly low; hence the electrons occupy the states near the bottom of the conduction band. In this case the band energy E(k), where k is the wave vector in the crystal, can be expanded about the minimum. The linear term of the expansion is zero at the minimum, and the energy dependence will have a familiar quadratic law, to which the effective mass tensor can be assigned. Furthermore assuming that the same conduction region occupied by the electrons is uniform and isotropic, the effective mass tensor can be replaced by a constant mass m^*. We shall also exclude spin-orbit coupling from the quantum dot model Hamiltonian. This relativistic effect can become important in small quantum dots but in large quantum dots, it is negligible.

It is worth to mention that spin-orbit interaction along with fluctuating nuclear spins of GaAs lattice [88-90] can have a large effect on the

decoherence times of spin states in large quantum dots, which are of great interest in future spin-based information processing [91]. The quantum dot is described as a closed system of interacting 2-D electrons in an external isotropic parabolic potential. Here the tunneling and the leads are not modeled as interest is in the case where tunneling is sufficiently weak so that the dot can be idealized as an isolated system with well define electron number and we seek for their interacting ground state. As a result of the given approximations, the model quantum dot Hamiltonian of N electrons in a homogenous external magnetic field along the z-axis ($\mathbf{B} = \mathrm{B}u_z = \nabla \cdot \mathbf{A}$) can be written as [92, 93]

$$\hat{\mathrm{H}} = \sum_i^N \left\{ \frac{\left(-i\hbar\nabla_i + \frac{e}{c}\mathbf{A}(\vec{r}_i)\right)^2}{2m^*} + V_{ext}(\vec{r}_i) + g^*\mu_B \mathbf{B}.\mathbf{S}_i \right\} + \sum_{i<j} \frac{e^2}{\varepsilon \left| \vec{r}_i - \vec{r}_j \right|} \qquad (70)$$

The part in parenthesis $\hat{H}_o$ show the sum over N electrons in the quantum dot and the second, interaction part H' contains the coulomb repulsion between pairs of electrons. Magnetic field appear in Hamiltonian in the kinetic energy term via the vector potential ($\mathbf{A}(\vec{r}_i)$) and also couples directly to the electron spins ($\mathbf{B}.\mathbf{S}_i = \mathbf{B}.\mathbf{S}_{z,i}$) which leads to the spin Zeeman splitting. The potential $\mathbf{V}_{ext}(\vec{r}_i)$ describes the quantum dot confinement of the electrons. We assume the electron motion in the quantum dot to be strictly restricted in two dimensions ($\vec{r} = x\vec{u}_x + y\vec{u}_y$). The semiconductor host of the quantum dot is taken into account also in the effective g-factor g^* and in the dielectric constant ε, in addition to the constant mass m^* discussed above. μ_B is the Bohr magneton.

Single-particle state

The direct solution of Schrödinger's equation for the Hamiltonian of equation (68) is a tedious task. The Schrödinger's equation for the single-particle part $\hat{H}_o$ on the other hand is straight forward to solve:

$$\hat{H}_o\phi_i = \varepsilon_i\phi_i \tag{71}$$

If we drop the interaction between electrons and the Zeeman coupling to the electron spin, the Hamiltonian for a single-electron reduces to

$$\hat{H}_o = \frac{(-i\hbar\nabla_i + \frac{e}{c}\vec{A}(\vec{r}_i))^2}{2m^*} + \vec{V}_{ext}(\vec{r}_i) \tag{72}$$

As can be guessed from figure 18, the confinement potential in the plane can be described as harmonic to a good approximation. Thus

$$V_{ext} = \tfrac{1}{2}m^*\omega_o^2 r^2 \tag{73}$$

where ω_o gives the strength of the confinement. In the case of large quantum dots (diameter~100nm), $\hbar\omega_o$ is typically of the order of few meV. Substituting harmonic $\mathbf{V}_{ext}$ and $\mathbf{A}$ in the symmetric gauge ($\mathbf{A} = \frac{1}{2}\mathbf{B}(-y,x,0)$) we can write equation (72) as

$$\hat{H}_o = \frac{-\hbar^2}{2m^*}\nabla^2 - i\hbar\frac{eB}{2m^*c}(-y\frac{\partial}{\partial x} + x\frac{\partial}{\partial y}) + \frac{e^2}{2m^*}\frac{B^2}{4c^2}r^2 + \tfrac{1}{2}m^*\omega_o^2 r^2 \tag{74}$$

which in a more compact form becomes

$$\hat{H}_o = -\frac{\hbar^2}{2m^*}\nabla^2 + \frac{1}{2}m^*\omega^2 r^2 + \frac{1}{2}\omega_c\hat{L}_z\ , \tag{75}$$

where $\omega^2 = \omega_o^2 + \omega_c^2/4$ and $\omega_c = eB/m^*c$, $\hat{L}_z$ is the z-components of the angular momentum operator, $\hat{L}_z = x\hat{P}_y - y\hat{P}_x = -i\hbar\frac{\partial}{\partial\theta}$.

A natural choice is to measure energy in oscillator units $\hbar\omega$, and length in effective harmonic oscillator lengths $l_\omega = \sqrt{\hbar/m^*\omega}$. The characteristic energy and length scales depend on both confinement strength and magnetic field because $\omega = \sqrt{\omega_o^2 + \omega_c^2/4}$. The Hamiltonian in oscillator units can be written as

$$\hat{H}_o = -\frac{1}{2}\nabla^2 + \frac{1}{2}r^2 + \frac{\omega_c}{2\omega}\hat{L}_z \tag{76}$$

The problem of a harmonic oscillator in a magnetic field of equation (76) was first considered by Darwin [94]. Since this Hamiltonian is spin-independent and invariant under rotation about the z-axis,

$$\left[\hat{H}, \hat{L}_z^{tot}\right] = \left[\hat{H}, S_{tot}^2\right] = \left[\hat{H}, S_z^{tot}\right] = 0 \tag{77}$$

The exact eigen funtions can be chosen as simultaneous eigen functions of the total angular momentum $\hat{L}_z^{tot}$, the total spin S_{tot}^2 and its z component S_z^{tot} where eigen functions and corresponding densities are then rotationally invariant. The solution in polar coordinates can be written using the associated Laguerre polynomials $L_n^\alpha(x)$;

$$\phi_{nl}(r,\theta) = \sqrt{\frac{n!}{\pi(n+|l|)!}} r^{[l} [L_n^{|l|}(r^2) e^{-r^2/2} e^{il\theta} \tag{78}$$

where the Laguerre polynomial is given by the formula

$$L_n^{|l|}(x) = \sum_{m=0}^{n} \frac{(-1)^m}{m!} \binom{n+|l|}{n-m} x^m \tag{79}$$

The wave functions ϕ_{nl} called the Fock-Darwin states form a complete orthonormal basis. Ten lowest eigenstates of $\hat{H}_o$ are

$$\phi_{00} = \frac{1}{\sqrt{\pi}} e^{-r^2/2}$$

$$\phi_{0\pm1} = \frac{1}{\sqrt{\pi}} r e^{-r^2/2} e^{\pm i\theta}$$

$$\phi_{0\pm2} = \frac{1}{\sqrt{\pi 2!}} r^2 e^{-r^2/2} e^{\pm 2i\theta}$$

$$\phi_{o\pm3} = \frac{1}{\sqrt{\pi 3!}} r^3 e^{-r^2/2} e^{\pm 3i\theta}$$

$$\phi_{0\pm10} = \frac{1}{\sqrt{\pi}} (1 - r^2) e^{-r^2/\,2}$$

$$\phi_{1\pm1} = \frac{1}{\sqrt{\pi 2!}} r(2 - r^2) e^{-r^2/2} e^{\pm i\theta} \tag{80}$$

The corresponding energy eigenvalues of the radial quantum number n and the angular momentum number l of $\hat{H}_o$ are given by

$$\varepsilon_{nl} = (\,2n + 1 + |l|\,)\hbar\omega - \frac{1}{2} l\hbar\omega_c \tag{81}$$

In absence of a magnetic field, the solution reduces to a two-dimensional harmonic oscillator. When **B** = 0, the last term of equation (81) vanishes $(\omega_c = 0)$ and all contributions of $(\,2n + |l|\,) = \text{constant}$ are degenerate in energy. The degeneracy becomes larger with higher energies. The energy levels ε_{nl} at B = 0T are plotted in the left panel and the radial part of the wave functions of equation (80) are plotted in the right panel of figure 26.

The application of a magnetic field destroys the degeneracy due to

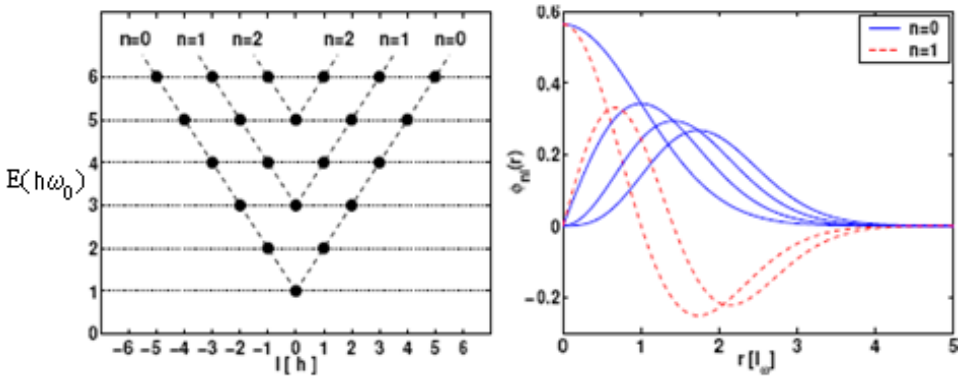

Fig 26: Left, Energy levels in the absence of magnetic field..

Right, Radial part of the wave function $\phi_{nl}(r)$ [94]

the term linear in l. The electron levels shift and split, resulting in many level crossings as the magnetic field strength increases. In the left panel of figure 27, the evolution of the five lowest energy levels (n,l) is plotted as a function of the magnetic field with the confinement strength $\hbar\omega_o = 3meV$. For a comparison, the single-particle energy levels of $\hbar\omega_o = 6meV$ parabolic quantum dots are plotted in the right panel of figure 27.

In the limit of very high magnetic field, the lowest energy levels condense into Landau levels. The lowest Landau level is composed of increasing l-values with $n = 0$, whose energy rises with increasing $\mathbf{B}$ but the separation between the energy levels decreases when the magnetic field increases. In the limit of $\mathbf{B} \to \infty$, the degeneracy in the lowest Landau levels become very high. In analogy to the hydrogen atom, their degeneracy leads to

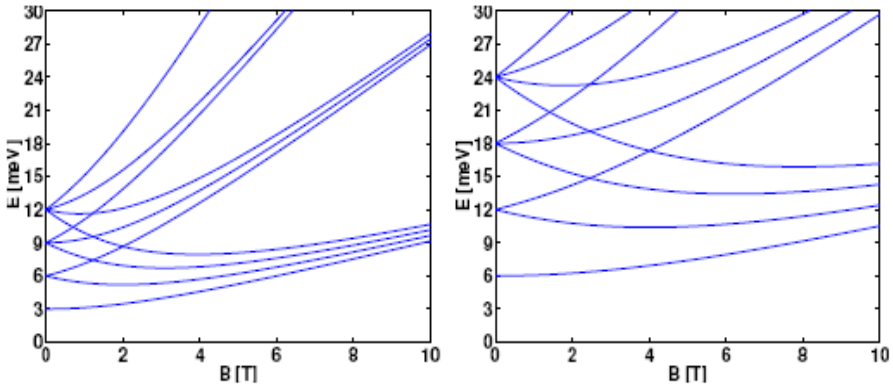

Fig 27: Fock-Darwin energy levels versus magnetic field with $\hbar\omega_o = 3meV$ in the left and $\hbar\omega_o = 6meV$ in the right panel [94].

the energetic shell structure for weak interaction. The degeneracy of the m-th level with energy $E_m = \hbar\omega(m+1)$ is $2m+2$ for spinful electrons. This gives the so called magic numbers which are total number of electrons in closed shells

$$N(m) = (m+1)(m+2) = 2,6,12,20,30,... \tag{82}$$

and correspond to energetically very stable fillings. A periodic table of the artificial atoms is displayed in figure 28.

With these one-particle states, one can now make the so called constant interaction approximation for the addition energies; one assumes that the total energy is given by the sum over the occupied oscillation states plus the coulomb interaction which is parameterized by a constant capacity C. The addition energies, equation (57) then reads

$$E_{add} = E(N+1) - 2E(N) + E(N-1) = \begin{cases} e^2/C + \hbar\omega, if\ N = 2,6,12\cdots \\ e^2/C \quad else, \end{cases} \tag{83}$$

and are maximal for closed shells. This is the atomic shell structure of the quantum dots which relies on the symmetry of the 2-D harmonic oscillator.

A periodic table of artificial atoms (quantum dots) is illustrated in figure 28.

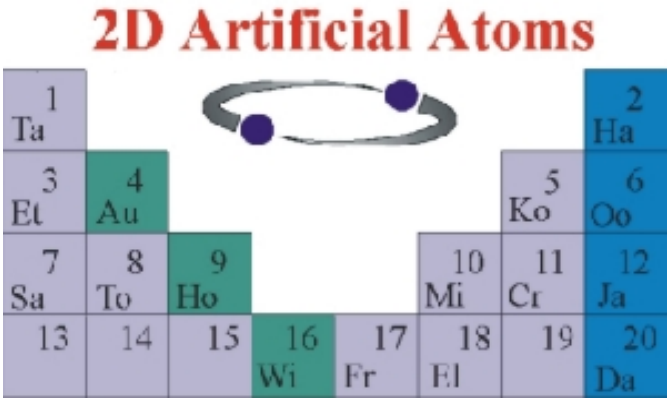

Fig 28: A periodic table of artificial atoms (quantum dots) [5]

The electronic state of a quantum dot

The simplest treatment of the electronic states of a quantum dot is based on the effective mass approximation (EMA). This rests on the assumption that if the quantum dot is larger than the lattice constant of the crystal structure, then it will retain the crystal properties of the infinite crystal and the same values of the carrier effective masses. The electronic states of the quantum dot can then be determined simply by considering the modification of the energy of the charge carriers provided by the quantum confinement.

The electronic and hole states illustrated in figure 29 are determined by solving the Schrödinger's equation for a particle in 3-dimensional box. The zeroth order approximation is a perfectly spherical quantum dot with infinite potential wells at the surface. Strong confinement is defined as the case where

the quantum dot size is small compared with the de-Broglie wavelength of the electrons in the box or small compared with the Bohr exciton radius of the bound electron-hole pair (exciton) in the bulk material. This is the case for II-VI and III-V semiconductors.

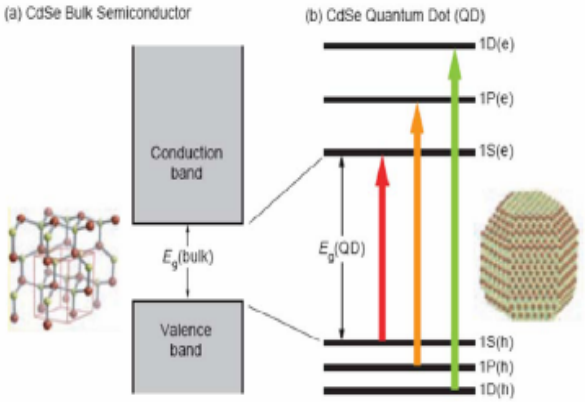

Fig 29: Comparison of energy levels between, (a) bulk semiconductor and (b) a quantum dot [5].

Taking into account the Coulomb interaction between electrons and holes which is enhanced due to the quantum confinement in the quantum dot, the Hamiltonian can be written as

$$\hat{H} = \frac{\hbar^2 \nabla^2_e}{2m^*_e} - \frac{\hbar^2 \nabla^2_h}{2m^*_h} - \frac{q^2}{\varepsilon |r_e - r_h|} + V_e(r_e) + V_h(r_h) \tag{84}$$

or
$$\hat{H}\Psi(r) = E\Psi(r) \tag{85}$$

where V_e and V_h are the confining potentials, r_e and r_h are the distances of the electron and hole from the center of the quantum dot and ε is the permittivity of the semiconductor. Analytical solutions of equations (84) and (85) are demanding because the center of mass motion and the reduced mass motion cannot be separated as independent coordinates.

Various approaches to solving this problem have been used. These include variational calculations (Schmidt et al, [95]; Ekimov et al, [96]; Kayanuma et al, [97]; Takagahara, [98, 99]), matrix diagonalisation (Hu et al, [100]; Park et al, [101]) and Monte Carlo methods (Pollodi et al [102]). Pertubation theory (Brus, [87,103]) and variational calculations (Kayanuma, [104]) lead to a solution of the form

$$E_{\min} = \frac{\hbar^2 \pi^2}{2R^2}\left[\frac{1}{m_e^*} + \frac{1}{m_h^*}\right] - \frac{1.8e^2}{\varepsilon R} - 0.25E_{Ryd} \qquad (86)$$

E_{min} is the lowest energy separation between the hole and electron states of the quantum dot (the energy gap between the lowest level of the conduction band (Lowest Unoccupied Molecular Orbital (LUMO)) and the highest level of the valence band (highest occupied Molecular Orbital (HOMO). R is the radius of the quantum dot and $E_{R\,y\,d}$ is the bulk exciton binding energy in meV. E_{min} is often referred to as the bandgap E_g of the quantum dot since it represents the threshold energy for photon absorption.

In equation (86), the first term relates to the quantum localization which shifts the energy gap to higher energies as R^{-2}. The second term is the coulomb term which shifts the energy to lower energies as R^{-1}, consequently, the total energy gap increases in energy when decreasing the quantum dot diameter [87]. By altering the boundaries of the band gaps, the energy levels of the valence and conduction bands of the quantum dot can be adjusted. This may be done by either subtracting or adding atoms to the dot or changing the shape (geometry) of the dot. Since the emission frequencies are dependent on the band gaps, the wavelengths can be controlled. The band gap of a quantum dot can therefore be precisely tuned to emit different wavelengths [6, 7].

One of the optical features of small excitonic quantum dots immediately noticeable to the unaided eye is coloration. As with bulk semiconductor material, electrons tend to make transitions near the edges of the bandgap. The coloration is directly related to the energy levels of the quantum dot. Quantitatively speaking, the bandgap energy that determines the energy (and hence color) of the fluoresced light is inversely proportional to the square of the size of the quantum dot. The smaller the dot, the bluer (the more towards the blue end of the spectrum) the emission colour reflecting the fact that electrons must fall a greater distance in terms of energy and thus produce radiation of a shorter and therefore 'bluer' wavelength. This is because a small dot has few atoms and energy levels which are widely spaced.

Also the larger the dot the redder (the more towards the red end of the spectrum) the emission colour because larger dot have many atoms and energy levels which are more closely spaced. This also accounts for the large difference between bulk and nanocrystal semiconductor materials. Figure 30 illustrates a matching of the output colour and the size of quantum dots. The dot's size thus dictates its wavelength emission; the smaller the dot the bluer the emission and the larger the dot, the redder the emission.

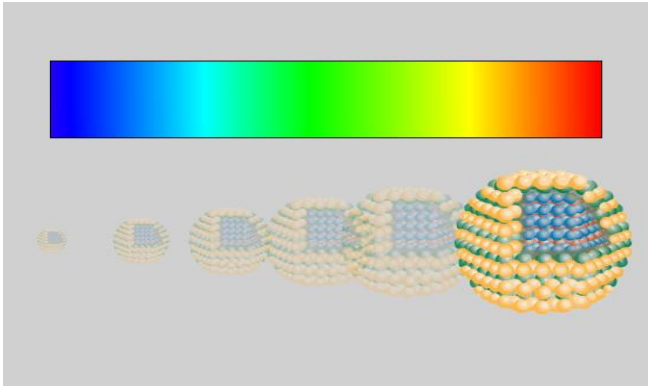

Fig 30: Matching of the output colour and the quantum dot size [5,105]

This allows the quantum dot to absorb photons containing less energy, i.e. those closer to the red end of the spectrum where as smaller size quantum dots have fewer atoms and therefore wider band-gaps, absorb photons of higher energy and hence fluoresce in the blue region. Recent research in nanotechnology seem s to suggest that the shape of the quantum dot may well also be a factor in the coloration, but as yet is still to be confirmed [105]. Table 1 show quantum dot material systems and their emission wavelength ranges.

Table 1: Quantum dot material systems and their emission wavelength range [106]

Quantum dot material systems	Emission Ranges	Quantum dot diameter Ranges
CdSe	465nm-640nm	1.9nm-6.7nm
CdSe/ZnS	490nm-620nm	2.9nm-6.1nm
CdTe/CdS	620nm-680nm	3.7nm-4.8nm
PbS	850nm-2100nm	2.3nm-9.0nm
PbSe	1200nm-234nm	4.5nm-9.0nm

Because of the 3-dimensional spatial confinement in quantum dots, the solution of the Schrödinger's equation results in describing the electronic states of the quantum dot by three quantum numbers plus spin. A commonly used notation by Woggon [107] and Xia [108] labels the electron states as nL_F, where n is the principal quantum numbers (1, 2, 3 etc), L is the orbital angular momentum (S, P, D, etc) and F is the total angular momentum (F = L + J, J = L + S), where S is the spin and the projection of F along a magnetic

axis is m_F = - F to + F. Thus the electron states become $1S_e$, $2S_e$, $1P_e$, etc and the hole states become $1S_{1/2}, 1S_{3/2}, 1P_{1/2}$ etc, shown in figure 29. For optical transitions in ideal quantum dots, the selection rules are $\Delta n = 0,\ \Delta L = 0, \pm 2$ and $\Delta F = 0, \pm 1$. These rules can be broken by non-spherical quantum dots and strong hole-state mixing.

Spectroscopy of quantum dots

The idea of quantum dot spectroscopy is to use light of a suitable wavelength to induce excitation between energy levels in the quantum dot and measure the absorption and photoluminescence spectral intensities as a function of their wavelengths. Due to their small sizes, quantum dots display remarkable spectroscopic properties. In this section, we seek to establish the difference in behaviour between quantum dots of different sizes and by describing several optical properties of (CdSe) quantum dot such as their absorption spectrum, photoluminescence spectrum, and quantum efficiency.

Absorption spectrum

The absorption spectrum of quantum dots (CdSe) was obtained from an absorption experiment using a Fourier Transform spectrometer (Biorad FTS-6000) operated at a resolution of $32cm^{-1}$. For the light source, an incandescent lamp (tungsten-halogen) which gives a very broad emission spectrum from the visible to the infra-red regime was used. The absorption spectrum was determined by comparing the spectrum of the quantum dot in chloroform to the spectrum of pure chloroform solution. Furthermore, the absorption spectrum can also be used to obtain the mean size of the dot. The

mean size is extracted by comparing the wavelength of the first absorption peak with the experimental results at [109-111].

The absorption experiment was performed for two mean sizes of CdSe quantum dots. The results are presented in figure 31. The thick line represents

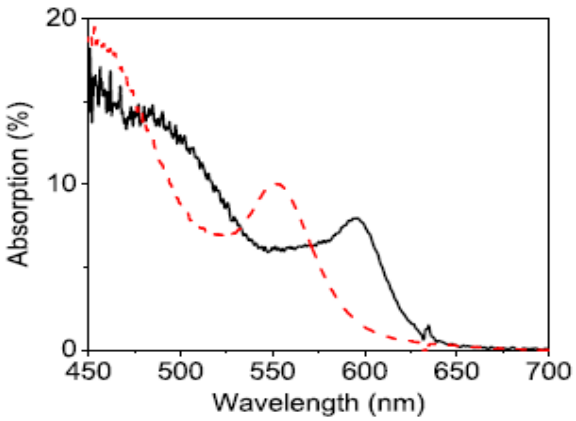

Fig 31: A typical absorption spectrum of CdSe quantum dots [109].

the absorption spectrum of CdSe quantum dot with (4.3 ± 0.4) nm in mean diameter. The first absorption peak occurs at the wavelength 595nm.

The dashed line displays the absorption spectrum for the (3.1 ± 0.3) nm quantum dot in mean diameter with the first absorption peak at the wavelength 551nm. The first absorption peak is associated with the transition between the LUMO and the HOMO band of the quantum dots.

Broadening of the absorption spectrum at the blue side as well as the red side of the first absorption peak is due to size dispersion of the quantum dots. Based on these absorption spectra, it is clear that the absorption spectra shift to shorter wavelengths as the mean size of the dot decreases. The blue shift proves that the LUMO-HOMO energy gap for small quantum dots is

wider than for larger dots. The absorption spectrum also gives information about the efficient wavelength to excite the dots. Moreover, the absorption spectrum can be used to determine the quantum efficiency of the dot (CdSe).

Photoluminescence spectrum

The quantum confinement also affects the photoluminescence of the quantum dots. That is the emission wavelength can be tuned by adjusting the size of the dots. The photoluminescence for two mean sizes of (CdSe) quantum dots were measured. The results are displayed in figure 32. The thick line represents the emission spectrum for the (4.3 ± 0.4) nm in mean diameter which is red shifted in comparison to the (3.1 ± 0.3) nm (dashed line) quantum dots. The band width of the quantum dots spectrum is associated with the polydispersity of the quantum dots size. The spectral band width for monodispersed quantum dots is narrower than those observed for the polydispersed quantum dots.

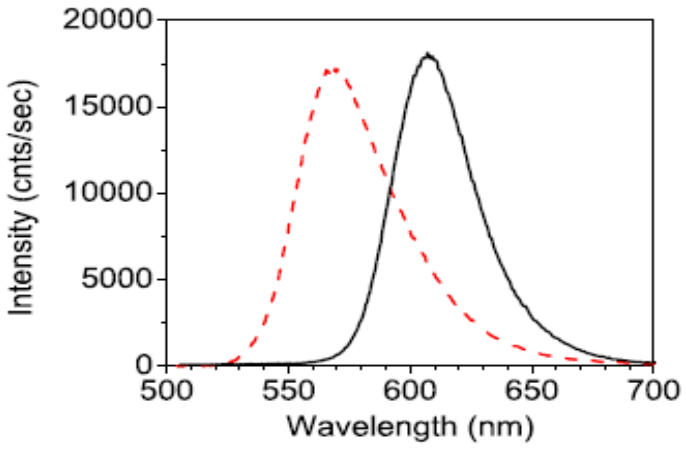

Fig 32: A typical photoluminescence spectrum of (CdSe) quantum dots [112].

Moreover, a specific wavelength component in the quantum dots spectrum originates from specific sizes of quantum dots with the smaller dots emission towards the blue side. Since the emission line width of a single quantum dot is very narrow, (~0.3nm at 10K) [112], the quantum dots spectrum has a narrow homogenous line width and a broad inhomogeneous line width.

Quantum efficiency

In general, the quantum efficiency of a quantum dot is defined as the ratio of the total number of photons emitted to the total number of photons absorbed. Experimentally, this quantity can be extracted by calculating the ratio of the luminescence to the absorption data, then compare the ratio with the quantum efficiency of a standard reference sample. For a reference, laser dyes Rhodamine 6G (R6G) in ethanol which has a quantum efficiency of $\eta_{R6G} = 95\% \pm 5\%$ [113] was used.

Calculation of the quantum dots efficiency can be expressed as follows [114];

$$\eta_{QD} = \frac{lu\,\mathrm{min}escence\ of\ QDot}{absorption\ of\ QDot} \qquad \eta_{R6G} = \frac{lu\,\mathrm{min}escence\ of\ R6G}{absorption\ of\ R6G}$$

The ratio of these two quantities gives

$$\eta_{QD} = \left[\frac{1-T_{R6G}}{1-T_{QD}}\right]\left[\frac{\Delta\Phi_{QD}}{\Delta\Phi_{R6G}}\right]\eta_{R6G} \tag{87}$$

where $1-T_{R6G}$ and $1-T_{QD}$ are the absorption values of R6G and quantum dots respectively, which are obtained from the absorption measurements. $\Delta\Phi_{QD}$ represents the total luminescence intensity of quantum dots extracted by integrating the emission intensity per wavelength interval $I(\lambda)$ over the whole

spectrum. $\Delta\Phi_{QD} = \int I(\lambda)d\lambda$. $\Delta\Phi_{R6G}$ is obtained using the same calculation for R6G. In these calculations, the wavelength used to get the absorption should be the same as the wavelength used to excite the quantum dots and R6G.

CHAPTER THREE

MULTIPLE EXCITON GENERATION AND INTERMEDIATE BAND SOLAR CELL CONCEPTS

Basic structure of solar cells

A Solar cell also called (photovoltaic, PV) converts the energy of the sun into electricity. It consists of a diode made of two layers of semiconductor materials one with an abundance of electrons that functions as the negative pole and the other with an abundance of holes (vacant positively charged spaces) that functions as the positive pole sandwiched between two electric contact layers. Sunlight that passes through the top contact is absorbed in the semiconductor and causes the electrons and holes to diffuse into the different contacts. The electrons and holes are separated by the diode and these charges drive a current in the circuit. Direct current (D.C.) electricity is generated when the solar cell is connected to a load. Solar cells may be integrated into larger modules and arrays to generate enough electricity. The spectrum of sunlight which can be successfully utilized by the solar cell depends on the type and configuration of material used.

Silicon is the most common element used to manufacture solar cells, however, other organic and inorganic materials and nanostructures may be used. Cheaper alternatives to Si do exist but these have much lower efficiencies and often more sensitive to environmental conditions.

They can be classified into:

1. Silicon (Si) – including single-crystalline Si, multi-crystalline Si and amorphous Si.
2. Poly-crystalline thin films – including Copper Indium diselenide (CIS), Cadmium telluride (CdTe) and thin film Silicon.
3. Single-crystalline thin films- including high efficiency materials such as Gallium arsenide (GaAs).
4. Organic sensitized cells which are thin layers of titanium dioxide nanoparticles onto which organic dye molecules are adsorbed, and an acqueous or gel-like electrolyte. Here the energy conversion process is similar to that used by plants during photosynthesis (electron transfer via dye molecules). An organic sensitized solar cell is inexpensive, but its efficiency is about 10% which is too low.
5. Polymer cells, semiconductor polymers which are mainly organic molecules (such as polyphenylene vinylene) have extended delocalized bonds that create bands similar to silicon. Ultrathin layers of these molecules are used in cells which are cheaper to manufacture but suffer from low efficiencies and sensitive to air and moisture.
6. Quantum dots cells, on account of their small size, are potentially more energy efficient, generating up to seven electrons per photons compared to one with existing silicon technologies. They can be incorporated in different matrices and applied as thin films potentially allowing a larger proportion of the spectrum to be absorbed by using different sized particles in stacked layers.
7. Quantum wells these: these allow potentially more energy to be captured from available light than materials in existing applications.

8. Carbon nanotubes and fullerens: when incorporated in matrices of other semiconductor materials, facilitate charge transfer thus increasing efficiency. In addition, they can be used as scaffolds for the deposition of other semiconductor, giving a much larger surface area per unit volume and boosting energy conversion.

Figure 33 is the design of a solar cell showing its essential features. It consists of a glass or plastic cover or other encapsulant, an antireflective layer, a front contact to allow electrons to enter a circuit, a back contact to allow them to complete the circuit, and a semiconductor layer where the electrons begin and complete their journey.

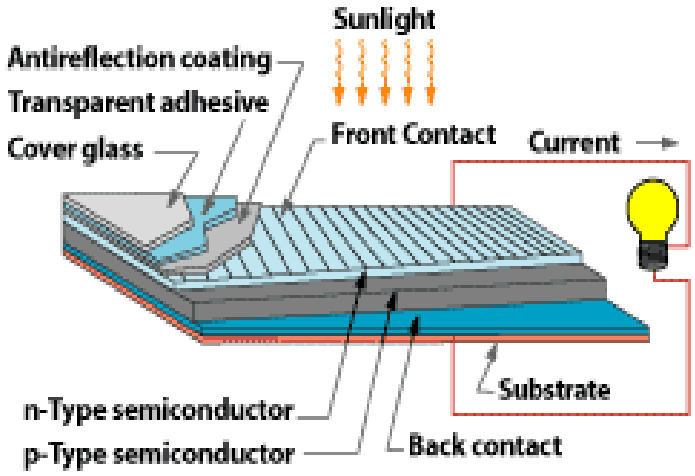

Fig 33: Structure of a conventional solar cell [115]

Solar radiation as an energy source

The major source of energy to operate a solar cell is the sun which radiates energy from gamma rays down to radio waves. Most of the energy is released as visible light even though visible light represents only a small

fraction of the total solar spectrum. The radiation from the sun consists of discrete packets of energy called photons that range in frequencies.

In terms of wavelength, the sun emits almost all of its energy in the range 2×10^{-7} *to* $2\times10^{-6}m$. Each wavelength corresponds to a particular frequency and energy $E=\hbar\upsilon$ where $\hbar$ Planck's constant is and υ is the frequency of radiation. The shorter the wavelength,, the higher the frequency and the greater the energy. Red and violet lights are at the low and high energy ends of the visible spectrum respectively with violet light having twice as much energyas red light. This is illustrated in figure 34.

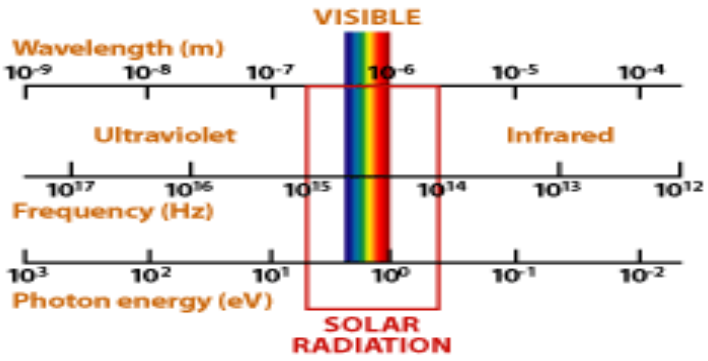

Fig 34: Representation of the solar radiation [115]

The sun may be considered as a black body at a temperature of nearly T_{sun} = 5767K radiating electromagnetic spectrum in the solar system.

Using a dilution factor $f_\omega=(\frac{R_{sun}}{R_{SE}})^2=\frac{\Omega_{sun}}{\pi}$ where R_{sun} and R_{SE} are the radii of the sun and earth respectively. Ω_{sun} is the solid angle subtended at the earth, we obtain the solar constant $S=f_\omega\sigma T_{sun}^4=1.367kW/m^2$ which is the average extraterrestrial irradiance, i.e. the radiation intensity that reaches the outer edge of the atmosphere when the earth is taken to be at its average

distance from the sun. The atmosphere reflects and absorbs most of the high energy radiations including gamma rays, x-rays and ultraviolet rays. Also, much of the residual energy is lost through absorption and scattering in travelling from the edge of the atmosphere to the surface of the earth depending on the thickness of the atmosphere that the energy must pass through. Hence the intensity available at the earth's surface is less than the solar constant.

Assuming a fraction 0.7 reaches the earth's surface when the sun is directly over head in clear sky, then the terrestrial irradiance is $S_E = 0.7S = 957W/m^2 \sim 1000W/m^2$ denoted by AM1.5G which is chosen as the standard value of radiant power. As the sun moves lower in the sky, the energy passes through a longer path of air, loosing more energy and thus reaches a value less than $1000W/m^2$. This radiation is distributed unevenly in different regions on the earth with the regions near the equator receiving more solar radiation than anywhere else. The number 1.5 indicates that the length of the path through the atmosphere is 1.5 times, the shorter path when, the sun is directly over-head. The standard spectrum outside the earth's atmosphere is AM0 which is useful for predicting the performance of a solar cell in space.

The mean daily irradiance is obtained with the use of a geometrical factor of $\frac{1}{4}$ which takes account of the angle between the sun rays and a plane parallel to the earth surface often called the peak solar hours (PSH) = $G_E = \frac{1}{4} x S_E$ x 24h ~ 5.75kW/h. This value is needed in the sizing of the stand alone PV system. In practice one uses the mean solar radiation near the site of installation and its variation throughout the year rather than the average hourly radiation which is $\frac{1}{4} S_E = 238W/m^2$. The amount of the sun's energy that

reaches the surface of the earth every hour is greater than the world's population energy needs in one year hence the sun represents an abundant source of renewable energy to humanity [116-120].

Solar cell performance parameters

When solar radiation or photons of sufficient energy from some other source incident on a solar cell, their energies are transferred to the extra electrons in the negative pole, causing them to flow to the positive pole and creating new holes that start to flow to the negative pole. Thus producing a direct electric current which can be used to power other devices. This current may be converted into an alternating current using inverters and subsequently fed into the grid. An ideal solar cell may be modeled by a current source in parallel with a diode. In practice no solar cell is ideal and so a shunt resistance and series resistance components are added to the model. The equivalent circuit and symbol are shown in figure 35

The performance of a solar cell is predicted from its current density-voltage characteristics. This is obtained by exposing the cell to a constant level of light while maintaining a constant cell temperature, varying the resistance of the load and measuring the current that is produced.

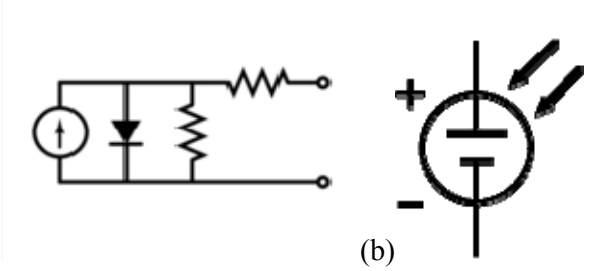

(a) (b)

Fig 35: Schematic diagram of the (a) equivalent circuit and (b) symbol of a solar cell

The current density-voltage curve illustrated in figure 36 passes through typically, two significant points

1. The intercept on the current axis called the short-circuit current (I_{SC}) which is the value of the current when the positive and negative terminals of the cell are short circuited and the voltage between the terminals is zero corresponding to a zero resistance.
2. The intercept on the voltage axis called the open-circuit voltage (V_{OC}) which is the value of the voltage over the terminals under open circuit conditions, when the current is zero corresponding to infinite resistance.

   P_m, is the maximum power point

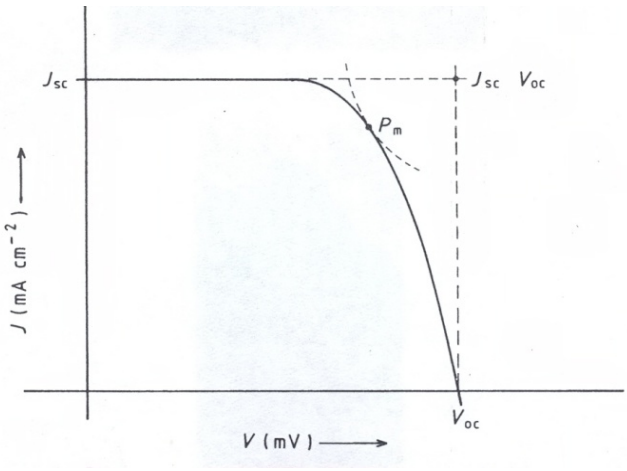

Fig 36: The Current-voltage characteristics of a solar cell.

The cell may be operated over a wide range of voltages and currents by varying the load resistance from zero (short circuit) to infinity (open circuit). From the equivalent circuit, the current produced by the solar cell is equal to

the photogenerated currnet, minus that which flows through the diode, minus that which flows through the shunt resistance.

$$I = L_P - I_O - I_{SH}$$

where

I is the output current

I_P is the photo –generated current

I_D is the diode current

I_{SH} is the shunt current

The current through these elements is determined by the voltage through them:

$$V_J = V + IR_S$$

where

V_J is the voltage across both the diode and shunt resistance R_{SH}

V is the voltage across the output terminals

R_S is the series resistance

Using the Shockley diode equation, the current diverted through the diode is

$I_D = I_O \left(\exp(qV_J)/nkT - 1\right)$

I_O is the reverse saturation current

n is the diode quality factor (1for an ideal diode)

where k is Boltzman's constant , q is the charge on an electron

T is the working temperature of the cell

By Ohm's law, the current diverted through the shunt resistance is

$$I_{SH} = \frac{V_J}{R_{SH}}$$

R_{SH} is the shunt resistance

Substituting these into the first equation, gives the characteristic equation which relates the solar cell parameters to the output voltage.

$$I = I_P - I_O\left(\exp q(V + I \times R_S)/nkT - 1\right) - \frac{V + IR_S}{R_{SH}}$$

If the shunt resistance is so high that the last term can be ignored, the n we have

$$I = I_P - I_O\left(\exp q(V + I \times R_S)/nkT - 1\right)$$

、 $$I_P = I_P(T_1)\left(1 + K_O(T - T_1)\right)$$

$$I_P(T_1) = G \times I_{SC}(T_1)$$

$$K_O = \left(\boldsymbol{I}_{SC}(T_2) - \boldsymbol{I}_{SC}(T_1)\right)\Big/(T_2 - T_1)$$

$$I_O = I_O(T_1) \times \left(T/T_1\right)^{3/n} \times \exp(-q\frac{V_g}{nk}(\frac{1}{T} - \frac{1}{T_1}))$$

$$I_O(T_1) = I_{SC}(T_1)\Big/\left(\exp q \times V_{OC}(T_1)/nkT - 1\right)$$

$$R_S = -\left(\frac{dV}{dI}\right)_{Voc} - 1/X_V$$

$$X_V = \left(I_O(T_1) \times q/nkT_1\right)\left(\exp qV_{OC}(T_1)/nkT_1\right) \qquad (88)$$

V_g is band gap voltage

T_1 and T_2 are reference temperatures in Kelvin

V_{OC} is the open circuit voltage

I_{SC} is the short circuit current

The highest efficiency can be determined as corresponding to the point normally at the knee of the I-V curve where the cell delivers maximum power

$$P_m = I_m V_m \qquad (89)$$

If the constant solar irradiance or light intensity is E and the surface of the solar cell receiving the light is A, then the total incident solar power is $E \times A$ and hence the efficiency of the solar cell is calculated from

$$\eta = \frac{P_m}{E \times A} = \frac{I_m V_m}{E \times A} \tag{90}$$

At the point of intercept of J_{SC} and V_{OC} the ratio

$$FF = \frac{I_m V_m}{I_{SC} V_{OC}} \tag{91}$$

is called the fill factor. The fill factor measures the 'squaredness' of the I-V curve and describes the degree to which the current at the maximum power point I_m matches the current I_{SC} and the voltage at the maximum power point V_m matches the voltage V_{OC}. From equation (89) $I_m V_m = FF \times I_{SC} V_{OC}$ and hence the cell's efficiency

$$\eta = \frac{I_m V_m}{E \times A} = \frac{FF \times I_{SC} V_{OC}}{E \times A} \tag{92}$$

The last equation shows that the higher the fill factor, the higher the efficiency and vice versa.

The widespread use of solar cells has been limited to date because of two factors;

1. High production cost and
2. Low efficiency.

The fabrication of the simplest semiconductor solar cells is a complex process that requires ultra-pure starting materials (Silicon) and takes place under exactly controlled conditions such as high vacuum and temperatures between 400 ^{o}C and 1400^{o}C. The market value of normal solar panels compared with other conventional sources, for instance fossil fuel are expensive and their size

is constrained by manufacturing techniques thus limiting their scalability to large area panels.

Factors affecting Solar cell conversion efficiency

The conversion efficiency of a solar cell is the percentage of the solar energy shinning on a PV device that is converted into electrical energy. This is currently between 20% and 30% for the most efficient solar cells even though the predicted theoretical limit is 67%. Much of the energy from sunlight reaching a PV cell is lost before it can be converted into electricity. But certain characteristics of a solar cell material limit the cell's efficiency. Some characteristics are fixed, while others can be improved by selecting appropriate materials and carefully designing the cell. The efficiency of solar cells is affected by a variety of factors which include the following:

Wavelength

The spectrum of sunlight covers a range of 0.5 eV to 3.5 eV. From infrared to ultraviolet, it covers a range of about 0.5eV to about 2.9eV in terms of energy. For example, red light has energy of about 1.7eV, and blue light has energy of about 2.7eV. (An electron-volt is equal to the energy gained by an electron when it passes through a potential difference of 1 volt in a vacuum.) When light shines on crystalline silicon, electrons within the crystal lattice may be freed. This is because only photons with a certain level of energy can free electrons in the semiconductor material from their atomic bonds to produce an electric current. This level of energy, known as the bandgap

energy, is the amount of energy required to dislodge an electron from its covalent bond and allow it to become part of an electrical circuit.

Crystalline silicon has bandgap energy of 1.1eV. The bandgap energies of other effective PV semiconductors range from about 1.0 to 1.7 eV. In this range, electrons can be freed without creating extra heat. To free an electron, the energy of a photon must be at least as great as the band gap energy. The primary reason why PV cells efficiency is small is because they cannot respond to the entire spectrum of sunlight. Photons with energy less than the band gap are not absorbed, or do not produce electronic transition, a deficiency, referred to as transmission losses. This constitutes about 20% of incoming solar energy.

Also, photons with more energy than the band gap energy will expend that extra amount as heat when freeing electrons; the resultant energy loss is referred to as thermalisation loss.This account for an additional loss of about 30%. Thus the inefficient interactions of sunlight with the cell material waste about 50% of the energy from the original sunlight, because the photon's energy is either below the band gap of the material or is in excess of the bandgap energy. Only photons with as much energy as the material band gap produce energy conversion with optimum efficiency [121]. A key to obtaining an efficient PV cell among others is to convert as much sunlight as possible into electricity or reduce both transmission and thermalisation losses to a minimum.

This requires a PV cell or solar radiation to be tuned through slight modifications to the silicon's molecular structure to optimize the photon

energy or to modify the solar radiation to obtain a better match between the incident radiation and the spectral response of the solar cell material or both.

Figure 37 illustrates the absorption and transmission relationship between solar energy and different solar cell materials. Different PV materials have different energy bandgaps. Photons with energy at least equal to the band gap energy are absorbed to create free electrons. Photons with less energy than the bandgap energy pass through the material.

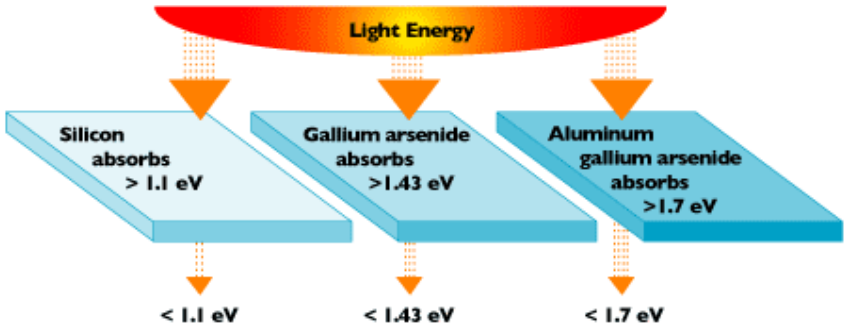

Figure 37: Different PV materials with different energy bandgaps [115].

Recombination

Charge carriers which are electrons and holes in a solar cell may inadvertently recombine before they make it into the electrical circuit and contribute to the cell's current. Indirect recombination may also occur where electrons or holes encounter an impurity, defect in the crystal structure or interface or surface that makes it easy for them to recombine.

Natural resistance

The natural resistance to electron flow in a cell decreases a cell's efficiency. This loss predominantly occurs in three places, in the bulk of the primary solar material, in the tin top layer typical of many devices and at the interface between the cell and the electrical contacts leading to the circuit.

Temperature

Solar cells work best at low temperatures as determined by their material properties. However, much of the light energy shining on the cell becomes heat, but all cell materials loose efficiency as the operating temperature rises. The solution is to match the material to the operating temperature or continually cool the cell.

Reflection

Silicon is a shiny gray material and can act as a mirror, reflecting more than 30% of the incident light. A cell's efficiency can be increased by minimizing the amount of light reflected away from the cell's surface. To improve the conversion efficiency of the solar cell, the amount of light reflected must be minimized. Two techniques are commonly used.

First a thin layer of silicon monoxide (SiO) which has anti reflecting (AR) properties is coated at the top surface of the solar cell. A single layer reduces reflection to about 10% but only at one wavelength. A second layer can lower the reflection to less than 4%. Better results are obtained by applying multiple AR layers.

Another way is to texture the top surface of the cell. Chemical etching creates a pattern of cones and pyramids which capture light rays that might otherwise be deflected away from cell. By texturing the surface, reflected light is redirected down into the cell where it has a second chance to be absorbed.

Interaction of solar radiation with bulk semiconductor material

A stimulus such as heat, voltage or photon flux in a semiconductor generates carrier distribution that is different from that in thermal equilibrium. After the removal of the excitation source, relaxation processes will force the system back into the equilibrium state. Even though the discrete levels in a quantum dot increases the complexity of the carrier dynamics, the underlying physical processes are the same as the bulk case.

Shining light on a semiconductor causes the following excitations; interband transitions and excitonic transitions or below bandgap transitions. These processes are shown schematically in figure 38.

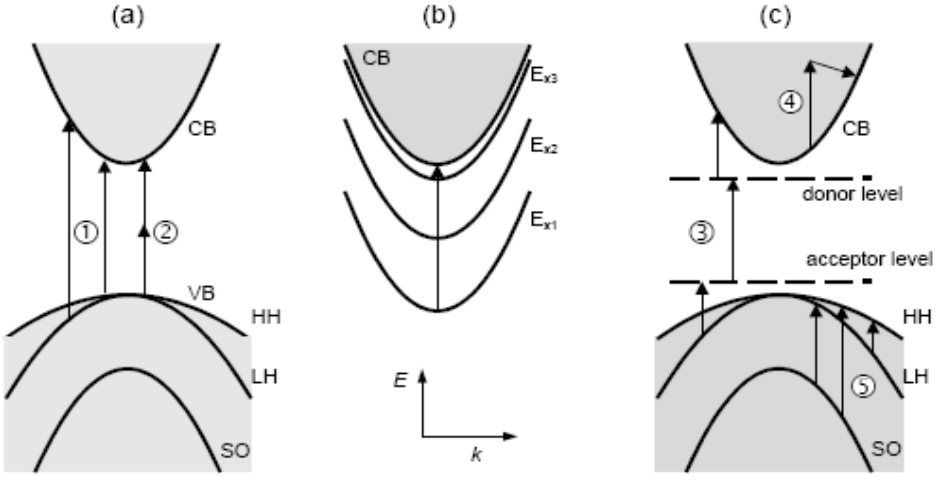

Fig 38: Schematic diagram of electronic excitation in a semiconductor due to interaction with photons [122].

(a) Bandgap excitation: (1) Single photon absorption, (2) multi-photon absorption. (b) excitonic transition and (c) below-bandgap transitions: (3) impurity related transition, (4) intra-band absorption, (5) intra-valence band transitions. The notations have the following meanings, E_{Xi}…..ith, excitonic levels, HH/LH/SO…., heavy hole/light hole/split-off valence band, for direct bandgap materials i.e. when the conduction band minimum is at the same position in k-space as the valence band maximum.

If the photon energy is larger than the bandgap, inter-band transitions dominate, exciting electrons from the valence band into the conduction band. Deviations from a perfectly periodic structure in a crystal lattice result in localized defect energy levels within the forbidden gap. These can be caused by either structural defects in the bulk (such as point defects, dislocations, stacking faults etc) or by the surface itself (so called surface states).

Depending on their energy levels, the defects are categorized as either traps or recombination centers. When the energy difference between the defect levels and the conduction band is small, an electron promoted from the top of the valence band can be captured at the defect level within the forbidden gap. The probability of recombination with the carrier of opposite sign is rather small as the energy difference to the valence is large. Consequently the electron and hole pair forming a bound system like a hydrogen atom via Coulomb interaction called an exciton, stay at the carrier traps for finite times and can return to the conduction or valence band through thermal excitation.

The possible energies of an exciton below the conduction band is described similar to the hydrogen atom as

$$E_n = -\frac{\mu e^4}{2\hbar^2}\frac{e^2}{n^2}\frac{1}{\varepsilon_r} \tag{93}$$

where μ is the reduced mass and ε_r is the relative dielectric constant of the material under consideration taking into account the changes arising from considering carriers in a semiconductor instead of free carriers in vacuum and *e* is the elementary charge. The reduced mass depends on the effective masses of the electrons $m_e^{\bullet}$ and holes $m_h^{\bullet}$ as $\frac{1}{\mu} = \frac{1}{m_e^{\bullet}} + \frac{1}{m_h^{\bullet}}$

For each material, there is a fixed physical average separation between the electron and the hole called the Bohr exciton radius (BER).The characteristic distance between these two charges is [81, 123, 124]

$$a_B^{ex} = \frac{\hbar^2}{e^2}\varepsilon\left[\frac{1}{m_e^*} + \frac{1}{m_h^*}\right] \tag{94}$$

Defects with energy levels deep within the forbidden gap, present a different situation. Thermal excitation of trapped carriers is significantly reduced (the probability of such an event decays exponentially with the energy difference of the defect and the band energy). Instead carriers recombine at the defects, which are called recombination centers, nonradiatively i.e. with the emission of phonons.

In bulk semiconductors, the crystals are much larger than the BER, the exciton stretches to its full extent leading to continuous energy levels both in the valence and conduction bands, meaning there is almost no energy difference between them. Although many above-bandgap solar photons carry enough energy to theoretically unleash several electrons or excitons, they almost never free more than one electron (i.e. the quantum efficiency is low, about 1.3 electron-hole pairs per absorbed photon) [50,125]. This is because

the photogenerated carriers with total excess kinetic energy equal to the difference between the photon energy and the bandgap (hot carriers) often collides with nearby atoms and is less likely to set other electron free to generate multiple excitons. Rather it creates atomic vibrations or phonons that squander the electron's excess energy as heat (Thermalization loss) leading to a fast relaxation of the exciton to their lowest energy levels and their subsequent recombination.

The distribution of the excess exciton kinetic energy between electrons and holes in bulk semiconductors is determined by their effective masses. The carrier having lower effective mass receives more of the excess energy [32] hence

$$\Delta E_e = (h\upsilon - E_g)\left[1 + m_e^* / m_h^*\right]^{-1} \tag{95}$$

$$\Delta E_h = (h\upsilon - E_g) - \Delta E_e \tag{96}$$

where ΔE_e is the difference in energy between the conduction band and the initial energy of the photo-generated electron and ΔE_h is the energy difference between the valence band and the photo-generated hole. This is illustrated in figure 39. This excess kinetic energy creates an effective temperature for the Boltzman ensemble of photogenerated carriers that can be much higher than the lattice temperature after the electrons and holes have equilibrated (thermalized) among themselves.

The initial carrier temperature on photon absorption can be much higher than 3000K with the lattice temperature at 300K.

The action of the built-in voltage in conventional bulk semiconductor solar cells is a fast extraction of the electrons away into the external circuit to

constitute a photogenerated current and a photovoltge [126] before the hot exciton relapse to their lowest levels and subsequently recombine. This accounts for the one-photon-one electron rule characteristic of bulk semiconductor solar cells which limits its efficiency to about 30% [2].

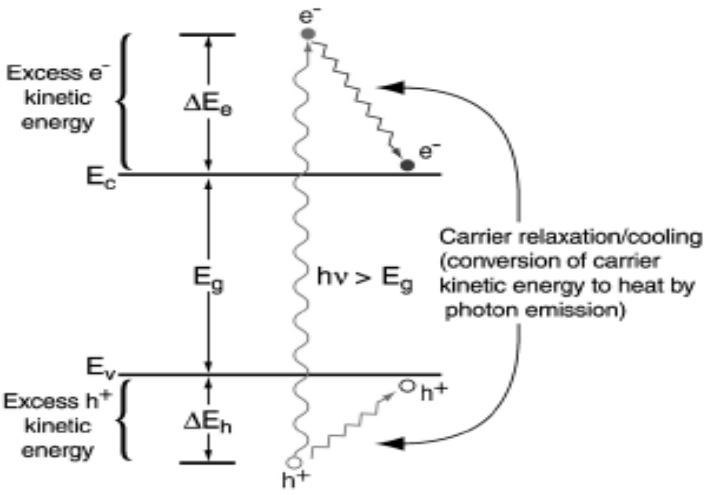

Fig 39: Hot carrier relaxation / cooling in semiconductor solar cell [32].

M. Califano et al [127,128] had suggested that the solutions to the loss in photon energy are alternative solar cell concepts that harvest the excess band gap energy of photons to produce photocurrents and photovoltages, rather than being lost to phonons. Then it would be possible to obtain two or more electron-hole pairs from one and this could possibly break the efficiency barrier of conventional solar cells caused by thermalization. Solar cells based on direct carrier multiplication are commonly referred to as third generation solar cells and among the several schemes are the following:

1. Hot carrier solar cells [129-131]

2. Solar cells producing multiple electron-hole pairs per photon (impact-ionization) [132-135]

3. Multiband and impurity solar cells [125,134-136]

4. Thermo-thermophotonic cells [125]

Impact-ionization in quantum dots

Two factors make low-dimensional structures such as quantum dots and MQW potentially useful for third generation solar cell implementation.

1 The mitigation of thermal scattering and

2 The control over light absorption.

About a decade ago, Murphy et al [137] hypothesized that the nano-size of quantum dots coupled with their quantum confinement effects could lead to impact-ionization which is a pre-requisite for improving on the performance of conventional solar cells.

Impact-ionization is a process by which the interaction between a photon with excess bandgap energy and an electron in a quantum dot produce several excitons. First the photo-generated electron with excess bandgap energy strikes an electron bound to an atom transferring energy to it and creating another exciton. If enough excess energy remains in the newly formed exciton, its electron can create another exciton and so on.

In quantum dots, the presence of discrete states means that energy must be transferred from the carriers in discrete steps. Since the spacing between the electronic (excitonic) levels (of the order of hundreds of meV) is large, compared to the longitudinal optical phonon frequency (~25meV), electron cooling via electron-phonon coupling requires the simultaneous emission of a large quantity of phonons, a process which is quantum mechanically of low probability. This retards hot exciton cooling and results in

cooling times in the nanosecond range [138]. It is such slow cooling properties of the quantum dot exciton that proves useful in the concept of quantum dot based solar cells [129] since slow cooling would allow the harvesting of the photons energy in excess of the band gap. As this energy may be available to generate other excitons, the process has the potential of nearly doubling the theoretical efficiency of conventional solar cells. This is the significance of impact-ionization.

Since then, there has been extensive research in this direction by various researchers notably groups from the National Renewable Energy Laboratory (NREL). Experiments conducted by Schaller et al [139] involving the interaction of high energy blue light with cadmium selenide (CdSe) and lead selenide (PbSe) quantum dots, produced two and three excitons respectively.The creation of three excitons using lead telluride(PbTe) quantum dots has been reported by Jiang et al [140]. Recently, Schaller etal [141] have reported the creation of as many as seven excitons by interaction of ultra violet light photons with lead selenide (PbSe) quantum dots. Hypothetically, the number of excitons created by a photon is related to the energy of the photon divided by the dot's band gap energy,

$$n(excitons) \sim h\nu / E_g \tag{97}$$

where E_g is the band gap energy of the quantum dot and υ is the frequency of the photon. This is because the photon must supply one band gap worth of energy to each electron. Therefore, using dots with smaller band gap energy produce a large number of excitons because less energy is needed to push the electron over the dot's bandgap threshold. However, in actual experimental work, it is observed that the distribution of photon energy between electrons

and holes often require the photon to have more energy to produce a specific number of excitons than suggested above. Schaller et al [139] have subsequently reported that the photon must have at least three band gaps of energy.

Computation of the conversion efficiency of MEG solar cells

This section considers the calculation of the conversion efficiency limit of a single junction solar device which employs quantum dot absorbers based on the principle of impact-ionization discussed by Hana et al [142]. In this calculation, the basic assumptions are:

1. All photons with energy above the absorption threshold are absorbed.
2. The quasi-Fermi level separation is constant and equal to qV across the device which is equivalent to the assumption of infinite carrier mobility and finally,
3. The only active recombination mechanism is radiative recombination.

The current-voltage relationship for a single junction device is given by

$$I(V,E_g) = I_G(E_g) - I_R(V,E_g) \tag{98}$$

where I_G is the photo generated current,

I_R is the recombination current associated with radiative recombination

E_g is the absorption threshold or band gap of the barrier

V is the photovoltage generated by the cell.

The photo generated current I_G and recombination current I_R are obtained from

$$I_G(E_g) = q \int_{Eg}^{E\max} QY(E)\Gamma(E)dE \tag{99}$$

and

$$I_R(V,E_g) = qg\int_{Eg}^{\infty}\frac{QY(E)E^2}{\exp\{[E-qQY(E)V]/kT\}-1}dE \qquad (100)$$

Where E is the photon energy

q is the electron charge

k is the Boltzmann's constant

T is the temperature of the solar device (T=300K)

$g = 2\pi/c^2h^3$ where c is the speed of light in vacuum and h is Planck's constant.

The quantum yield QY(E) allows for the generation and recombination of multiple charge pairs per photon over the appropriate energy range. $\Gamma(E)$ is the photon flux associated with the AM1.5G spectrum. E_{max} is the maximum photon energy in the solar spectrum; For AM1.5G, E_{max} = 4.428eV approximated to E_{max} = 4eV for practical purposes, the resultant integrated solar current above 4eV in the standard AM1.5G spectrum is $\sim 5\mu A cm^{-2}$. In equation (99), carrier generation from ambient black body radiation is neglected which is a reasonable approximation for E_g = 0.2eV.

Multiple exciton generation is implicit in the analysis through the energy dependent quantum yield QY(E) which may exceed one over certain photon energy ranges. For an ideal MEG quantum dot absorber, the form of QY(E) is given by a sum of the step function

$$QY(E) = \sum_{m=1}^{M}\theta(E,mE_g) \qquad (101)$$

where $\theta(E,mE_g)$ is the Heaviside unit step function. m = 1, gives the usual one-photon, one-electron-hole pair.

$m = m_{\max} = E_{\max} / E_g$ gives the maximum number of excitons and the highest possible efficiency for an MEG device. MEG absorbers may be denoted by M = 1, M = 2 and M = M_{max} respectively by M_1, M_2 and M_{max}. The conversion efficiency of a photovoltaic device at a given point is

$$\eta_{pv}(V) = I(V)V / P_{in} \tag{102}$$

where P_{in} = 100mW/cm^2 is the integrated optical power in the AM1.5G spectrum.

The value of the voltage V in equation (102) is obtained by the following consideration of actual water splitting devices. The photochemical conversion efficiency for the production of stored chemical energy as H_2 from water splitting is given as

$$\eta_{H_2}(V) = I(V)U_{H_2} / P_{in} \tag{103}$$

where $U_{H_2} = 1.23V$ is the minimum thermodynamic potential required for water splitting at 300K. The operating voltage or bias point of the cell will be larger than U_{H_2} by the sum of the anode and cathode over potential (loss) and the resistive potential drop of the electrolyte. Denoting the sum of these over potentials (loss) by V_{over} and assuming it is independent of the current, then the operating voltage

$$V = V_{over} + U_{H_2} \tag{104}$$

By maximizing the efficiencies of equations (103) and (104), the maximum efficiency of a single junction photovoltaic device with a given threshold E_g and quantum yield QY(E) can be obtained from equations (98) to (104).

Several authors [143-148] have subsequently reported values of the efficiency of single junction solar cell devices which rely on carrier

multiplication by impact-ionization exceeding the Shockley and Queisser limit. Under standard AM1.5G illumination, the maximum efficiency for single junction solar cells operating at 300K with quantum yield determined from equations (98) to (104) is shown in figure 40 for single junction devices with the following absorber types; M_1 (no exciton multiplication), M_2 (two excitons per photon above $\hbar\upsilon = 2E_g$) and M_{max} (maximum possible number of excitons per photons from solar spectrum).

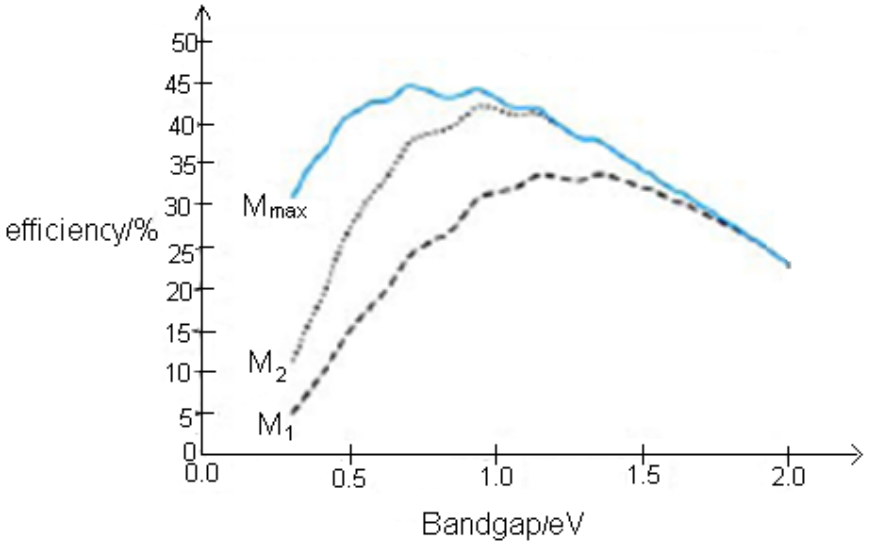

Figure 40: PV conversion efficiency as a function of quantum dot bandgap [142].

The curve M_1 is without carrier multiplication and corresponds to the usual one-photon-one-exciton rule i.e. the Shockley and Queisser limit with maximum efficiency 33.7%, occurring at E_g = 1.3 eV. The curve M_{max} is obtained by using the maximum integral number of carrier multiplication possible with the available excess energy $m_{max} = E_{max}/E_g$. This corresponds to a maximum efficiency of 44.4% for a single junction with bandgap E_g = 0.7 eV where m_{max} = 6. From the graph, an efficiency value of ~ 42% is obtained

with carrier multiplication of M = 2 i.e. curve M_2 which is 94% of the absolute maximum. The implication is that higher multiplication values greater than 2 are not the only pre-requisite for substantially increasing the efficiency of a single junction solar device based on impact-ionization.

Intermediate band solar cell concept

In order to achieve higher conversion efficiencies, multi-bandgap absorber systems such as multiple quantum wells (MQW) and superlattice (SL) have been suggested [149]. Due to quantum mechanical effects, the effective band gap of the MQW is lower than $E_g^{barrier}$ and thus a MQW can expand the light absorption range to longer wavelengths. The enhanced well number and the formation of continous minibands in a superlattice contribute to the easy spread of the charge carriers through the whole structure resulting in high conductivity. This can improve its efficiency by increasing the short-circuit current [150]. In the presence of the built-in electric field, in the depletion layer, the photogenerated carriers produced by absorbing extra photons in the well escape to the adjacent barrier layer, and thus contribute extra current with high escape efficiency at room temperature [151-153].

To avoid defect formation and degradation of the photovoltaic properties, lattice matched MQW materials are used. Based on current technology, lattice matched absorbers with thickness up to 1μm have been made possible [154]. As a way of minimizing the effect of lattice dislocations, the component materials as well as the values of L_b and L_w are carefully selected. The MQW could be fabricated with quantum dot arrays produced by self assembled growth [155,156] or by patterning techniques.

The concept of intermediate band solar cells (IBSC) involves the insertion of a narrow additional level (isolated or forming bands) in the regular bulk semiconductor material at the p-n junction to provide additional absorption channels that can accept electronic excitations from the valence band and allow transitions to the conduction band [157-159] as shown in figure 41.

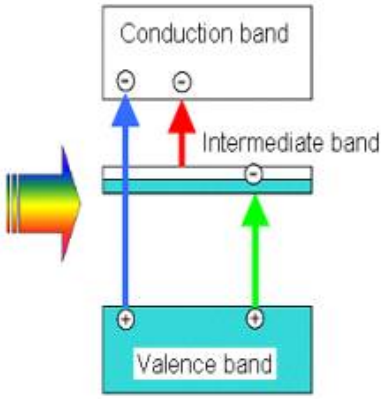

Fig 41: Photon absorption processes in the Inter mediate band solar cell [160]

Thus the operation of the IB solar cell depends on a material with three bands, i.e. a conduction band, a valence band and an inter mediate band. Due to the existence of three bands, there exist three band gaps: A bandgap between the conduction and valence bands, $E_{CV,}$ a bandgap between the conduction and inter - mediate bands, $E_{CI,}$ and a bandgap between the valence and inter-mediate bands, $E_{VI.}$ Each of these bands is associated with a distinct quasi-Fermi level. E_{FV} , E_{FI} and E_{FC} are the Fermi levels of the valence, inter - mediate and conduction bands respectively.

Under non equilibrium conditions, three chemical potentials exist, one for each of the carrier populations associated with the three bandgaps as

shown in figure 42. μ_{IV}, μ_{CV} and μ_{CI} are the chemical potentials between the intermediate band and the valence band, the conduction band and the valence band and finally the conduction band and the inter mediate band respectively. $qV = \mu_{CI} - \mu_{IV}$, V is the photogenerated voltage across the cell.The A_{IV}, A_{CI}, and A_{CV} are respectively, the energy difference between middle level of the intermediate band and the lowest level of the valence band, the energy difference between the middle levels of the conduction and intermediate bands, and finally the energy difference between the lowest level of the conduction band and the highest level of the valence band.

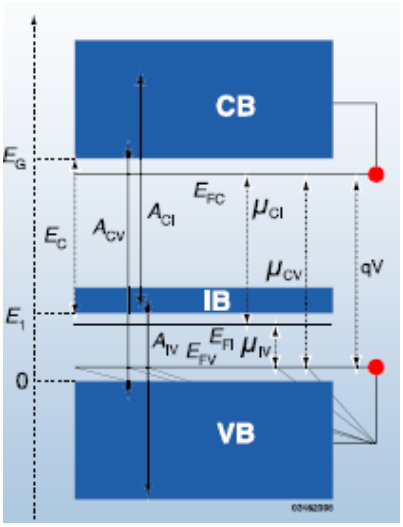

Fig 42: Schematic diagram of IBSC showing the energy intervals, chemical potentials and Fermi levels [161]

Due to increased photon induced carrier generation, the existence of the intermediate band provides more efficient solar energy conversion as compared to single junction solar cell whose band gap is E_{CV} [162], as a result, such intermediate band solar cells could work close to their optimum

efficiencies without current flowing in the intermediate band itself if the band(s) are suitably populated with electrons and holes. In order to provide high likelihood of carrier advancement to and from the intermediate band, the Fermi levels must exist near the intermediate band. Also, the conduction and valence bands are not directly electrically contacted although radiative transitions between the intermediate band and the two other levels are allowed [158,163]. The advantage derived from here is that the IB helps to receive photons with energies less than the bandgap of the host material (which could otherwise not produce any electronic transitions) by a two-step process thus improving the short-circuit current without degrading the open circuit-voltage. [159, 164-167].

The IBSC could be implemented by introducing QWs into the intrinsic region of the p-i-n solar cell [149,168], where the minibands constructed with 3-dimensionally ordered assemblies of quantum dots or quantum dot supracrystals [149,169,170] constitute the intermediate bands. [154].This can provide the required electron and hole dispersion, and charge transport expected to increase the spectral range leading to higher efficiency. Here, the requirement of a narrow band (to reduce thermalisation losses) and high mobility (to avoid serial resistance) are somewhat conflicting from the fundamental point of view of quantum mechanics because they vary inversely as a function of the overlap integral of the electronic wave functions of the centers (transition metals, quantum dots) forming the bands.

In these structures, interband electron-phonon relaxation can be reduced substantially [171] though this effect can be overturned by many-body effects and high temperatures. Intersubband absorption of phonons [172],

intersubband transitions due to electron-electron scattering or the inverse Auger effect can constitute ways to have multiple quasi-Fermi levels under detailed balance conditions and thus leading to an increase in efficiency beyond the single gap limit.

Another mechanism that comes into play which could lead to an enhancement of the efficiency of solar cells even when the local distribution of charge carriers is well described by two quasi-Fermi levels is the heating of the optically active regions of the semiconductor.

As a result, the thermoelectric due to temperature gradients in the cell may enhance the output voltage. There may also be the enhancement of current and output voltage due to thermionic emission from the optically active regions if a semiconductor with a lower band gap than the traditional semiconductor material is inserted within the main band gap [173].

In general, the conversion efficiency of inorganic solar cells decline with a rise in temperature which is due to the decrease in optical bandgap. In contrast, the MQW solar cells exhibit excellent temperature dependence because of the multi-bandgap structure [174] such as p-i-n single-junction concentrators e.g. AlGaAs/InGaAs or InGaAs/InP MQW. These also show excellent radiation hardness, useful for space solar cells.

Even though the concept of IB solar cell seems promising, several difficulties have been identified with its practical implementation.

One of the main challenges associated with this concept is ensuring practically and efficiently, optimal optical transitions which depend on obtaining the required exact energy spacing among all three bands. The most efficient conversion process is realized if each photon is absorbed using the transition

with the highest threshold possible [158, 164, 175]. In figure 41, the transitions with the lowest energies are to proceed according to the path coloured red until the energy is high enough to proceed along the path coloured green which should be dominant for energies upwards until the path coloured blue becomes in turn possible and dominant. Therefore, an optimal use of energy imposes very different transition rates between bands.

Another difficulty encountered in this concept is that practically, these transitions described above do not occur naturally since in general, absorption coefficients tend to vary as 1/E where E is the transition energy. Even though there are considerable degree of freedom with the density of states and transition matrix elements, obtaining efficient absorption reqiures that optical absorptions are allowed and therefore can be described in the dipolar (first order) approximation as proposed by Nelson [176] .Therefore The optical transitions are not expected to depend much on energy for a given transition between two bands.

The three matrix elements corresponding to the three transitions of figure 40 are not completely independent and it seems difficult to have cross sections in the order of the transitions described especially keeping them all as high as possible. Notably, if the bands are suitably narrow or if the valence band-width is equal to the difference in the absorption threshold between transitions coloured red and green, then the transitions described will occur naturally. Yet this will lead to an unpleasant implication, considering the solar spectrum, the width of the valence band should be of the order of 1eV which is quite narrow and therefore with likely implications for the hole mobility.

Another factor to consider is the electron and hole concentrations in the intermediate band. One requires a sufficiently high electron and hole concentrations in the this band to ensure an efficient transition coloured red and green respectively.

This may be achieved in two ways: either

1) the intermediate band is populated (with both electrons and holes) by photon absorption or
2) the intermediate band is naturally rich in both species and therefore behave as a metallic band [157].

However it is necessary that such a metallic band will not impact negatively on the optical properties of the device (e.g. increased reflectivity).

Case (1) gives an absorption cross section that depends on the square of the intensity of illumination, so that most likely, high illumination levels will have to be reached for the process to be efficient.

Case (2) relaxes the constraint on illumination levels but it makes the recombination kinetics much faster. As a result of the micro-reversibility principle, in the radiative limit, both absorption and recombination are enhanced in the same ratio and this has no net influence on the efficiency. This is not so any more if non radiative recombination is included.

In the metallic IB concept, there is a strong absorption probability of the intermediate band. The problem of course is that such metallic IB is very likely to be a source of recombination in real systems. The high concentration of both holes and electrons in the IB necessary for having good absorption will increase the kinetics of any recombination path and this is likely to make the system specially sensitive to non radiative recombination in

the paths coloured red and green. It will also strongly increase the recombination of carriers generated by the path coloured blue.

Notably in this scheme, there is some up conversion at play whereby two low -energy photons are used to produce an electron with a higher kinetic energy. Here the stringent requirement on the closeness to the radiative limit can be somewhat relaxed because the optical transitions of the two step promotion of the valence band electrons take place in different parts of the device and are not therefore strongly coupled as in the metallic intermediate band version. The mobility necessary in the intermediate band to avoid resistive losses under AM1.5G illumination can be estimated around $100 cm^2/Vs$ (for typical carrier concentrations of $10^{17} cm^{-3}$). This value can be achieved in minibands in multiple quantum well structures but not in solids having narrow bands (d or f bands) such as transition metal oxides or chalconides.

We next consider 3-dimensionally ordered QDS with closely spaced quantum dots and high quality interfaces in which there is a strong overlapping of the electronic wave functions leading to the formation of minibands [177]. Figure 43 is a schematic diagram of the supposed supracrystal structure showing the periodically arranged quantum dots.

The QDS is sandwiched between p and n type layers of the host material. In principle the IB must be half populated with electrons which could be achieved by modulation doping at the barrier region. To achieve maximum efficiency, one has to engineer the QDS parameters such as quantum dot size, shape, inter-dot spacing and dot arrangement.

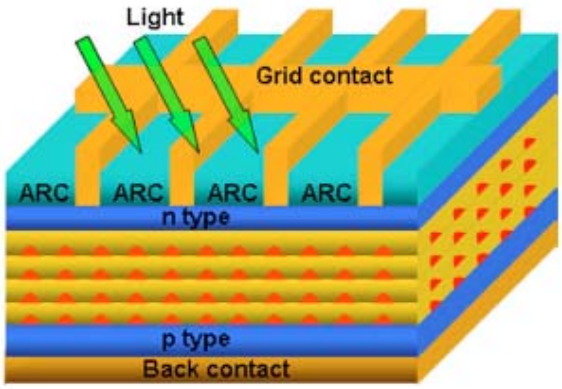

Fig 43: Schematic diagram of quantum dot supracystal [177]

In order to demonstrate the possibility of QDS forming optimum IB, the electron dispersion in such structure is first calculated by solving the Schroedinger's equation. This has been successfully carried out by Lazarenkova et al [178] using semianalytical approach which gives the solution in the 3-D ordered QDS through the Kronig-Penny type of expression. This has been further verified to ensure its accuracy by the finite-element simulation [177,179]. 3-D analysis of QDS made of $InAs_{0.9}N_{0.1}/GaAs_{0.98}Sb_{0.02}$ material systems has been performed by Q. Shao et al [180].

It has been found that the valence band offsets are negligible in this system while the conduction band offset is equal to $E_{barrier} \approx 1.29eV$ [181].

The values of the electron effective masses, $m^*_{InAsN} = 0.035m^o$ and $m^*_{GaAsSb} = 0.066m^o$ where m^0 is the electron rest mass and the other band parameters are obtained from [181]. The results are presented in figure 44

showing the calculated electron dispersion E(k) in the simple cubic QDS as a function of the electron wave vector q with quantum dot size W = 4.5nm and inter-dot spacing H = 2nm along the [[100]] quasi crystallographic direction.

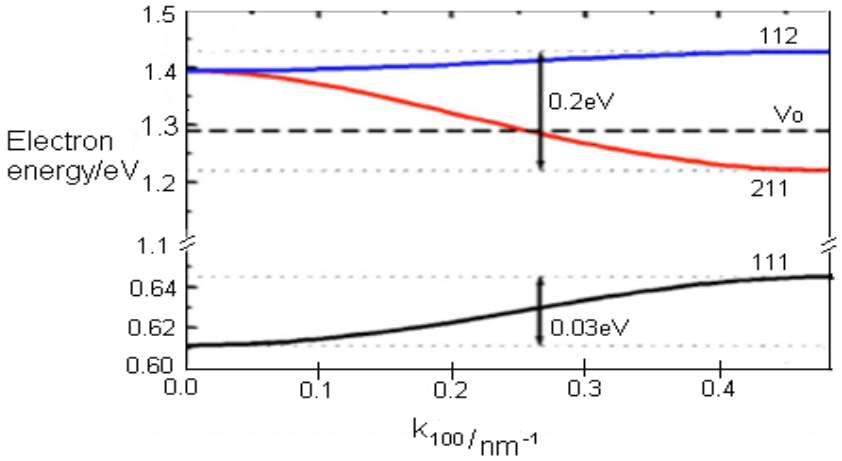

Fig 44: Electron dispersion in $In As_{0.9}N_{0.1}/Ga As_{0.98}Sb_{0.02}$ quantum dot supracrstal [178].

Parameters of the IB solar cell

The analysis leading to obtaining the efficiency of the IBSC is carried out with the standard assumptions of the ideal solar cell specified by Luque et al [158] i.e. non radiative transitions are forbidden, the quasi-Fermi levels are constant throughout the whole cell volume, the photovoltaic cell is thick enough to assure full absorption of photons with enough energy to induce any of the transitions shown in figure 41 and ohmic contacts applied such that only electrons (holes) can be extracted from the conduction (valence) to form the external current.

For an ideal solar cell, the photogenerated current is proportional to the difference between the number of photons absorbed by the device and the

number of photons emitted from the device. In the IBSC, the short circuit current density J_{SC} is given by [158]

$$J_{SC}/q = [\dot{N}(E_{13},\infty,T_S,0) - \dot{N}(E_{13},\infty,T_a,\mu_{13})] + [\dot{N}(E_{23},E_{12},T_S,0) - N(E_{23},E_{12},T_e,\mu_{12})] \quad (105)$$

where T_S is the temperature of the sun (6000K) regarded as a black body, T_a is the temperature of the solar cell (300K), $\dot{N}$ is the flux of photons, absorbed or emitted from the semiconductor and E_{13}, E_{23}, E_{12} $\mu_{13}, \mu_{23}, \mu_{12}$ are the energy differences and chemical potential difference between the conduction and valence bands, the conduction and intermediate bands and finally the intermediate and valence bands respectively. $E_{F!}, E_{F2}, E_{F3}$ are the Fermi levels of the valence, intermediate and conduction bands respectively and Δ_1 is the width of the intermediate band as shown in figure 45.

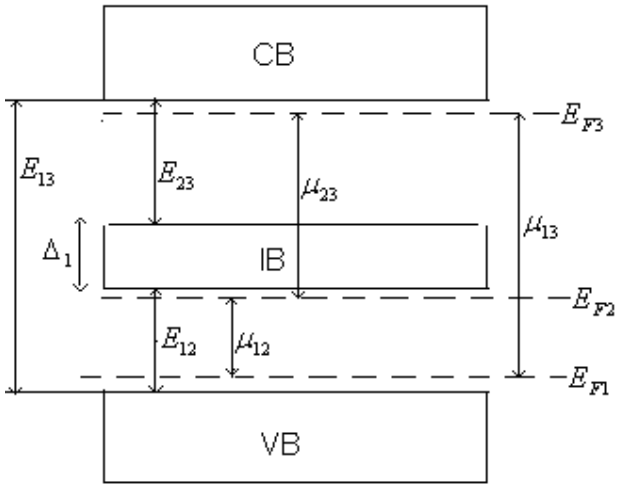

Fig 45: Band diagram of a solar cell with intermediate band

The first term in equation (105) is the photon flux that produces transitions from the valence band to the conduction band. The second term is the photon flux emitted as a result of charge recombination between the conduction and valence bands. The third term is the photon flux that produce transitions between the valence band and the intermediate band and between the intermediate band and the conduction band. The fourth term is the photon fluxdue to recombination of charge carriers between the conduction band and the intermediate band and between the inetermediate band and the valence band.

In thermodynamic equilibrium, the photon flux $\dot{N}$ is given by the general form of the Kirchoff's law of thermal radiation [161]

$$\dot{N}(E_l, E_h, T, \mu) = \frac{2\pi}{h^3 c^2} \int_{E_l}^{E_h} \frac{E^2}{e^{(E-\mu)/k_B T} - 1} dE \tag{106}$$

where E_l and E_h are the lower and upper energy limits of the photon flux for the corresponding transitions respectively. μ is the chemical potential of the transitions, k_B is the Boltzman's constant, E is the photon's energy and c is the speed of light. The output voltage is the difference between the chemical potentials of the conduction and valence bands.i.e

$$qV_{oc} = \mu_{13} - \mu_{12} \tag{107}$$

Assuming the fill factor is unity, then substituting the values of V_{OC} and J_{SC} in the efficiency equation $\eta = \frac{FFJ_{SC}V_{OC}}{P_{in}}$, where the incident power $P_{in} = \sigma T_S^4$, and σ is the stefan-Boltzman constant, we obtain the efficiency upper limit for the optimum quantum dot supracrystal parameters of the IBSC.

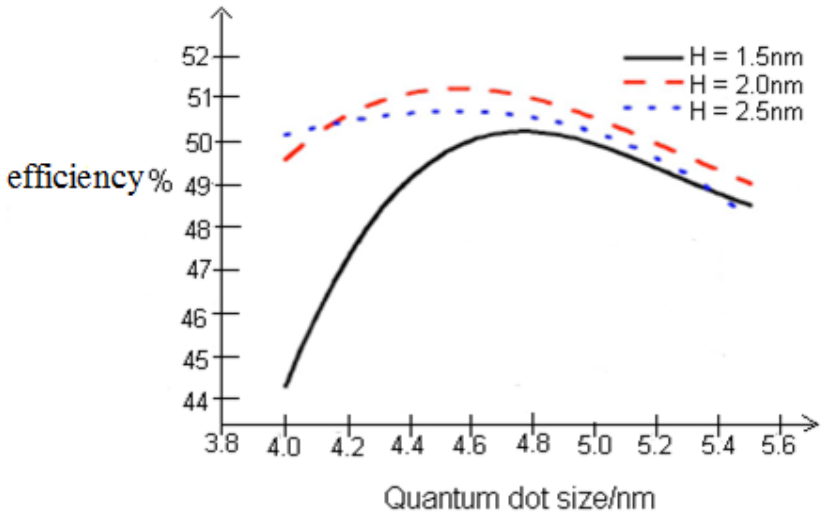

Fig 46: PV power conversion efficiency versus quantum dot size in $InAs_{0.9}N_{0.1}/GaAs_{0.98}Sb_{0.02}$ quantum dot supracrystal [158].

Figure 46 illustrates the power conversion efficiency of the IB solar cell based on quantum dot supracrystals as a function of the dot size which shows a maximum efficiency of 51.2% obtained from QDS with W = 4.5nm, H = 2nm having band parameters close to the ideal one. Though in comparism, this value is smaller than the thermodynamic values, it is still higher than the Shockley and Queisser limit of ~30% for bulk semiconductor materials [2].

Lastly, the electron density of states DOS must be as high as possible in order to restrict the IB quasi-Fermi level to its equilibrium position [182]. The electron DOS is given by

$$G(E) = \frac{2}{(2\pi)^3} \oint \frac{dS_E}{|\nabla_k E(k)|} \tag{108}$$

where E(k) is the electron energy and the integration is carried out over the surface of constant energy S_E. The DOS for IB ([[111]] miniband) in the

simple cubic supracrystal is shown insert in figure 44, the area under the curve is $7.395\times10^{18}cm^{-3}$ which is of the same order of magnitude as the DOS in the valence and conduction bands sufficient for the IB quasi-Fermi level pinning.

Typical theoretical values of efficiency of both one and two level bands as obtained by Brown et al [149] with the intermediate band scheme are shown in figure 47.

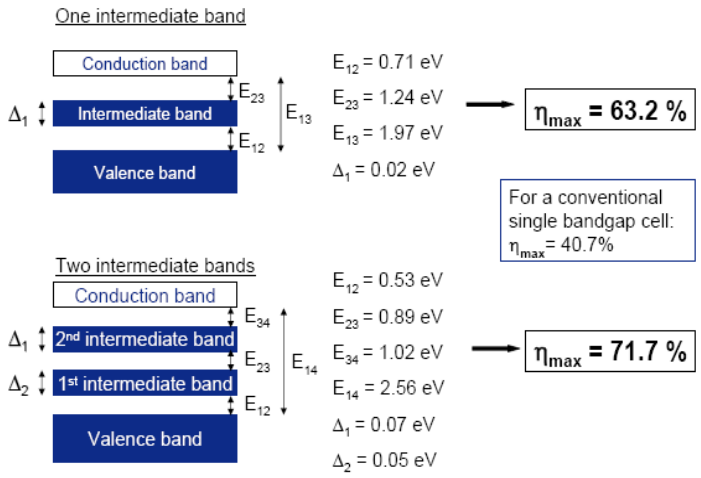

Fig 47: One and two level IBSC systems with efficiency values [149].

In these calculations, all optimum bands and energy separations are assumed to be exact. The intermediate band solar cell has remained largely conceptual due to difficulty in materializing it. However, recently some attempts to obtain the intermediate band structure using InAs [183,184] , Si/SiO_2 [185,186] or Si quantum dots embedded in hydrogenated amorphous Silicon carbide (a-SiC:H) multilayer [187] has been reported.

Compatibility of quantum dots

Quantum dots are a versatile kind of structure, apart from their small size and quantum confinement effect, quantum dots, in particular colloidal nanocrystals are not rigid like bulk semiconductor materials and can be molded into a variety of different forms. Such dots are free-floating in solution and can be combined easily with conductors and semiconductor polymers or sol-gels or implemented into porous films. Also due to the possibility of using liquid-phase with relatively low temperature processing, it permits the creation of junctions on inexpensive substrates such as coated glass, metal sheets etc. at the expense of the expensive microfabrication processes used in manufacturing conventional Silicon and thin-film based solar cells

Lastly, quantum dots can be prepared with a protective shell which increases its stability and therefore can lead to long lasting solar cells with little or no degradation in performance. All these constitute a huge advantage over conventional semiconductor solar cell devices which do not have molecular shells to protect them against harmful solar effects thus requiring periodic replacement [188]. These properties of quantum dots can enhance the ease of their inclusion in conventional solar cells to improve their performance. The way forward is to exploit the tunable band gap property of quantum dots to design them with different sizes to match and absorb all the photons in the solar spectrum in the same cell.

CHAPTER FOUR

CONCLUSION AND RECOMMENDATIONS

Conclusion

The advancement in nanofabrication methods especially lithography, molecular beam epitaxy and colloidal synthesis, coupled with the development of Scanning Tunneling microscopy and Atomic Force microscopy, allows for the accurate observation and positioning of atoms and molecules on substrates at the nanoscale . This has led to the production of nanostructures such as quantum dots and quantum well structures with strong quantum confinement effects and desirable properties that can be controlled at will.

The theory of the electrostatically gated quantum dot elaborated in chapter two, yield quantitatively a correct interpretation of the electronic properties of aquantum dot.The analysis indicate that like naturally occurring atoms, the electrons confined in aquantum dot form localized bound states with discrete energy levels and tunable band gaps.The spectroscopic analysis also indicates a good agreement between theory and experiment mainly that the absorption and emission spectra shift to shorter wavelength as the mean size of the dot decreases.

The interaction of quantum dot with a photon flux also show that the quantum confinement effect retards hot exciton cooling and allows the excess bandgap energy to be harnessed to produce several excitons thus breaking the one-photon, one-exciton rule which effectively limits the efficiency of

conventional solar cells. Also inter dot coupling could form minibands which provide additional channels for charge transport. These properties lend a quantum dot as suitable material for implementation in a solar cell as a way of improving its efficiency.

In this review, it has been demonstrated theoretically, that through multiple exciton generation (MEG) or impact ionization in quantum dots, the conversion efficiency of a quantum dot solar cell attains a value of 42% which nonetheless, is less than the thermodynamic limit but much higher than the Shockley and Queisser detailed balance limit. Secondly, that a single junction cell with properly located band of intermediate states using quantum dot supracrystals achieves a power conversion efficiency of up to 51.2%. Higher efficiencies of up to 71.7% have been reported for materials with two bands of intermediate steps.

Recommendations

There still remains a gap between the ideal and real values of the conversion efficiencies and further investigation into quantum dot carrier dynamics should be on-going, even though the problem of large area, cost-effective and highly reproducible fabrication processes for mass production seem mitigated.

Future ultra- efficient solar cells should incorporate a 3-D array of quantum dots of different sizes to respond to different portions of the solar spectrum and thus increase the spectral absorption range and also with inter-dot spacing sufficiently small such that strong coupling occurs and minibands formed to allow long-range eletron transport. The delocalized quantized 3-D

miniband states could be expected to slow carrier cooling and permit the on-set of impact-ionization to enhance both the photocurrent and photovoltage.

However, these schemes are largely theoretical and successful experimental back-ups with improvements and fine tuning are expected to boost the efficiency, reduce the cost of solar cells in comparison with other currently available energy sources and lead to the wide-spread use of solar cells and to secure a future based on clean and sustainable energy.

REFERENCES

[1] Kastner M., The single-electron transistor, Rev. Mod. Phys. **64**, 849 (1992).

[2] Jacak L., Hawrylak P. and Wojs A., *Quantum dots*, Springer (1998).

[3] Ashoori R., Electrons in Artificial atoms, Nature, **379**,413 (1996)

[4] Kouwenhoven L. P., Austin D. G. and Tarucha S., Few-electron quantum dots, Rep. Prog. Phys. **64**,701 (2001).

[5] http://www.evidenttech.com/nanomaterials, 18/7/2006

[6] Alivisatos A. P., Pespectives on the Physical Chemistry of Semiconductor Nanocrystals, J. Phys. Chem, **100**, 13226 (1996)

[7] Gaponenko S.V., *Optical Properties of Semiconductor nanocrystals* Cambridge Univ. Press, Cambridge, (1998)

[8] Grossard A. C., The coulomb blockade in coupled quantum dots, Science **274**, 1332, (1996)

[9] OosterkampT.H., Fujisawa T., Van der Wiel W.G., Ishibashi K., Hijman R.V., Tarucha S. and Kouwenhoven L.P., Microwave spectroscopy of a quantum dot molecule, Nature **395**, 873 (1998)

[10] Brodsky M., Zhitenev N.B., Ashoor R.C., Pfeiffer I. L. N.and West K.W., Localisation in artificial disorder: Two coupled quantum dots, Phys. Rev. Lett. **85**, 2356 (2000)

[11] Holleitner A. W., Blick R.H., Huttel A.K., Eberl K. and Kotthaus J. P., Probing and controlling the bonds of an artificial molecule, Science **297**, 70 (2002)

[12] Sakaki H., New Self-organised Growth Methods for InGaAs Quantum Dots on GaAs, Jpn. J. Appl. Phys. **28**, L314 (1989)

[13] King H. M., The world's evolving energy systems, Am. J. Phys. **49**, 1007 (1982)

[14] Shockley W. and Quesser H.J., Detailed balance limit of efficiency of p-n junction solar cells. J. Appl. Phys. **32**,510 (1961)

[15] Landsberg P. T. and Baruch P., Third Generation Photovoltaics. J. Phys. A 22, 19111(1989)

[16] Green M. A., *Third generation photovoltaics. Advanced Solar Energy Conversion,* Springer. Berlin, (2003)

[17] Bimberg D., Grundmann M. and Ledetsov N. N., *Quantum dot heterostructures,* Wiley, New York (1999).

[18] Dingle R., Wiegmann W. and Henry C. H., Quantum states of confined carriers in very thin $Al_XGa_{1-X}As$-GaAs-Al_XGa_{1-X} as heterostructures, Phys. Rev. Lett. **33**, 827 (1974)

[19] Nozik J. A. and Memming R., Physical chemistry of semiconductor-liquid interfaces, J. Phys. Chem. **100**, 13061 (1996).

[20] Miller R. D. J., Mclendon G., Nozik A. J., Schmickler W. and Willig F., *Surface Electron Transfer Processes.* VCH Publishers, New York (1995)

[21] Dingle R., *Semiconductor and semimetals: Applications of Multiquantum Wells, Selective Dopping, and Superlattices, Vol **24***, Academic Press, New York (1987)

[22] Peterson M.W., Turner J. A., Parson C. A., Nozik A. J., Baren't D. J., Van Hoof C., Borghs G., Houdre R. and Morkoc H., Miniband dispersion in GaAs/$Al_XGa_{1-X}As$ superlattices with wide and very thin barriers, Appl. Phys. Lett. **5**, 2666 (1988)

[23] Mensah S. Y., Allotey F. K. A., Nkrumah G. and Mensah N. G., Ground state Energy of a Polaron in a Superlattice, Superlattice and Microstructures, **29**(5), 336 (2001).

[24] Mensah S. Y., Owusu A., Mensah N. G. and Edziah R., Determination of the effective Mass of Semiconductor Materials using Faraday Rotation, **1**(2) 33 (2001)

[25] Mensah S. Y., Allotey F. K. A. and Clement A., Effect of ionization of impurity centres by electric field on the conductivity of Superlattice, Journal Superlattice and Microstructures, **19**(2), 151 (1996)

[26] Pearson C. A., Thacker B. R., Szmyd D. M., Peterson M. W. and Nozik A. J., Characterization of photocurrent spectroscopy of single quantum wells, J. Chem. Phys. **93**, 7706 (1990)

[27] Bastard G., *Wave Mechanics Applied to Semiconductor Heterostructures* Halsted Press, New York (1988).

[28] Jaros M., *Physics and Application of Semiconductor Microstructures,* Oxford University Press, New York (1989).

[29] Weisbuch C. and Vinter B., *Quantum Semiconductor Structures,* Academic Press, New York (1991).

[30] Yoffe A. D., Low-dimensional systems-quantum-size effects and electronic-properties of semiconductor microcrystallites (zero-dimensional systems) and some quasi 2-dimensional systems, adv. **42**, 173 (1993)

[31] Cuadra L., Marti A. and Luque A., IEEE Trans Electron Devices. **51**, 6 (2004).

[32] Nozik A. J., Spectroscopy and hot electron relaxation dynamics in semiconductor quantum wells and quantum dots, Annu. Rev. Phys.**52**, 193 (2001).

[33] Davies J. H., *The physics of low-dimensional semiconductors,* Cambridge University Press, Cambridge (1999).

[34] Madelung O., *Introduction to solid-state Theory*, Springer, New York, (1978).

[35] Harrison P., *Quantum Wells, Wires and Dots,* Wiley, Chester (2000).

[36] Bimberg D., Ggrandmann M. and Ledenstov N. N., *Quantum dot Heterostructures,* Wiley, New York, (1999)

[37] Pearsal T. P. (Ed.), *Quantum Semiconductor Devices and Technologies, Electronic Matrials Series,* Kluwer, Boston (2000)

[38] OosterkampT. N., Artificial atoms and Molecules, Phd. Thesis Technical University Delft, The Netherlands, (1999)

[39] Ashoori R. C.,Stormer H.L., Wieher J. S., Pfieffer L. N., Pearson S. J., Baldwin K. W. and West K. W., Single-electron capacitance spectroscopy of Discrete Quantum levels, Phys. Rev. Lett. **68**, 3088 (1992).

[40] Ashoori R. C., Stormer H. L., Wieher J. S., Pfieffer L. N., Pearson S. J., Baldwin K. W. and West K. W., N-electron ground state energies of a quantum dot in magnetic field, Phys. Rev. Lett. **71**, 613 (1993)

[41] Shedelbeck G., Wegscheder W., Bicher M. and Abstrieter G., Coupled Quantum Dots Fabricated by Cleaved edge Overgrowth: From artififcial atoms to molecules, Science **278**, 1792 (1997)

[42] Alivisatos A. P., Synthesis and characterization of CdS quantum dots in polystyrene, Science **271**,933 (1996)

[43] Overbeek J. T. G., Monodispers colloidal systems, fascinating and useful, Adv. Colloidal Interface Sci. **15**, 251 (1982)

[44] Murray C. B., PhD Thesis: Synthesis and Characterization of II-VI Quantum Dots and Their Assembly into 3D Quantum Dot Superlattices, Department of Chemistry, Massachusetts Institute of Technology (1995)

[45] Weller H. and Eychmuller A., Preparation and characterization of semiconductor nanoparticles ,in Kamat P. V. and Meisel D., eds, Semiconductor Nanoclusters, Elseviier Science B. V., Amsterdam, 5 (1997)

[46] Murray C. B., Norris D. J. and Bawendi M. G., Synthesis and Characterization of nearly monodisperse CdE (E = S, Se,Te) semiconductor nanocystallites , J. Am. Chem. Soc **115**, 8706 (1993).

[47] Micic O. I., Sprague J. R., Curtis C. J., Jones K. M., Machol J. L., Nozik A. J., Giessen H., Fluegel B., Mohs G. and Peyghambarian N., Synthesis and characterization of InP, GaP and $GaInP_2$ quantum dots, J. Phys. Chem. **99**, 7754 (1995)

[48] Micic O. I., Sprague J. R., Lu Z. and Nozik A. J., Highly efficient band-edge emission from InP quantum dots, Appl. Phys. Lett. **68**, 3150 (1996).

[49] Micic I. O., Cheong H. M., Fu H., Zunger A., Sprague J. R., Mascarenhas A. and Nozik A. J., Size-dependent spectroscopy of InP quantum dots, J. Phys. Chem. B. **101**, 4904 (1997).

[50] Guzelin A. A., Katar J. E. B., Kadananich A. V., Binan U., Hamad K., Juban E., Alivisatos A. P., Wolters R. H., Arnold C. C. and Heath J. R., Synthesis of size-selected, surface-passivated InP nanocrystals, J. Phys. Chem. **100**, 7212 (1996).

[51] Banin U.,Cerullo G., Guzelin A. A, Bardeen C. J., Alivisatos A. P. and Shank C. V, Quantum confinement and ultrafast dephasing dynamics in InP nanocystals, Phys. Rev. B **55**, 7059 (1997)

[52] Micic O. I., Lumin J. and Nozik A. J., Synthesis and characterization of binary and ternary III-V quantum dots, **70**, 95 (1996).

[53] Olshavsky M. A., Goldstein A. N. and Alivisatos A. P., Organometallic Synthesis of gallium-arsenide crystallites exhibiting quantum confinment, J. Am. Chem. Soc. **112**, 9438 (1990).

[54] Guzelin A. A, Banin U., Kadavanich A. V., Peng X. and Alivisatos A. P., Colloidal chemical synthesis and characterization of InAs nanocrystals quantum dots, Appl. Phys. Lett. **69**, 1432 (1990)

[55] Murphy J. E., Beard M. C., Norman A. G., Alhrenkiel S. P., Johnson J. C., Yu P., Micic O. I., Ellingson R. J. and Nozik A. J., PbSe colloidal nanocrystals: synthesis, characterization and multiple exciton generation, J. Adm. Chem. Soc. **128**, 3241 (1999).

[56] Sugawawara. M., *Self-assembled InGaAs/GaAs Quantum Dots, Vol. 60 of Semiconductors and Semimetals*, Academic Press, San Diego (1999)

[57] Hanna M. C., Lu Z. H., Cahill A. F., Heben M. J. and Nozik A. J., MOCVD growth and optical chararcterization of strain-induced quantum dots with InP island stressors, J. Cryst. Growth **174**, 605 (1997).

[58] Ruminov S. and Scheerschmidt K., TEM/HREM visualization of nm-scale coherent InAs islands (quantum dots) in a GaAs matrix, Phys. Status Solid A **150**, 471(1995).

[59] Lee H., Yang W., Lowe-Webb R. and Sercel P. C., Shape of InAs/GaAs quantum dots: relation to optical properties, Proc. 24th. Int. Conf. Phys. Semicond., world scientific, Singapore, 205 (1998).

[60] Yang W., Lee H., Johnson T. J., Sercel P. C. and Norman A. G., Electronic structure of self-organised InAs/GaAs quantum dots bounded by {136} facets, Phys. Rev. B **61**, 2784 (2000).

[61] Vurgaftman I., Meyer R. and Ram-Mohan L. R., Band parameters for III-V compound semiconductors and their alloys, J. Appl. Phys. **89**, 5815 (2001).

[62] Leosson K., Birkedal B., Magnusdottir I., Langbein W. and Hvam J. M., Homogeneous linewidth of self-assembled III-V quantum dots observed in single-dot photoluminescence, Physica E **17**, 19 (2003).

[63] Uskov A. V., Magnusdottir I., Tromborg B., Mork J., and Lang R., Line broadening caused by Coulomb carrier-carrier correlation and dynamics of carrier capture and emission in quantum dots, Appl. Phys. Lett. **79**, 1679 (2001).

[64] Santoprete R., Koiller B., Capaz R. B., Kratzer P., Liu Q. K. K. and Scheffler M., Tight-binding study of the influence of the strain on the electronic properties of InAs/GaAs quantum dots, Phys. Rev. B **68**, 235311 (2003).

[65] Shumway J., Williamson A. J., Zunger A., Passaseo A., Degiorgi M., Cingolani R.,Catalani M.and Crozier P., Electronic structure consequences of In/Ga composition variations in self-assembled $In_xGa_{1-X}As$/GaAs alloy quantum dots, Phys. Rev. b **64**, 125302 (2001).

[66] Goldhaber-Gordon D., Shtrikman H., Mahalu D., Abusch-Magder D., Mierav U. and Kastner M. A., Kondo Effect in a Single-Electron Transistor, Nature, **391**, 156 (1998).

[67] Goldhaber-Gordon D., Gores J., Kastner M. A, Shtrikman H., Mahalu H. D. and Meirav U., From the Kondo regime to the Mixed-Valence Regime in a Single-Elctron Transistor, Phys. Rev. Lett. **81**, 5225 (1998).

[68] Kastner M., Artificial Atoms, Physics today, **46**, 24 (1993).

[69] Tarucha S., Austin D. G., Honda T., van Der Hage R. J. and Kouwenhoven L. P., Shell Filling and Spin Effects in a Few Electron quantum dots. Phys. Rev. Lett. **77**, 3613 (1996).

[70] Kouwenhoven L. P., Oosterkamp T. H., Daneosaastro M. W. S., M. Eto, Austing D. G., Honda T. and Tarucha S., Excitation Spectra of Circular Few-Electron quantum Dots, Science **278**, 1788 (1997).

[71] Oosterkamp T. H., Janssen J. W., Kouwenhoven L. P., Austing D. G., Honda T. and Tarucha S., Maximum-Density Droplet and Charge Redistribution in Quantum Dots at High Magnetic Fields, Phys. Rev. Lett. **82**, 2931 (1999).

[72] MacDonald A. H., Yang E. S. R. and Johnson M. D., Correlation effects in vertical gated quantum dots, Aust. J. Phys. **46**, 345 (1993).

[73] Jauregui K., Hausler W. and Kramer B., Wigner molecules in quantum dots, Europhys. Lett. **24**, 581 (1993).

[74] Tarucha S., Honda T., van der Hage R. J. and Kouwenhoven L. P., Shell filling and spin effects in a few electron quatum dot, Phys. Rev. Lett. **77**, 3613 (1996).

[75] Bednarek S., Szafran B. and Adamowski J., Microelectron Eng, **99**, 51 (2000).

[76] Thoules D. J., Maximum Metallic Resistance in Thin Wires, Phys. Rev. Lett. **39**, 1167 (1977).

[77] Kulik I. O. and Shekhter R. L., An Electrochemical Coulomb Stair Case: Detection of Single Electron-Transfer Events at Nanometer Electrodes, Sov. Phys.-JETP, **41**, 308 (1975).

[78] Kouwenhoven L. P. and Marcus C. M., Quantum dots. Physics World, **11**. No. 6, 35 (1998).

[79] Kouwenhoven L. P., Marcus C. M., S.Tarucha S., Westervelt R. M. and Wingreen N. S., Electron Transport in in quantum dots, Proceedings of the NATO Advanced study Institute on Mesoscopic Electron Transport, (Kluwer Series E **345**, p. 105 (1997).

[80] Kouwenhoven L. P., Austin D. G. and Tarucha S., Few-electron Quantum dots. Phys. **64** (6), 701 (2001).

[81] di Vincenzo D. P., Low-dimensional systems in nanostructures, Phys. **48**, 771 (2000).

[82] De Franceschi S., Sasaki S., Elzerman J. M., van der Wiel W. G., Tarucha S., and Kouwenhoven L. P., Electron Cotunelling in Semiconductor Quantum Dots, Phys. Rev. Lett. **86**, 878 (2001).

[83] Loss D., and diVincenzo D. P., Quantum Computation with Quantum Dots, Phys. Rev. A **57**, 120 (1998).

[84] Cronewett S. M., Oosterkamp T. H. and Kouwenhoven L. P., A Tunable Kondo effect in quantum dots, Science **281**, 540 (1998).

[85] Schmid J., Wies J., Eberl K. and Klitzing K. V., Strongly electrostaticallycoupled quantum dots with separate leads, Physica B**182**, 256 (1998).

[86] Simmel F., Blick R. H., Kotthaus J. P., Wegsheider W. and Bichler M., Anomalous Kondo Effect in a Quantum Dot at Non-zero Bias, Phys. Rev. Lett. **83**, 804 (1999).

[87] Brus L. E., Elecron-electron and Electron-Hole interaction in small semiconductor crystallite: The size dependence of the lowest excited Electronic state, J, Chem, Phys. **80**, 4403 (1984).

[88] Johnson A. C., Petta J. R., Taylor J. M., Yacoby A Lukin M. D., Marcus C. M., Hanson M. P. and Grossard A. C., Triplet-singlet spin relation via nuclei in a double quantum dot Nature,**435**, 925 (2005)

[89] Koppens F. H. L., Folk J. A., Elzerman J. M., Hanson R.,.Van Beveren L.H.W., Vink I. J.,Tranitz H. P.,Weggcheider W., Kouwenhoven L. P. and Vandesypen L. M. K., Control and detection of singlet-triplet mixing in a random nuclear field, Science, **309**, 1346 (2005).

[90] Petta J. R., Johnson A. C.,Taylor J. M., Laird E. A., Yacoby A., Lukin M. D., Marcus C. M., Hanson M. P. and Grossard A. C., Coherent manipulation of coupled electron spin in semiconductor quantum dots, Science, **309**,2180 (2005)

[91] Loss D. and di Vicenzo D. P., Quantum computation with quantum dots, Phys. Rev. A 5**7**, 120 (1998).

[92] Kumar A., Laux S. E. and Stern F,. Electronic states in GaAs quantum dots in a magnetic field. Phys. Rev. B **42**, 5166 (1992)

[93] Reimann S. M., Koskinen M. and Manninen. M., On the formation of Wigner molecules in small quantum dots. Phys. Rev. B **62**, 8108, (2000).

[94] Darwin C. G., The diamagnetism of the free electron, Proc. Cambridge Phil. Soc **27**, 86 (1930).

[95] Schmidt H. M. and Weller H., Photochemistry of colloidal Semiconductors: Quantum size effects in semiconductor crystallites-calculation of energy spectrum for the confined exciton, Chem. Phys. Lett. **129**, 615 (1986).

[96] Ekimov A. I., Efros A. L., Ivanov M. G., Onushenko A. A. and Shumilov S. K., Donor-like exciton in zero-dimensional semiconductor structures, Solid State Comm. **69**, 565 (1989).

[97] Kayanuma Y.,and Momiji H., Incomplete confinement of electrons and holes in microcrystals, Phys. Rev. b **41**, 10261 (1990).

[98] Takagahara T., Effects of dielectric confinement and electron-hole exchange interaction on excitonic states in semiconductor quantum dots, Phys. Rev. B **47**, 4569 (1993).

[99] Takagahara T., Electron-phonon interaction and excitonic dephasing in semiconductor nanocystals, Phys. Rev. Lett. **71**, 3577 (1993).

[100] Hu Y. Z., Lindberg M. and Koch S. W., Theory of optically excited intrinsic semiconductor quantum dots, Phys. Rev. B **42**, 1713 (1990).

[101] Park S. H., Morgan R. A.,Hu Y. Z., Lindberg M., Koch S. W. and Peyghambarian N., Non linear-optical properties of quantum-confined CdSe microcrystallites, J. Opt. Soc. Adm. **7**, 2097 (1990).

[102] Pollock E. L. and Koch S. W., Path-integral study of excitons and biexcitons in semiconductor quantum dots, J. Chem. Phys. **94**, 6776 (1991).

[103] Brus L. E., Electronic wavefunctions in semiconductors clusters; experiment and theory, J. Phys. Chem. **90**, 2555 (1986).

[104] Kayanuma Y., Quantum-size effects of interacting electrons and holes in semiconductor microcrystals with sphereical shape , Phys. Rev. B **38**, 9797 (1988).

[105] http://www.evidenttech.com/nanomaterials/quantum-dot-nanomaterials.php, 18/7/2006

[106] http://www.evidenttech.com/nanomaterials/evidots/quantum-dot-introduction.php, 18/7/2006

[107] Woggon U, *Optical Properties of Semiconductor quantum Dots,* Springer Tracts in Modern Physics, Springer-Verlag, Berlin-Heidelberg (1997).

[108] Xia J. B., Electronic structures of zero-dimensional quantum wells, Phys. Rev. B **40**, 8500 (1989).

[109] Murray C. B. Norris D. J., and Bawendi M. G., Synthesis and Characterisation of Nearly Monodisperse CdE (E = Sulfur, Selenium, Tellurium) Semiconductor Nanocrystallites, J. Am. Chem. Soc. **115**, 8706 (1993).

[110] Katari J. E. B., Colvin V. L. and Alivisatos A. P., X-ray Photoelectron Spectroscopy of CdSe Nanocrystals with Applications to studies of The Nanocrystal Surface, J. Phys. Chem. **98**, 4109 (1994).

[111] Jacobsohn M. and Banin U., Size Dependence of Second Harmonic Generation in CdSe Nanocrystals Quantum Dots, J. Phys. Chem. B**1**, 104 (2000).

[112] Empedocles S. A, Neuhauser R., Shimizu K. and Bawendi M. G., Photoluminescence from Single Semiconductor Nanostructures, Adv. Mater. **11**, 1243 (1999).

[113] Kubin R. F.,Lumines J. and Fletcher A. N, Florescence quantum Yields of Some Rhodamine Dyes. **27**, 455 (1982)

[114] de Mello Donega C., Hickey S. G., Wuister S. F., Vanmaekekberg D. and Meijerink A., Single-Step to Control the Photoluminescence Quantum Yield and size Dispersion of CdSe Nanocrystals, J. Phys. Chem. B **107**, 489 (2003)

[115] http://www1.eere.energy.gov/solar/solar cell structures.html. 27/7/2007

[116] http://www1.eere.energy.gov/solar/index.html. 27/7/2007

[117] http://www.eere.energy.gov/ 27/7/2007

[118] http://www.energy.gov/ 27/7/2007

[119] http://www1.energy.gov/solar/webmaster.html. 27/7/2007

[120] Nault R. M., In: Basic research needs for solar energy utilization. Report on the basic energy source workshop on solar energy utilization. Argonne National Laboratory U.S.A. (2005).

[121] Green M. A., *Solar cells: Operating Principles, Technology and Systems Application,* Prentice-Hall, Eglewood Cliffs, N.J., U.S.A. (1982)

[122] Shah J., *Ultra-fast spectroscopy of semiconductors and semiconductor nanostructures,* Springer- Verlag, Berlin (1999)

[123] Krishna M. V. R., Friesner R. A., Quantum Confinement in Semiconductor Clusters, J. Chem. Phys. **95**, 8309 (1999)

[124] Kittel C., *Introduction to Solid State Physics*, Sixth Edition, John Wiley and Sons Inc., New Edition John Wiley and sons Inc., New York, Chichester, 299 (1996)

[125] Kolodinski S., Werner J. H., Wittchen T. and Queisser H. J., Quantum Efficiencies exceeding unity due to impact ionization in silicon solar cells, Apply. Phys. Lett. **63**, 2405 (1993)

[126] Sze S., *Physics of Semiconductor Devices,* Wiley, New York, (1981)

[127] Califano M., Zunger A., and Franceschetti A., Efficient Inverse Auger Recombination Threshold in CdSe Nanocrystals, Nano lett.**4**, (2004)

[128] Califano M., Zunger A. and Franceschetti A., Direct Carrier Multiplication due to Inverse Auger Scattering in CdSe Quantum Dots, Appl. Phys. Lett., **84**, 2409 (2004)

[129] Green M. A., *Solar Cells*, The University of New South Wales, Kensington, Aust, (1992)

[130] Nozik A. J., High Efficiency carrier Multiplication in PbSe Nanocrystals: Implications for Solar energy Conversion, Annu. Rev. Chem., **52**, 193 (2001)

[131] Ross R. T. and Nozik A. J., Efficiency of hot-carrier solar energy converters, J. Appl. Phys. **53**, 3813 (1982).

[132] Boudreaux D. S. and Williams F., A. Nozik A. J., Hot Carrier Injection at Semiconductor-Electrolyte Junctions, J. Appl. Phys. **51**, 21581(1980)

[133] Landsberg P. T., Nussbaumer H. and Willeke G., Band-band impact ionization and solar cell efficiency, J. Appl. Phys. **74**, 1451 (1983)

[134] Green M. A., *Third Generation Photovoltaics*, Bridge Printery, Sydney, (2001).

[135] Nozik A. J., Quantum dot solar cells, Physica E, **14**, 233 (2002)

[136] Schaller R. C. and Klimov V., High Efficiency Carrier Multiplication in PbSe Nanocrysrtals: Implications for solar Energy Conversion, Phys. Rev. Lett. **92**, 186601(2004)

[137] Murphy J. R., Ellingson R. J. and Nozik A. J., PbTe Colloidal nanocrystals: Synthesis, characterization and multiple exciton generation. Journal of the American Chemical Society, **128**, 3241 (2006)

[138] Brunner K., Brunner K., Abstreiter G., Bastard G. and Vogl P., Exciton relaxation and radiation recombination in semiconductor quantum dots, Phys. Rev. Lett. **69**, 3216 (1992)

[139] Schaller R. C., Petruska M. A. and Klimov V. I., Effects of electronic structure on carrier multiplication efficiency: comparative study of Pbse and CdSe nanocrystals. Appl. Phys. Lett. **87**, 253102 (2005)

[140] Jiang X., Zikhidov A. and Klimov V., Photovoltaic responses of solar cells based on lead selenide quantum dots and conducting polymers,.American Physical society meeting , Baltimore.

[141] Schaller R. C. and Klimov V. I., Seven excitons at a cost of one: redefining the limits for conversion efficiency of photons into charge carriers. Nano Lett. **6**, 424 (2006)

[142] Hanna M. C. and Nozik A. J., Solar conversion efficiency of photovoltaic and photoelectrolysis cells with carrier multiplication absorbers, J. Appl. Phys. **100**, 74510 (2006)

[143] Ellingson R. J., Beard M. C., Johnson J. C., Yu P., Micic O. I., Nozik J. J., Shabaev A. and Efros A. L., Highly efficient multiple exciton generation in colloidal PbSe and PbS quantum dots, Nano Lett. **5**, 865 (2005).

[144] Werner J. K. H., Kolodonski S. and Queisser J. H., Novel optimisation principles and efficiency limits for semiconductor Solar cells, Phys. Rev. Lett. **72**, 3851 (1994).

[145] Spirkel W. and Ries H., Lumunescence and efficiency of an ideal photovoltaic cells with charge multiplication, Phys. Rev. B **52**, 11319 (1995)

[146] Brendel R., Werner J. H. and Queisser J. H,.Thermodynamic efficiency limits for semiconductor solar cells with carrier multiplication sol. Energy Mat. Sol. Cells **41**, 419 (1996).

[147] Wurfel P., Solar energy conversion with hot electrons from impact-ionization, Sol. Energy Mat. Sol. Cells **46**, 43 (1997).

[148] de Vos A. and Desoete B., On the ideal performance of solar cells with larger than-unity quantum efficiency, Sol. Energy Mat. Sol. Cells **51**, 415 (1998).

[149] Landsberg P. T. and Badescu V., Solar cell thermodynamics including multiple impact-ionization and concentration of radiation, J.Phys. D **35**, 1236 (2002).

[150] Barnham J. W. K., Duggan G., A new approach to high efficiency multi-bandgap solar cells, J. Apply. Phys. **67**, 3490 (1990).

[151] Bushel D. B.l, Tibbits F. N. D. and Barnham K. W. J., Effect of well number on the performance of quantum well solar cells, J. Apply. **97**, 124908 (2005).

[152] Nelson J., Paxman M., Barnham J. W. K., Roberts J. S. and Button C., Steady-state carrier escapefrom single quantum wells, IEEE J. Quantum Electron **29**, 1460 (1993).

[153] Alemu A., Coaquira J. A. H. and Freundlich A., Dependence of device performance on carrier escapes sequence in multi-quantum-well p-i-n solar cells, J. Apply. Phys. **99**, 084506 (2006).

[154] Barnham J. W. K., Braun B., Nelson J., Paxman J. M., Button C., Roberts J. S. and Foxon C. T., Short-circiut current and energy efficiency enhancement in low-dimensional structure photovoltaic devices, Apply. Phys. Lett. **59**, 135 (1991).

[155] Freundlich A. , Renaud P., Vilela M. F. and Bensaoula A., Strained quantum well photovoltaic energy converter, US 5851310 (1998).

[156] Yakimov A. I., Dvurechenski A. V., Proskuryakov Y. Y., Niliforov A. I., Pchelyakov O. P., Teys S. A. and Gtaskovskii A. K., Normal-incidence infra-red photo-conductivity in Si p-i-n diode with embedded Ge self-assembled quantum dots, Apply. Phys. Lett. **75**, 1413 (1999).

[157] Walther T., Cullis A. G., Noris D. J. and Hopkins M., Nature of the Stranski-Krastanov Transition During Epitaxy of InGaAs on GaAs, Phys. Rev. Lett. **86**, 2381 (2001).

[158] Caudra L. R. and Marti A., Luque A., Design Constraints of the Quantum-Dot Intermediate Band Solar Cell, Physica E **14**, 150 (2002).

[159] Luque A. and Marti A., Increasing the efficiency of Ideal Solar Cells by Photon Induced Transitions of intermediate levels, Phys. Rev. Lett. **78**, 5014 (1997).

[160] Wolf M., Limitations and possibilities for improvements of photovoltaic solar cells, Proc. IRE **48**, 1246 (1960).

[161] http://emet-solar.ibl.gov/index.html, 15/2/2008

[162] Luque A. Marti A. and Caudra L., Quantum Dot Intermediate Band Solar Cell, Poltcnica de Madrd U., Phys. Rev. Lett., **78**, No.26, (1997).

[163] Luque A. and Marti A., Increasing the Efficiency of Ideal Solar Cell by Photon Induced Transitions at Intermediate Levels, Phys. Rev. Lett. **78**, 5014 (1997).

[164] Green M. A., Handbook of semiconductor Nanodevices, Photovoltaic Applications of Nanostructures Vol.4, edited by A.A. Baladin and Wang K. L.(ASP Stevens Ranah, California 219 (2006).

[163] Green M. A., Nanotchnology, **11**, 401 (2000).

[165] Canovas E., Stanley C., Farmer C., Cuadra L. and Luque A., Thin Solid Films, **511**, 638 (2006).

[166] Sinhavoy S., King C. W., Bailey S. G. and Raffaelle R. P., Proceedings of the 31st IEEE Photovoltaic specialists Conference (IEEE, New Jersey,. 94 (2005).

[167] Cuadra L., Marti A. and Luque A., Thin Solid Films **451**, 593 (2004).

[168] Honsberg C. B., Corkish R. and Brener S.P., Thermoelectric Field Effects in Low Dimensional Structure Solar Cells, Proc. Of Glasgow (2000)

[169] Kettemann S. and Guillemoles J. F., Proceedings of the 13th Photovolts. Sol. Energy Conference, Nice (1995).

[170] Nelson J., Barnes J., Ekins-Daukes N., Kluftinger B., Tsui E., Barnham K., Foxon T., Cheng T. and Roberts J. S., Observation of Supressed Radiative Recombination in Single Quantum well p-i-n Photodiodes, J. Appl. Phys. **82**, 6240 (1997).

[171] Urayama J., Noris T. B., Singh J. and Bhattacharya P., Observation of Phonon Bottleneck in quantum Dot electronic relaxation, Phys. Rev. Lett. **86**, 4930 (2001).

[172] Keevers M. J., and Green M. A., 23rd IEEE. Photovoltaics Spec. Conf. Proc., Loisville, Efficiency improvements of silicon solar cells by impurity photovoltaic effect, (1993), 140; R. Corkish, M. A. Green, ibid., 675.

[173] Tritt T. M. (ed.*), Recent Trends in Thermo-electric Materials Research, Semiconductors and Semimetals,* Academic Press, San Diego, 69 (2001).

[174] Aperathitis E., Varonides A. C., Scott C. G., Sand D., Foukaraki V., Androulidaki M., Hatzopoulos Z. and Panoyotatos P., Dependence of photo current components on enhanced performance GaAs/AlGaAs multiple quantum well solar cells. Sol. Energy Mater Sol. cells; **70**, 49 (2001).

[175] Brown A. S., Green M. A. and Corkish R. P., Diluted II-VI Oxide semiconductor with Multiple Band Gap, Physica, E (Amsterdam) **14**, 121 (2002).

[176] Nelson J., *The physics of solar cells,* Imperial College Press, (2003).

[177] Lazarekova O. L., and Baladin A. A., Electron and phonon energy spectra in a three-dimensional regimented quantum dot superlattice, Phys. Rev. B **66**, 245319 (2002).

[178] Lazarenkova O. L. and Baladin A. A, Miniband formation in a quantum dot crystal, J. Appl. Phys. **89**, 5509 (2001).

[179] Niker D. L., Pokatilov E. P., Shao Q. and Baladin A. A., Energy Harvesting - From Fundamentals to Devices, Phys. Rev. B **76**, 125417 (2007).

[180] Shao Q. and Baladin A. A., Charge carrier states and light absorption in ordered quantum dot superlattices, Appl. Phys. Lett. **91**, 163503 (2007).

[181] Levy M. Y., Honsberg C., Marti A. and Luque, A. Proceedings of the 31st IEEE Photovoltaics Specialists Conference , IEEE, New Jersey, 90 (2005).

[182] Vugaftman I., Meyer J. R., and Ram-Moham R., III-V Semiconductor Band Parameters, J. Appl. Phys. **89**, 5815 (2001).

[183] Luque A., Marti A., Lopez N., Antolin E., Canovas E., Stanley C., Farmer C, Cabellero L. J.,Caudra L. and Balenzotegui J. L., Experimental analysis of the quasi-fermi level split in quantum dot intermediate-band solar cells. Apply. Phys. Lett. **87**, 083505 (2005).

[184] Luque A., Marti A., and Lopez N., et al. Operation of the intermediate-band solar cell under non ideal space charge region and self- filling of the intermediate-band. J. Apply. Phys. **99**, 94503 (2006).

[185] Cho E., Green M. A., Xia J., Corkish R., Reece P. and Gal M., Clear quantum confined luminescence from crystalline silicon/SiO_2 single quantum wells. Apply. Phys. Lett. **84**, 2286 (2004).

[186] Jiang C. and Green M. A., Silicon quantum dot superlattices: Modelling of energy bands, density of states and mobilities for silicon tandem. Solar cell applications. J. Apply. Phys. **99**, 114902 (2006).

[187] Kurokawa Y., Miyajima S., Yamada Y., and Konagai M., Preparation of nanocrystalline silicon in amorphous silicon carbide matrix, Jpn. J. Phys. **45**, 1064 (2006).

[188] http://www.evidenttech.com/nanomaterials/quantum, 5/10/2007